INTERFEROMETRIC MEASUREMENT OF BRIGHTNESS DISTRIBUTIONS IN DISCRETE RADIO SOURCES

Thesis by

Alan Theodore Moffet

In Partial Fulfillment of the Requirements

For the Degree of

Doctor of Philosophy

California Institute of Technology

Pasadena, California

1961

ACKNOWLEDGMENTS

I am grateful to J. G. Bolton, former Director of the Owens Valley Observatory, for assigning to me a most fruitful task and for providing the observing time necessary to carry it out. G. J. Stanley, Acting Director of the Observatory, has advised on the preparation of the data for publication and was also responsible for the design of the receiving equipment. Consultations with R. B. Leighton, thesis advisor since Professor Bolton's departure, have been of great value.

The burden of making the observations was shared by D. Morris, V. Radhakrishnan, and D. E. Harris. Data on source positions and identifications were provided by T. A. Matthews, who has also critically reviewed the manuscript. Information on galactic sources was supplied by R. W. Wilson. Many useful discussions with P. Maltby are gratefully acknowledged.

During the course of my graduate study I have held a National Science Foundation Predoctoral Fellowship. The work of the Observatory is supported by the United States Office of Naval Research under Contract Nonr 220(19).

ABSTRACT

Information about the brightness distributions in 110 extragalactic and 17 galactic radio sources has been obtained from observations with the Caltech variable spacing interferometer at a wavelength of 31.3 cm. In these observations, the amplitude and phase of the complex visibility function were measured at transit with antenna spacings of 195λ, 389λ, 779λ, and 1557λ along an east-west baseline. Using these same basic spacings, and by observing at large hour angles, the visibility amplitude was measured at ten other effective spacings between 126λ and 1363λ. Not all sources were observed at all spacings.

Of the 110 extragalactic sources, 47 are found to have angular diameters greater than 1'.5. Only 4 of these 47 appear to have smooth, simple structure, while the remaining 43 show some form of complexity, many having two fairly well separated components. It is suggested that the majority of all extragalactic sources have complex structure. For three extragalactic sources (M 87, NGC 5128, and Cygnus A) comparable measurements at other wavelengths have been published, and in each case, significant changes in structure with wavelength are noted.

The theory of interferometric investigation of discrete sources is developed in some detail, and previous work in the field is reviewed. Calculations on a number of model sources are described.

TABLE OF CONTENTS

CHAPTER I

Introduction

In one of the first surveys of cosmic radio noise, Hey, Parsons and Phillips, in 1946, observed fluctuations in the emission received from the Cygnus region. To explain this phenomenon they postulated the existence of an intense, small-diameter radio source (1). The presence of such a source was soon confirmed by Bolton and Stanley, who found its angular diameter to be less than 8' (2).

In the fifteen years since these first observations, several thousand discrete radio sources have been catalogued. The positions and intensities of many have been measured at several different wavelengths and with different types of instruments. Most are known to have apparent diameters of less than 10', but detailed brightness distributions have been obtained for fewer than a dozen of the brightest or largest sources. The reason for this is that previous investigations with high resolution interferometers have been limited by low sensitivity to only the strongest sources, while other instruments with high sensitivity have had sufficient resolving power to reveal details of structure in only the very largest sources. The construction of the variable spacing interferometer at the Owens Valley Observatory has made available for the first time an instrument with high resolving power and enough sensitivity to enable brightness

distribution measurements to be carried out on at least several hundred sources.

The object of this investigation has been to obtain detailed information about the brightness distributions of a large group of sources. One hundred twenty seven sources were observed, of which 60 were found to contain structural details having characteristic sizes within the 1'.0 to 15' range over which the instrument was most sensitive. Several sources were found to consist of two roughly equal centers of emission, thus resembling in structure the well-known example of Cygnus A.

In the following chapter the theory of interferometric investigations of discrete sources is developed, and previous work in the field is briefly reviewed. In Chapter III the observations and the analysis of the data are described, while the visibility functions are tabulated in Chapter IV with graphs for the more interesting sources. The interpretation of the visibility functions is given in Chapter V, and an Appendix contains calculations made on several types of model sources.

CHAPTER II

Interferometry of Discrete Sources

Resolution of fine detail within a radio source requires that the antenna sensitivity pattern have a commensurate degree of fineness. This implies a large antenna size, since beamwidth and aperture are inversely proportional. For instance, to obtain a 1' pencil beam with a paraboloid which was illuminated in such a way as to have reasonably low sidelobes, the diameter of the aperture would have to be about 4500 wavelengths. Antennas with pencil beams approaching 1' have only been constructed for wavelengths of about 1 cm. At these short wavelengths only a few of the brightest sources can be detected with the best of currently available receivers. It is, however, possible to investigate the fine details of a source distribution by introducing fine structure within a gross primary sensitivity pattern. The requirement of a large over-all aperture is the same, but the aperture no longer need be completely filled in. The principles of this method were set forth by Michelson in a series of papers in the 1890's (3,4). The method is that of the wave interferometer or Michelson interferometer.

Interferometric measurements were first made in radio astronomy by Ryle and Vonberg (5) and by McReady, Pawsey, and Payne-Scott (6) to determine the sizes of active

regions on the Sun. Ryle first developed the two element radio interferometer which is directly analogous to the Michelson stellar interferometer. This chapter will be devoted to the theory of interferometric techniques, using such an instrument, as applied to studies of discrete sources.

Bracewell (7,8) has reviewed the interferometry of discrete sources, and this discussion will follow his general line of development. It will, however, deal more extensively with brightness distribution measurements which can be made with currently available instruments similar to the California Institute of Technology interferometer (9), the interferometer at Nançay (10), or that at Malvern (11).

The Geometry of the Interferometer

Each of the above-mentioned instruments consists of two steerable paraboloids mounted on railroad tracks in such a way that the length and orientation of the baseline may be varied within certain limits. The baseline is defined as the line joining the vertices of the two paraboloids (which are assumed to be identically mounted and illuminated). Its length is s wavelengths at the operating frequency, and its azimuth is a. The baseline is ideally level when both antennas are pointed in the same direction, but we will consider the effect of a non-zero elevation ℓ.

The response pattern of a phase-switched (12) or a continuous multiplication (9) interferometer consisting of two antennas with isotropic sensitivities is a function only of the angle θ between the source direction and the median plane of the interferometer and is

$$R(\theta) = G\,A\cos(2\pi s \sin\theta + \Psi) \quad , \tag{1}$$

where A is the collecting area of each antenna, Ψ is an instrumental phase error which must be determined, and G allows for receiver gain changes. It can be seen that the interferometer response pattern is a series of sinusoidal fringes having a period of $1/s$ in $\sin\theta$. If the individual antennas do not have isotropic responses, then A must be replaced by the product of their <u>voltage</u> responses. In the case we are considering, of two identical antennas, this product is equal to the square of the voltage response of one antenna and hence to its <u>power</u> response, $A(\theta,\psi)$. The angles θ and ψ form a system of spherical polar coordinates having the interferometer baseline as polar axis.

For astronomical purposes, the interferometer response pattern is more conveniently dealt with in terms of hour angle and declination, so we seek an expression for $\sin\theta$ in terms of these quantities. Referring to figure 1, let N be the north celestial pole, Z the local zenith, ϕ the geographic latitude, S the position of the source

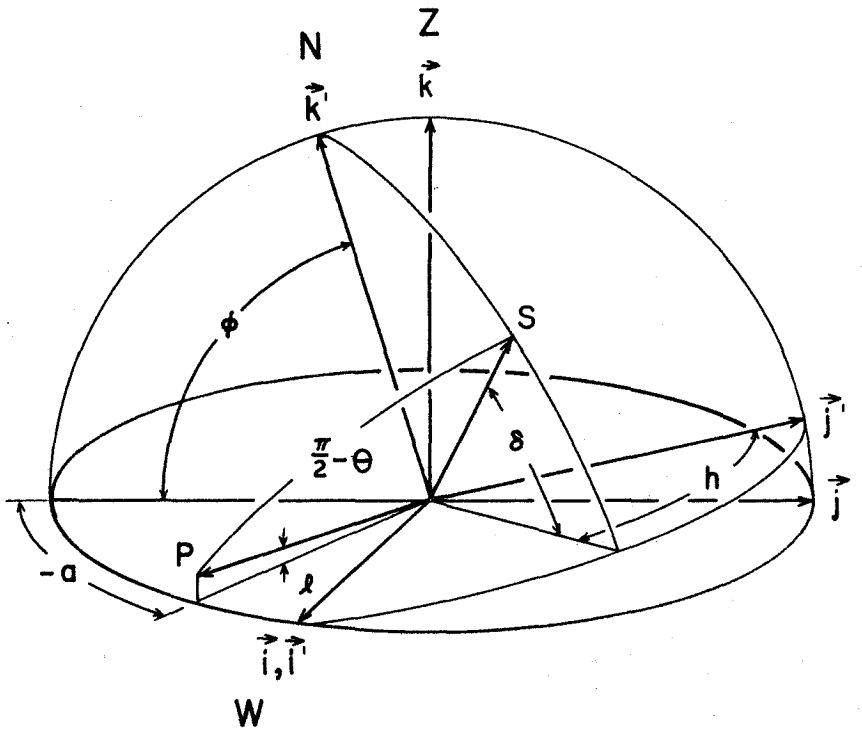

Figure 1. The geometry of the interferometer

at hour angle h and declination δ. Point P is the interferometer pole, i.e. the intersection of the projected baseline with the unit sphere, and is defined by the azimuth a and elevation ℓ of the baseline.

Let $\vec{i}$, $\vec{j}$, and $\vec{k}$ be the unit vectors of a Cartesian system with $\vec{k}$ pointing towards the local zenith and $\vec{i}$ and $\vec{j}$ in the local horizontal plane. Another system $\vec{i}'$, $\vec{j}'$, and $\vec{k}'$ is rotated by the complement of the latitude ϕ, so that $\vec{k}'$ points at the north celestial pole. The unit vector along the baseline is

$$\vec{e}_P = -\vec{i}\cos\ell\sin a - \vec{j}\cos\ell\cos a + \vec{k}\sin\ell \quad , \tag{2}$$

while that in the direction of the source is

$$\vec{e}_S = \vec{i}'\cos\delta\sin h + \vec{j}'\cos\delta\cos h + \vec{k}'\sin\delta \quad . \tag{3}$$

But we may express $\vec{i}'$, $\vec{j}'$ and $\vec{k}'$ as

$$\begin{aligned} \vec{i}' &= \vec{i} \\ \vec{j}' &= \vec{j}\sin\phi + \vec{k}\cos\phi \\ \vec{k}' &= -\vec{j}\cos\phi + \vec{k}\sin\phi \quad . \end{aligned} \tag{4}$$

Then $\vec{e}_S$ becomes

$$\begin{aligned} \vec{e}_S = {} & \vec{i}\cos\delta\sin h + \vec{j}(\sin\phi\cos\delta\cos h - \cos\phi\sin\delta) \\ & + \vec{k}(\cos\phi\cos\delta\cos h + \sin\phi\sin\delta) \quad , \end{aligned} \tag{5}$$

and $\vec{e}_P\cdot\vec{e}_S = \cos(\frac{\pi}{2} - \theta) = \sin\theta$ may be written as

$$\begin{aligned}\sin\theta = &- \cos\ell \sin a \cos\delta \sin h \\ &- \cos\ell \cos a (\sin\phi \cos\delta \cos h - \cos\phi \sin\delta) \\ &+ \sin\ell (\cos\phi \cos\delta \cos h + \sin\phi \sin\delta) ,\end{aligned} \tag{6}$$

or

$$\begin{aligned}\sin\theta = &(\cos\ell \cos a \cos\phi + \sin\ell \sin\phi) \sin\delta \\ &-(\sin a \sin h + \cos a \sin\phi \cos h) \cos\ell \cos\delta \\ &+ \sin\ell \cos\phi \cos\delta .\end{aligned} \tag{7}$$

If the baseline is level, then $\ell = 0$, and this expression simplifies to

$$\begin{aligned}\sin\theta = &\cos a \cos\phi \sin\delta \\ &- (\sin a \sin h + \cos a \sin\phi \cos h) \cos\delta .\end{aligned} \tag{8}$$

In two important special cases, the expression for $\sin\theta$ may be simplified still further. These are the cases of an east-west baseline, for which $a = 270^\circ$, $\ell = 0^\circ$, and

$$\sin\theta_{EW} = \sin h \cos\delta \tag{9a}$$

and the case of a north-south baseline, for which $a = 0^\circ$, $\ell = 0^\circ$, and

$$\sin\theta_{NS} = \cos\phi \sin\delta - \sin\phi \cos\delta \cos h . \tag{9b}$$

In order to interpret interferometric observations it is necessary to know the orientation of the interference fringes with respect to the source being studied, i.e. with respect to the grid of celestial coordinates in the neighborhood of the source. The fringes follow lines of constant

$\sin\theta$, and hence are normal to the gradient of $\sin\theta$, as is seen in figure 2. If ρ is the angle between this gradient and the direction of increasing hour angle, then ρ satisfies the relation

$$(10) \qquad \tan\rho = \frac{(\nabla \sin\theta)_\delta}{(\nabla \sin\theta)_h} = \frac{\frac{\partial(\sin\theta)}{\partial\delta}}{\frac{1}{\cos\delta}\frac{\partial(\sin\theta)}{\partial h}}$$

The partial derivatives of $\sin\theta$ may be obtained from equation 7 or equation 8, if the latter is applicable. For the two special cases mentioned above we have

$$(11a) \qquad \tan\rho_{EW} = -\sin\delta \tan h$$

$$(11b) \qquad \tan\rho_{NS} = \cot\phi \cos\delta \csc h + \sin\delta \cot h \quad .$$

The orientation of the fringes will frequently be specified by their position angle, which is defined as the angle between a fringe crest and an hour circle, modulo 180°. Position angles are conventionally taken as zero at the north and as increasing toward the east. From figure 2 it can be seen that the position angle of the fringes is just ρ.

Returning to figure 1, it can be seen that the gradient of $\sin\theta$ must point along the great circle from the source S to the interferometer pole P. Therefore, if the baseline were projected onto a plane normal to the source direction, i.e. normal to $\vec{e}_S$ of equation 3, it would lie parallel to $\vec{\nabla}\sin\theta$. The unit sphere is also

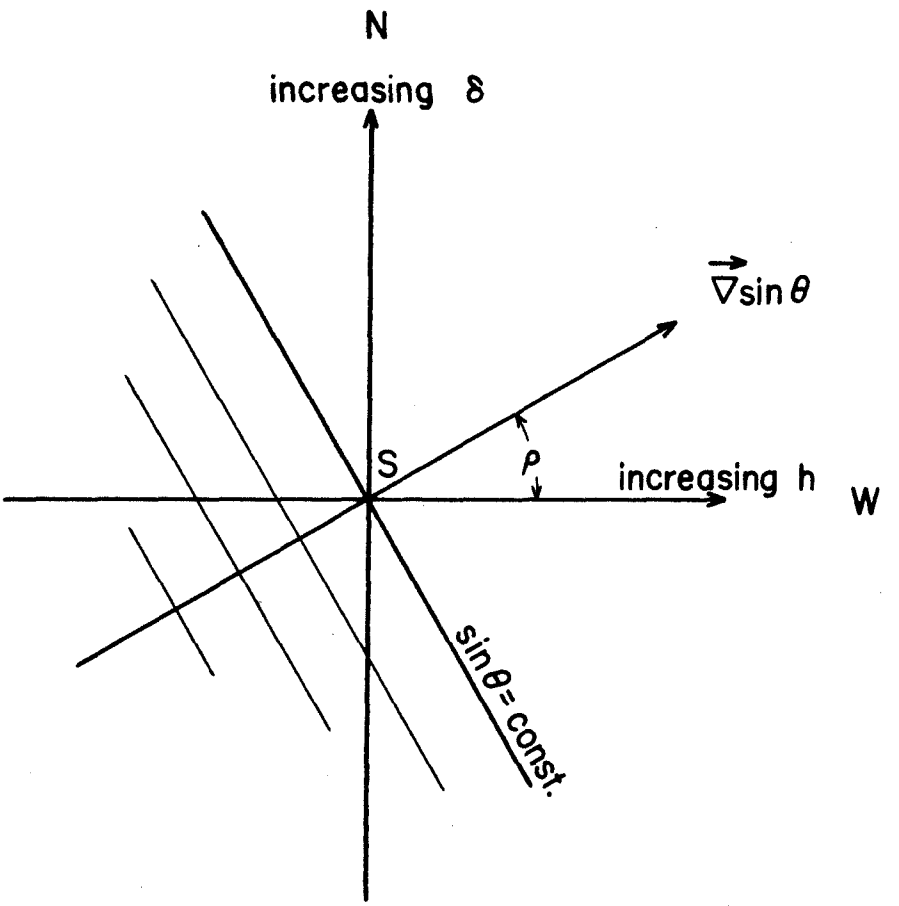

Figure 2. The sky in the neighborhood of the source, S. The lines of constant $\sin\theta$ are the crests of successive fringes, and the orientation of the fringes is defined by the angle ρ.

normal to $\vec{e}_S$ at S , so the projection of the baseline onto this sphere will lie along $\vec{\nabla}\sin\theta$. The position angle of the projected baseline is thus $90^\circ + \rho$. The projection of the baseline onto the unit sphere in the direction of the source can be called the effective baseline. If the length of the baseline is s wavelengths, that of the effective baseline is $s \cos\theta$.

Brightness Distributions and the Visibility Function

Now that the necessary geometric relationships have been established, we can show how the brightness distribution of a radio source may be investigated with a two element interferometer. A source is located by the right ascension α_o and the declination δ_o , at a specified epoch, of the centroid of its emission*, and it is described in detail by the brightness temperature distribution $T(\alpha-\alpha_o,\delta-\delta_o)$ of that emission. The right ascension and the hour angle are associated by the relation $\alpha = \Omega t - h$, where t is the sidereal time and Ω is the rate of rotation of the Earth. In the neighborhood of a small source the α,δ coordinate system will closely approximate a Cartesian grid, and it will simplify the analysis to make this approximation.

---

*The position of the centroid of the emission may, in some cases, be a function of the wavelength of observation.

Consider a Cartesian coordinate frame x,y fixed in a small region of the sky centered at right ascension α_o and declination δ_o, such that x increases toward the west along a circle of declination and y increases toward the north along an hour circle. Provided δ_o is not too close to 90^o, the x,y grid will correspond to the grid of celestial coordinates. The units of x and y are radians, and the transformation is

$$(12) \qquad \begin{aligned} x &= -(\alpha - \alpha_o) \cos \delta_o \\ y &= (\delta - \delta_o) \end{aligned} \qquad \text{for } x,y \ll 1 \quad .$$

Using the relation $\alpha = \Omega t - h$, x can be expressed in terms of t and h. Provided the chosen region of the sky is not too near the interferometer pole, the interferometer coordinates θ and ψ will also form a good approximation to a Cartesian system, rotated locally with respect to the x,y system by the angle ρ. In the x,y system the response pattern of equation 1 then becomes

$$(13) \quad R(x,y) = G\, A(x,y) \cos\left[2\pi\left[s_x(x + \Omega t) + s_y y\right] + \Psi\right] \quad ,$$

where s_x and s_y are the projections of the baseline onto the x and y axes, i.e. the x and y components of the effective baseline.

$$(14) \qquad \begin{aligned} s_x &= s \cos \theta_o \cos \rho_o \\ s_y &= s \cos \theta_o \sin \rho_o \end{aligned} \quad .$$

The relationships among the coordinate systems are illustrated in figure 3.

We now wish to describe the response of the interferometer to a discrete radio source passing through its sensitivity pattern. Let the source be described by its brightness temperature distribution $T(x,y)$. This is generally a function of the wavelength of observation λ . The integral of $T(x,y)$ over the source is related to S , the flux density of the radiation from the source, by the Rayleigh-Jeans approximation to the Planck radiation law.*

$$S = \frac{2k}{\lambda^2} \iint T(x,y)\, dx\, dy \quad . \tag{15}$$

The response of the interferometer to such a source will be given by the result of integrating equation 13 over the source distribution.

$$\begin{aligned} R(t) &= \frac{2k}{\lambda^2} G \iint A(x,y)T(x,y) \cos\left[2\pi\left[s_x(x+\Omega t)+s_y y\right]+\Psi\right] dx\, dy \\ &= \frac{2k}{\lambda^2} G \left[\begin{array}{l} \cos(2\pi s_x \Omega t + \Psi) \\ \quad \iint A(x,y)T(x,y) \cos 2\pi(s_x x+s_y y)\, dx\, dy \\ -\sin(2\pi s_x \Omega t + \Psi) \\ \quad \iint A(x,y)T(x,y) \sin 2\pi(s_x x+s_y y)\, dx\, dy \end{array}\right] . \end{aligned} \tag{16}$$

Here we have assumed that the paraboloids track the source at the sidereal rate so that $A(x,y)T(x,y)$ is not a function of t . We make the following definitions:

---

*The units of S are watts $m^{-2}(c/s)^{-1}$, and the compact expression $S\, d\nu = 2kT/(\lambda^2)\, d\nu$ is used rather than the homogeneous form $S\, d\nu = 2\nu^2 kT/(c^2)\, d\nu$.

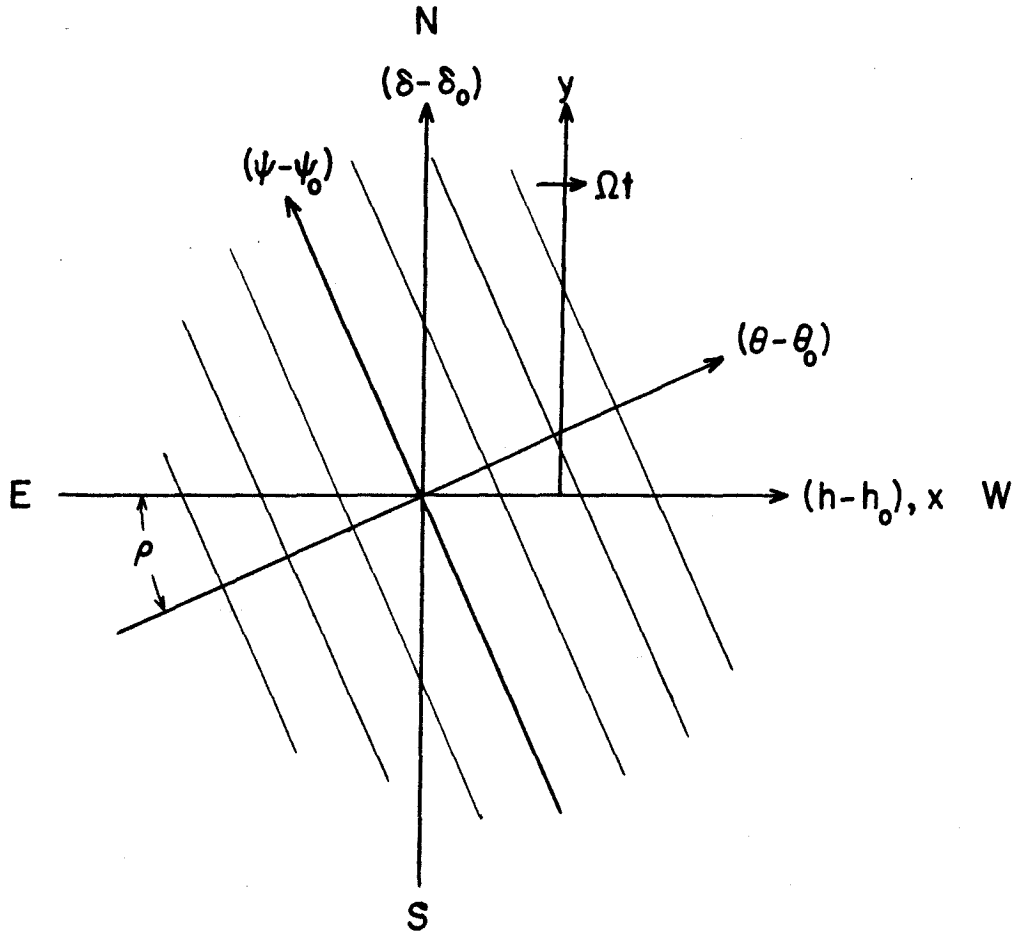

Figure 3. The x,y , h,δ , and θ,ψ coordinate systems projected on the sky near the point h_o,δ_o . The faint lines of constant θ are the crests of successive fringes.

$$A(x,y)\ T(x,y) = A\ T'(x,y)$$

(17) $$A = A(0,0)$$

$$S' = \frac{2k}{\lambda^2}\iint \frac{A(x,y)}{A}\ T(x,y)\ dx\ dy \quad .$$

Then it can be shown that equation 16 can be written as

(18) $$R(t) = G\ A\ S'\ V(s_x,s_y)\ \cos\left[2\pi s_x \Omega t + \Phi(s_x,s_y) + \Psi\right] \quad ,$$

where V and Φ define the complex visibility function ν and are given by

(19) $$\nu(s_x,s_y) = Ve^{i\Phi} = \frac{\iint T'(x,y)\ e^{i2\pi(s_x x + s_y y)} dx\ dy}{\iint T'(x,y)\ dx\ dy}$$

The identity of equations 16 and 18 is evident if the sines and cosines are expressed in exponential form and coefficients of like terms are collected. It is seen that the visibility function is the complex, two-dimensional Fourier transform of T', normalized to approach unity as s_x and s_y approach zero. Examples of visibility functions calculated for various models are given in the Appendix.

The procedure for measuring $T(x,y)$ with a two element interferometer is one of measuring R, and hence V and Φ, at a sufficient number of values of s_x and s_y to determine the transform $\nu(s_x,s_y)$. The brightness temperature distribution can then be recovered by Fourier inversion of the visibility function. Inversion of ν as defined above will actually produce T', the source distribution as

modified by multiplication with $A(x,y)$, the antenna power pattern. For most discrete sources, $T(x,y)$ will be appreciably different from zero only within a region where $A(x,y) \approx A(0,0)$, in which case $T(x,y) \approx T'(x,y)$ and $S \approx S'$. If this is not the case, $T(x,y)$ can be recovered from $T'(x,y)$ by dividing by $A(x,y)/A(0,0)$. If the source extends to regions where this ratio is very small, this procedure will introduce appreciable errors. Such a source can, in principle, be studied by letting it drift through the primary antenna pattern at different declinations, making ν a function of α_o and δ_o as well as s_x , s_y and $T(x,y)$. The required generalization of equations 16-19 is evident, but the method would be very cumbersome in practice. A two element interferometer of the type we are considering can be used efficiently only for studies of sources which are compact with respect to the primary antenna pattern.

There remains the question of choosing suitable values of s_x and s_y for a given source. These depend on the overall extent of the source. Suppose the following condition holds:

(20) $$T(x,y) = 0 \quad \text{for } |x| > X \text{ or } |y| > Y \quad .$$

Then Bracewell (8) has demonstrated that T is uniquely determined by the values of ν at a lattice of points s_x and s_y such that

(21) $$s_x = \frac{m}{2X} \quad , \qquad s_y = \frac{n}{2Y} \quad ,$$

where m and n are integers. Since $\nu(-s_x,-s_y) = \nu^*(s_x,s_y)$, observations need not be taken for negative values of one of the indices. Multiples of any spacings smaller than $1/(2X)$ and $1/(2Y)$ can be used, but the values of ν so obtained contain some redundancy. It is the experience of the writer that a redundancy factor in the observations of three or four is often welcome, particularly when the total number of points at which ν is measured is small.

Practical Limitations

The recovery of the source brightness distribution from its measured transform would be correct in every detail if error-free measurements could be made over the whole range of spacings for which V is greater than zero. This is, of course, not possible. The measured visibility function contains errors due to receiver noise, gain, and phase fluctuations. Furthermore the range of available spacings is limited, and in many cases the visibility is still appreciable at the largest available spacing. We know that the effect of this limited aperture should be a limited resolution, a smoothing out of fine details in the recovered brightness distribution.

In order to describe this smoothing we introduce an aperture function $K(s_x,s_y)$, representing the cutoff of

the observations at large spacings. For instance, a hypothetical case might be

$$(22) \qquad K(s_x,s_y) = \begin{cases} 1 & \text{when } s_x^2 + s_y^2 \leq s^2 \\ 0 & \text{when } s_x^2 + s_y^2 > s^2 \end{cases} .$$

If we neglect, for the moment, the errors in the measured values of the visibility function, then the available observational data are $K(s_x,s_y)\,\nu(s_x,s_y)$. Let the recovered source distribution, which is the Fourier inversion of this product, be denoted by $T_1(x,y)$, and let $\overline{K}(x,y)$ represent the inversion of $K(s_x,s_y)$. Then by a well-known theorem of Fourier analysis (see, for example, Sneddon (13)), T_1 is equal to the convolution of T and $\overline{K}$,

$$(23) \qquad T_1(x,y) = \overline{K}(x,y) * T(x,y) \quad .$$

Thus $\overline{K}$ describes the smoothing effect of the finite aperture. For the hypothetical K of equation 22, the transform is

$$(24) \qquad \overline{K}(x,y) \propto \frac{J_1(2\pi s\sqrt{x^2+y^2})}{\pi s\sqrt{x^2+y^2}} \quad .$$

This transform has been worked out in detail in connection with the visibility function of a uniform disk source, and a graph of it is given in the Appendix.

The solution obtained for T_1 when K , the aperture function, is unity out to the limiting values of the spacings and zero thereafter is known as the <u>principal solution</u> for the aperture (14). In many cases the principal

solution will not be a good approximation to the real source distribution $T(x,y)$. For instance, if a point source were studied with an interferometer having the aperture function of equation 22, the recovered distribution $T_1(x,y)$ would be just the transform given in equation 24, since $T(x,y)$ for a point source is a δ function. The function of equation 24 is graphed in figure 21 , and it can be seen that it has the expected broad central peak due to the smoothing-out of the point source, but it also has a number of secondary responses, the first of which is negative with an amplitude of about 0.12 of the main response.

Unwanted secondary responses can be reduced by tapering the value of the aperture function $K(s_x,s_y)$ from unity at small spacings to zero or nearly zero at the spacings where the observations are cut off. This procedure yields a brightness distribution $T_1(x,y)$ which is less confused by spurious responses, but from which some real detail has been lost. If desired, the analysis may be repeated with different tapers and the results compared. A discussion of suitable tapering functions and their transforms has been given in connection with crystallographic problems by Waser and Schomaker (15). Discussions of the problem with specific reference to radio astronomy have been given by Covington and Harvey (16) and by Bracewell and Roberts (14).

Errors in either the amplitude or the phase of the

measured visibility function are passed on as errors in the recovered brightness distribution. If the errors in the visibility function take the form of an added random "noise", then the transform of this noise will be added to the desired brightness distribution to produce a random error. If the source distribution is a simple one, it may be possible to remove this error by a smoothing operation. In this process, faint details of the source distribution may be smoothed away along with the noise. The exact treatment will depend very much on the particular situation, and no concise, general prescription for dealing with such errors seems possible.

With a suitable choice of aperture function K, the variable spacing interferometer can be made to simulate a large single antenna having the same overall aperture. This means that the recovered brightness distribution $T_1(x,y)$ would be identical to the response of a radiometer using the large antenna and studying the same source. The requirement is that $\overline{K}(x,y)$ should equal $A(x,y)$, the power sensitivity pattern of the large antenna. This equivalence has been pointed out by Ryle, who calls the method that of aperture synthesis (17). Bracewell has described another very general method for interpreting the response patterns of this and various other interferometer configurations (8).

The One-Dimensional Case

The complete two-dimensional analysis of a small source has never been done with a two element interferometer of the type we are considering; nor has it in the present investigation. A complete analysis of a discrete source requires measurement of the complex visibility function at all the lattice points given by equation 21, namely $s_x = m/(2X)$, $s_y = n/(2Y)$. If the indices go from $-M$ to M and 0 to N , respectively, this means $M(2N+1)+N$ observations, or a total of 220 for $M = N = 10$. This gives a ten-line scan through the source, to borrow a term from television usage. On the other hand, but ten observations with a single baseline orientation will give equivalent detail about the distribution of the source in one dimension. We now consider modifications of the previous theory to enable us to describe such one-dimensional observations.

Suppose the orientation of the baseline is such that its projection onto the sky is parallel to the x axis of figure 3. Then the orientation angle ρ is zero, and the components of the effective baseline are

$$s_x = s \cos \theta_o \qquad (25)$$
$$s_y = 0$$

This will be the case for observations at transit ($h = 0$) with an east-west baseline.

Since s_y is zero, equation 19 becomes

$$(26)\quad \nu(s_x,0) = V(s_x,0)\, e^{i\Phi(s_x,0)} = \frac{\iint T'(x,y)\, e^{i2\pi s_x x} dx\, dy}{\iint T'(x,y)\, dx\, dy}$$

Now let us integrate the two-dimensional brightness distribution along the direction of the fringes, or perpendicular to the projection of the baseline on the sky. We call the result the one-dimensional brightness distribution. In the particular case we are considering, we integrate along y and designate the one-dimensional distribution $T(x)$.

$$(27)\quad T(x) = \int T(x,y)\, dy$$

Let $T'(x)$ be the one-dimensional analog of $T'(x,y)$ (see equation 17), and let $\nu(s_x) = \nu(s_x,0)$ be the one-dimensional visibility function. Then we can re-write equation 26 as

$$(28)\quad \nu(s_x) = V(s_x)\, e^{i\Phi(s_x)} = \frac{\int T'(x)\, e^{i2\pi s_x x}\, dx}{\int T'(x)\, dx}$$

The one-dimensional Fourier inversion of $\nu(s_x)$ would clearly produce $T'(x)$. The inversion of a truncated visibility function, known only out to some limiting spacing, would produce a one-dimensional solution $T_1(x)$, in direct analogy to the two-dimensional case. If no tapering were used, $T_1(x)$ would be the principal solution for the source in one dimension. A particular selection of the tapering function will cause the recovered source distribution to be equivalent to the response of a radiometer using a long,

narrow antenna having a length equal to the longest spacing used with the interferometer. In Ryle's terminology, a two element interferometer with a single baseline orientation may be used to synthesize a long, narrow antenna having the same overall aperture. Such an antenna has a fan-shaped sensitivity pattern with high resolution in one dimension only.

Just as we could make a scan across a source with a fan beam oriented in any direction, so we could make a one-dimensional interferometric investigation using observations along a single baseline having an arbitrary orientation with respect to the source. The direction of resolution is the direction in which the baseline is projected onto the source, i.e. the direction given by position angle $90^\circ + \rho$. No information is obtained about the distribution of the source normal to this direction.

It should be noted that two one-dimensional analyses with different orientations do not constitute a full two-dimensional analysis. Thus in figure 4, observations with $\rho = 0^\circ$ and 90° cannot distinguish between two very different source distributions. They can, however, give a limit for the overall size of the source, and this is often very useful.

If a source contains two fairly well-separated centers of emission, measurements of this sort along two different axes allow the positions of the components to be determined.

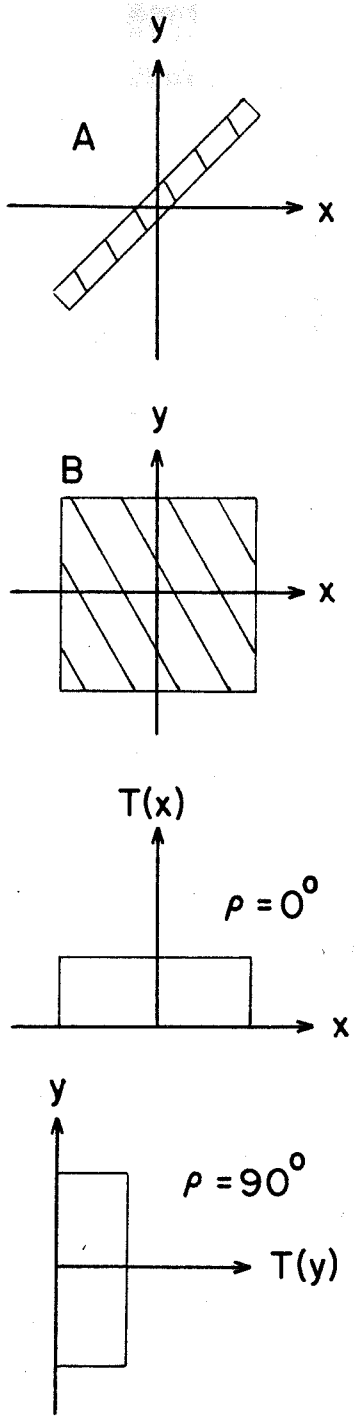

Figure 4. The two sources A and B give the same results for one-dimensional scans using $\rho = 0^{\circ}$ and 90°.

If the two components are identical, measurements along a third axis are required to remove the final ambiguity.

Model Fitting

There is an alternative to the method of Fourier inversion for the interpretation of interferometric data on brightness distributions, namely that of model fitting. The procedure is to calculate exact visibility functions for various physically reasonable source models. Free parameters in a model are then adjusted to make its calculated transform fit the observed portion of the visibility function of the source. If a perfect fit were obtained, the model would then be one possible distribution which could give rise to the observed visibility function.

The actual source distribution could differ from the model, provided that the visibility function of the differences between the source distribution and the model were non-zero only for spacings greater than those where the observations were cut off. Another way of stating this is that the source and the model have the same principal solutions, but they may differ by the addition or subtraction of high-frequency Fourier components to which the interferometer is not sensitive. Bracewell and Roberts (14) discuss this method in detail and give examples of source distributions having the same principal solution.

The advantage of this method is that it eliminates the problem of the spurious responses in the principal solution

and results in a recovered source distribution that is ab initio physically reasonable. The possible differences between the source and the model should always be kept in mind, however. The only thing the observation proves is that the source and the model have the same principal solutions within the limits of observational error.

The method of model fitting is particularly useful in the one-dimensional case, where the visibility function depends only on a single experimental variable, the spacing along one baseline. In this case it is often possible to fit the observed portion of the visibility function with the calculated transform of a very simple model such as a circular Gaussian "mound" of brightness or a uniformly bright disk. One-dimensional visibility functions have been calculated for these and also for some two-Gaussian models. The calculations and graphs of the results are given in the Appendix.

The Limiting Case

It is of interest to consider the behavior of the visibility function in the region where the source is beginning to be resolved. Consider the one-dimensional case.

$$(29) \qquad \nu(s_x) = V(s_x)e^{i\Phi(s_x)} = \frac{\int T(x)\ e^{i2\pi s_x x}\ dx}{\int T(x)\ dx}$$

For small values of s_x we may expand the exponential and retain only the leading terms,

$$V(s_x)e^{i\Phi(s_x)} = \frac{\int T(x)\left[1 + i2\pi s_x x - 2(\pi s_x x)^2 + i\frac{4}{3}(\pi s_x x)^3 + \ldots\right] dx}{\int T(x)\, dx}$$

$$= 1 - 2(\pi s_x)^2 \frac{\int x^2 T(x)\, dx}{\int T(x)\, dx} \tag{30}$$

$$+ i2\pi s_x \frac{\int xT(x)\, dx}{\int T(x)\, dx} + i\frac{4}{3}(\pi s_x)^3 \frac{\int x^3 T(x)\, dx}{\int T(x)\, dx} + \ldots$$

If the origin is chosen at the centroid of the source, the first moment of the brightness distribution vanishes; hence, the departure of Φ from zero is cubic in s_x, while the departure of V from unity is quadratic and is proportional to the second moment of $T(x)$. If $V(s_x)$ is observed only in the region where it can be represented as

$$V(s_x) = 1 - U\, s_x^2 \quad , \quad \text{where} \quad U = \int x^2 T(x)\, dx \quad , \tag{31}$$

then it is clear that any model having that value of U as its second moment will adequately represent the observations. It is customary to choose a circular Gaussian model for this purpose and to quote the diameter of its half-brightness contour as the "diameter" of such a barely-resolved source.

Review of Previous Work

As was mentioned before, the complete two-dimensional analysis of a discrete source has never been carried out with a two element interferometer of the type we are considering. Most of the existing work has been done with transit interferometers having nominally east-west baselines, thus resol-

ving the source only in the east-west direction, or in position angle 90°. In a few cases measurements have been made along other axes, thus setting limits on the overall size of the source.

The following is a brief review of published data on interferometric investigations of the brightness distributions in discrete radio sources. The work done up to 1957 is reviewed in greater detail by Shklovsky (18).

Systematic studies of the brightness distributions of the strongest sources were begun about 1950 at Manchester, Sydney, and Cambridge, and preliminary results were reported simultaneously (19,20,21). Wavelengths of around two meters were used, and rough estimates were obtained for the diameters of Cas A, Cyg A, Tau A, Vir A, and Cen A. Measurements with other than E-W baselines were made only on the first two of these sources, and showed that Cyg A was highly elongated, while Cas A was nearly circular. Mills (22) extended his work at 3 m on the last four of these sources, using baseline azimuths of 24°, 90°, and 164° and spacings as great as 3400λ. He fitted elliptical Gaussian models to his data on Tau A, Vir A, and Cen A.

Jennison and Das Gupta (23) continued the 2.5 m Manchester observations of Cyg A and Cas A out to spacings of about 5000λ along a baseline with an azimuth of 113°. The Cygnus source was found to consist of two equal centers of emission spaced by 1'.5, having individual diameters of 0'.8.

Observations have been made of more-extended sources by using antenna separations of three wavelengths to a few hundred wavelengths. Baldwin (24) showed that M 31 has a diameter at 3.7 m wavelength of $2^{\circ}.5$ and is almost circular. With Smith (25) he examined the region of the Virgo cluster and found that an extended source was present in addition to the well-known source Vir A; with Dewhirst (26) he studied the emission from IC 443. Brown, Palmer, and Thompson investigated five galactic sources of large diameter (27).

To check the possibility of a dependence of the structure of a source on wavelength, Conway (28) observed Cyg A at 60 cm with E-W spacings to 550λ. He found no differences from the visibility function of Jennison and Das Gupta, but this conclusion has been shown to be in error (29). Rowson (29,30) has observed Cyg A, Cas A, and Tau A at 10.7 cm with E-W spacings to 1750λ; Cyg A and Cas A were also observed with N-S spacings to 3380λ. He found that the separation of the two centers of emission in Cyg A was greater at the shorter wavelength, but that their individual diameters were virtually unchanged.

Biraud, Lequeuex, and Le Roux (31) have investigated the brightness distributions at 21 cm of Cyg A, Sgr A, Vir A, and the supernovae of Tycho and Kepler using E-W spacings to 2080λ. Sgr A and Vir A were both found to contain small diameter, bright components surrounded by more extended regions of lower surface brightness.

A program has been undertaken at Manchester to obtain diameter measurements for radio sources of very small angular extent. In the initial phase of this program, Morris, Palmer, and Thompson (32) reported on five sources, of which three had E-W diameters of $< 12"$. Work has continued on a list of 301 sources, with observations at 1.89 m, using E-W spacings of 310λ, 2200λ, 9700λ, and $32\,000\lambda$. Allen, Palmer, and Rowson (33) have reported on studies of 91 sources observed at the two greatest spacings. Of these, 32 produced a measurable interference pattern, and 8 have diameters of $< 3"$.

All the measurements reported above have been of the visibility amplitude V alone, with no attempt made to recover the phase of the complex visibility function. The effect of neglecting the phase is to symmetrize the recovered brightness distribution, as was first pointed out by Michelson (4). If the source itself is symmetric, then no error is introduced.

A phase sensitive interferometer for meter wavelengths has been described by Jennison (34). With it, he and Latham measured the complex visibility functions of Cyg A and Cas A at 2.36 m, using an E-W baseline with separations of up to 2160λ (35). The two components of Cyg A were found to differ in intensity by 20%, while Cas A was found to have a low intensity spur projecting towards the east from the main body of the source.

Using various elements of the Christiansen solar inter-

ferometer, Twiss, Carter, and Little have observed both the amplitude and the phase of the visibility function for seven strong sources at 21 cm, using E-W and N-S separations to 1800λ. They have reported some preliminary results on Tau A, Cyg A, Cen A, and the Orion Nebula (36). Cen A was found to have two, roughly equal components.

Some information on source diameters has come from the various surveys of radio sources (37,38,39,40,41). This information can at times be misleading, for it is obtained by comparing the amplitude of the visibility function at only two spacings and fitting a simple model to give the same ratio of visibilities. However, one of the results of the current investigation is that few sources are well described by a simple, symmetrical model.

CHAPTER III

Observations and Analysis

The amplitude, and in some cases the phase, of the complex visibility function has been measured for 127 discrete radio sources, using spacings within the range of 126 to 1557 wavelengths along an east-west baseline. The sources were mainly selected from the list of Harris and Roberts (42), which will subsequently be referred to as CTA. Most of the CTA sources were, in turn, selected from the third Cambridge catalog (38), which we designate 3C. Several galactic sources of relatively small diameter were selected from Wilson and Bolton's survey of the galactic plane (43), which we will call CTB. A few additional sources from the 3C catalog or from the first catalog of Mills, Slee, and Hill (44) were added to fill gaps in the observing program. In this chapter we describe the observations and the reduction of the observations to produce the visibility functions for these sources.

All observations were made with the Caltech variable spacing interferometer at the Owens Valley Observatory. The instrument has been described by Read (9,43). Briefly, it consists of two equatorially mounted, 90 ft paraboloids which can be moved along railroad tracks to certain fixed observing stations. The receiver used was a conventional superheterodyne with a crystal mixer and an intermediate frequency preamplifier at the focus of each antenna.

Coherent local oscillator signals were supplied to the mixers from a centrally placed oscillator, using a combination of coaxial and open wire transmission lines. A few observations at the longest spacing made use of klystron oscillators at each antenna, which were phase locked to signals radiated from the central local oscillator. Details of this system are included in Read's thesis (45). The IF signals were multiplied to produce the sensitivity pattern characteristic of the two element interferometer, which is given in equation 1.

The receiver accepted radiation in both the signal and the image bands, each of which was about 5 Mc wide with its center frequency displaced 10 Mc above or below the local oscillator frequency of 958 Mc. All observations thus involve an average over these two bands, which have a total spread of less than 3% of the 958 Mc center frequency. The corresponding center wavelength is 31.3 cm, and all spacings have been calculated in terms of this value.

At the time these observations were made, in the spring of 1960, the available observing stations were at spacings of 200 ft, 400 ft, 800 ft, and 1600 ft east of a central base station. With one antenna at the central station and the other at each of these stations successively, two series of observations were made: a primary series as the sources crossed the local meridian, and a secondary series at various distances east or west of the

meridian. In taking these observations the writer received assistance from D. Morris, V. Radhakrishnan, and D. E. Harris.

Observations at Transit

At each station the apparent intensity and position of a source was measured as the source transited. By comparison with similar measurements made at the other stations, both the amplitude V and the phase Φ of the complex visibility function were determined.

For an observation at transit the hour angle is zero. With an east-west baseline the local meridian lies in the median plane of the interferometer, and the position angle of the fringes is zero. This is confirmed by equations 9a and 11a, which show that with an east-west baseline, when $h = 0$, then $\sin \theta = 0$ and $\tan \rho = 0$. From equation 14 we find that in this case the effective baseline has only one component s_x, and this equals the actual baseline s. The fringe period is $1/s$ in angle or $1/(s \cos \delta)$ in time.

Table 1 summarizes the transit observations and gives the dates of each series. The coverage across the sky was not uniform, since observations were taken only at night at the 200 ft and 400 ft stations*, while one 24 hour-long run was made at 800 ft and again at 1600 ft. Right ascensions

*One 400 ft run was begun in late afternoon, starting at 01^h local sidereal time.

from 19^h to 01^h were not covered at all at 400 ft. The gap from 17^h to 03^h in the 200 ft data has been filled in with data taken from records obtained by Matthews and others as part of a position finding program. These records were made in January-February, June, and October-November of 1960. Of the 127 sources in the brightness distribution program, the 79 lying between right ascensions 03^h and 19^h were particularly well covered.

Table 1

Transit Observations

Station	Spacing λ	Fringe Period seconds time at equator	Fringe Period minutes arc	Dates 1960
200 ft	195	$70^s.6$	$17'.66$	25-29 Feb
400 ft	389	35.3	8.83	30 Mar-4 Apr
800 ft	779	17.7	4.42	28 Apr-2 May
1600 ft	1557	8.83	2.21	15-20 May

To take an observation of a source, the antennas were made to track its position as it approached the meridian. About ten or fifteen fringes of the interference pattern were recorded, centered about the time of transit. Marks were automatically placed on the record at the beginning of each sidereal minute.

The amplitude of the interference pattern was measured from the record, as was the sidereal time of the maximum in

the pattern nearest to the time of transit. The amplitude, corrected for variations in the gain of the receiver and for the attenuation of the output time constant, gave the apparent intensity of the source at the spacing then in use. Six of the strongest sources required an additional correction for the departure of the detector law from linearity. The time of a fringe maximum near transit, corrected for the instrumental phase shift and the delay of the output time constant, gave a measure of the apparent right ascension of the source.

To see how these measurements relate to the visibility function, we refer to the theory of Chapter II. The response of the interferomter to a discrete source is expressed in equation 18. We repeat this equation here, using the one-dimensional modification of equations 26-28:

$$R(t) = GSV(s_x)\cos\left[2\pi s_x \Omega t + \Phi(s_x) + \Psi\right] \quad . \tag{32}$$

Remembering that V and Φ are the amplitude and phase of the complex visibility function, S is the intensity of the source, and that G and Ψ account for gain and phase shifts in the instrument, we can see that the apparent intensity of a source at different spacings is given by $SV(s_x)$, while an apparent displacement in position is given by $\Phi(s_x)/(360^\circ)$ multiplied by the fringe period at that spacing.

As was noted following equation 30, V tends toward

unity at small spacings, while Φ tends toward zero. Thus as the antenna spacing is reduced, the apparent intensity tends toward the true intensity, while the apparent position tends toward the true position of the centroid of the source. For some sources a reasonably accurate extrapolation of the apparent intensity $SV(s_x)$ can be made from the smallest spacing used back to the limit at "zero spacing", which is $SV(0) = S$, the flux from the source. (The terms "flux" and "intensity" will be used interchangeably.) The fluxes for many of the sources observed in the present program have been measured by Harris and Roberts or by Wilson and Bolton and are given in the CTA or CTB lists (42,43). The amplitude of the visibility function $V(s_x)$ is taken to be the observed intensity divided by the best available measure of the total flux from the source.

In principle the true position of the centroid of a source, and hence the normalization of Φ, can also be determined by measurements with a single antenna as in the CTA or CTB surveys. In practice, the positional accuracy obtainable by that method is too poor to be of much use in determining Φ, though the CTA or CTB positions have been used to normalize the phases observed for several of the sources with large diameters. Most of the sources observed have diameters small enough that the phase can be normalized by assuming its value to be zero at the 195λ spacing. Thus

the phase shifts for the longer spacings are given by

$$(33) \qquad \Phi(s_x) = \frac{\alpha(195\lambda) - \alpha(s_x)}{\text{fringe period}} \times 360^\circ \quad .$$

If the right ascension measured at the 195λ spacing should not be that of the centroid, the value of $\Phi(s_x)$ obtained by this method would differ from the correct value by a linear function of s_x, and this possibility can be allowed for in the analysis of the brightness distribution. Matthews (46) has made available the right ascensions, measured at the 195λ spacing, for nearly all the sources observed. The phases of the 195λ records obtained in the brightness distribution program were not reduced.

Calibrations

The receiver gain variations were calibrated by observing, at each spacing, the three sources of very small diameter in the list published by Morris, Palmer, and Thompson (32); namely 3C 147, 3C 196, and 3C 295. These were reported to have diameters of less than 12" if they were uniformly bright, circular sources. The corresponding limit for a circular Gaussian model is < 7". The visibility amplitude for such a source at a spacing of 1557λ would differ from unity by only 1%, which is negligible when compared with other errors present. A fourth source, 3C 123, was used as a secondary standard, and measurements at Jodrell Bank (47) have now shown that its diameter is

only 12", which is still too small to introduce any serious error.

Implicit in this method of calibration is the assumption that these four sources do not have very much greater angular extents at 31 cm wavelength than they do at 2 m. There seems to be no reason to doubt this assumption; indeed, the consistency of the results of the present observations tends to confirm that it is true.

A second assumption basic to the whole method of measurement is that the radiation from the discrete sources is constant in intensity, at least over periods of several months. A slow decrease in intensity has been observed for Cass A, a relatively nearby galactic source, but even this is only about 1% per year (48). Variations in intensity have been reported for only one other source, Hydra A (49,50), and it seems possible that these may have been due to instrumental factors or ionospheric effects.

Returning to the subject of gain calibrations, a complete knowledge of the receiver gain variations could not be obtained from measurements on just the four small sources. However, at a given spacing all sources should have a constant apparent intensity. Among the sources observed were a number which were strong enough to give signal to noise ratios of fifty or more. Variations in the intensities observed for these sources from night to night at a given spacing must have been due to gain variations, since noise

fluctuations for these sources were negligible. By adjusting the gain calibration factor G for each night to give both constant intensities for these sources at a given spacing and constant intensities for the four small sources at all spacings, the uncertainty in gain was reduced. There was a residual uncertainty of between 3% and 7%, depending on the number and consistency of the observations. This uncertainty has been included in the estimate of the error in the final values of the visibility amplitudes, as will be explained in the section on errors.

The phase calibrations were made only after the amplitude calibrations were complete. About half of the sources observed were unresolved, i.e. $V(s_x)$ for these sources differed from unity by less than the error of measurement. These sources were thus expected to show no phase shifts, and all were used as calibrators.

At each spacing the apparent right ascensions, at epoch 1950.0, were computed for all the sources, temporarily assuming the instrumental phase shift Ψ to be zero. Allowance was made for precession, aberration, and nutation, using the Besselian star constants for the sources, as computed by Matthews and Roberts (46). Then the discrepancies, in minutes of arc, between these positions and the positions measured by Matthews with a 195λ baseline were plotted as a function of sidereal time for each night of observation. A smooth curve was drawn as nearly as possible through the points representing the unresolved

sources, which were scattered in a band along the curve. Apparent displacement of an individual source due to a real phase shift was then evident if the point representing this source fell outside this band. The variations in Ψ which had to be calibrated by this method were as great as 200° in the course of a night. The final uncertainty in the measured phase shift was almost entirely due to uncertainty in the placement of the calibration curve. This uncertainty amounted to about $\pm 20^{\circ}$ at 400 ft, $\pm 30^{\circ}$ at 800 ft, and $\pm 40^{\circ}$ to 50° at 1600 ft.

Off-Transit Observations

Since the number of effective spacings available at transit was rather small, a second series of observations was made at each station to take advantage of the foreshortening of the baseline which occurs when a source is observed at large hour angles. We recall that if a source is observed at an angle θ with respect to the median plane of the interferometer, the effective baseline is less than the real baseline by a factor of $\cos \theta$. On any one night, all measurements were made with a constant effective baseline.

In observations off the meridian, the interferometer fringes are rotated with respect to the source by the angle ρ , and ρ is given for an east-west baseline by equation 11a,

(11a) $$\tan \rho_{EW} = - \sin \delta \tan h \quad .$$

By inserting a constant value of θ , say θ_o , in equation 9a, we obtain a relation for the hour angle of observation as a function of declination,

$$\sin h = \frac{\sin \theta_o}{\cos \delta} \tag{34}$$

These two equations may be combined to give an expression for ρ as a function of δ and θ_o ,

$$\tan \rho = \frac{- \sin \delta \sin \theta_o}{\sqrt{\cos^2 \delta - \sin^2 \theta_o}} \quad . \tag{35}$$

An alternative, somewhat simpler form is

$$\sin \rho = - \tan \delta \tan \theta_o \quad . \tag{36}$$

We note that for sources near the celestial equator, ρ is small. Thus the off-transit observations for such sources could be used to supplement the transit observations, for which ρ is zero. For sources with large positive or negative declinations, ρ becomes large and has opposite signs on opposite sides of the meridian. For such sources, several observations with the same value of ρ but different effective antenna spacings (i.e. taken at the same hour angle, but at different stations) could give a one-dimensional analysis of the source with resolution along an axis in position angle $90^o + \rho$. The transit observations, of course, resolve the source in PA 90^o.

For a fixed effective spacing, equation 34 gives the variation of hour angle with declination. We see that near

the equator, h is just equal to θ_o, but that h increases at large positive or negative declinations. Because the antennas are limited in coverage by their construction and by the surrounding terrain to $\pm 4^h$ at most declinations, narrowing below $\delta = -20^o$ to a limit of $\pm 1^h$ near the southern horizon, not all sources can be observed at a given effective spacing.

At the 1600 ft and 800 ft stations, observations were made with values of $\cos \theta_o$ of 5/8, 3/4, and 7/8. At the 400 ft station, observations were made with $\cos \theta_o = 3/4$. At the 200 ft station, a rather limited series of observations was made with values of $\cos \theta_o$ of 0.646 and 0.867. These observations were grouped with the 5/8 and 7/8 measurements for purposes of analysis. A short series of observations was also taken at 1600 ft with a value of $\cos \theta_o$ of 0.788. In each group, measurements were made both east and west of the meridian in order to obtain the two possible values of the rotation ρ.

Table 2 gives the particulars of the off-transit observations, while table 3 gives, for the three principal values of $\cos \theta_o$, the declination limits imposed by the restricted hour angle coverage. For all off-transit observations the path lengths traversed by the signals from the two antennas were equalized by adding cable with an electrical length of $s \cos \theta_o$ to the IF lead coming from whichever antenna was nearer to the source. The effects of

unequal path lengths for the two signals are discussed by Read (9).

Table 2

Off-Transit Observations

Station	cos θ_o	Effective Spacing λ	Dates 1960	No. of Nights E	No. of Nights W
200 ft	0.646	126	2-4 Mar	1	1
	0.867	169	29 Feb-2 Mar	1 1/2	1/2
400 ft	0.750	292	4-9 Apr	2	2
800 ft	0.625	487	7-9 May	1	1
	0.750	584	2-5 May	1	2
	0.875	681	5-7 May	1	1
1600 ft	0.625	973	24,27-29 May	2	1
	0.750	1168	19-24 May	2	2
	0.788	1226	29 May	1/2	1/2
	0.875	1363	25-27 May	1	1

Table 3

Declination Limits

cos θ_o	δ
0.625	-38° to $+55^\circ$
0.750	-32 to +40
0.875	-25 to +25

The amplitudes of the off-transit records were analyzed in the same way as those of the transit records,

using the same four small sources as calibrators. A possibility which was considered is that one or more of these sources might be appreciably extended in the north-south direction. Such an extension would become apparent for observations with large values of ρ. Subsequent measurements by Maltby with a north-south baseline have shown that this is not the case for the three primary calibrators (51). Maltby does find a diameter of 0.'5 for 3C 123, but this is too small to have been of consequence in the observations reported here.

For measurements with $\cos \theta_o = 5/8$, none of the four calibrators were within the declination limits. The calibrators for these measurements were two moderately strong, small sources near the equator, 3C 161 and 3C 273. These sources were only slightly resolved with the 1557λ east-west spacing, so it was felt safe to interpolate the transit observations to obtain intensities for them at 126λ, 487λ, and 973λ effective spacing.

No attempt was made to recover the phases in the off-transit observations. While this would have been possible in principle, it was not thought to be worthwhile in this particular instance. The declination of a source would enter strongly into the recovery of phase information off transit, and for most sources the declination is not yet well enough known to permit this. The phases at the 1200 ft effective spacing would have been very useful in

order to fill in the large gap in the phase information between 800 ft and 1600 ft at transit. However, a fringe following scheme (45) was used with the klystron oscillators during the 1200 ft measurements, and information about the phase of the visibility function at this spacing was lost completely.

Errors

Receiver noise and instabilities in gain and phase shift were the principal sources of error in the measurement of the visibility functions. The method of calibrating the receiver gain variations has been described above. This method was most successful for the transit observations, where there were usually four sets of comparable data at a given spacing. The rms error Δ in the gain calibration factor was estimated on the basis of the consistency of all the data taken at one spacing. The estimate of this error varied from 0.03 for the best sets of transit runs to about 0.10 for some of the off-transit runs in which observations were made on only a single night.

While the uncertainty in the gain calibration dominated the error for the stronger sources, noise fluctuations became important for the weaker ones. The receiver noise fluctuations were equivalent in amplitude to the interference pattern of a source with an apparent intensity of between 0.4 and 0.8 x 10^{-26} wm^{-2}(c/s)$^{-1}$, while the faintest source included in the program had a flux of 1.2 x 10^{-26}.

The effect of noise was to produce a scatter in the apparent intensities of a weak source as observed with the same antenna spacing on successive nights. The variance σ^2 of this scatter, defined by

$$\sigma^2 = \sum_{i=1}^{n} \frac{\left[V_i(s_x) - \langle V(s_x) \rangle\right]^2}{n - 1} \quad , \tag{37}$$

was combined with the estimated mean-square gain uncertainty Δ^2 to give the final error in the visibility amplitude at that spacing:

$$\text{rms error in } \langle V(s_x) \rangle = \left[\sigma^2 + \Delta^2 \langle V(s_x) \rangle^2\right]^{\frac{1}{2}} \quad . \tag{38}$$

This method of combining the two errors was chosen because the two sources of error were more or less unrelated and both errors were unlikely to be at a maximum at the same time. In the cases where only one observation was available, σ^2 was replaced by the square of a maximum reading error estimated from the noise on the record involved.

Explicit amplitude errors were calculated by this method for all the observations at transit and for the observations with the 1200 ft effective spacing. They are given with the amplitudes in tables 4 and 7 in the next chapter. Errors were not calculated for the other off-transit observations, but they may be estimated using the following formula:

$$(39) \qquad \text{rms error in } V = \left[(0.6/S)^2 + 0.01\ V^2\right]^{\frac{1}{2}} \quad ,$$

where S is the flux for the source in units of 10^{-26} $wm^{-2}(c/s)^{-1}$ as given in table 4. Equation 39 is seen to be equivalent to equation 38 if we assume a value of 0.1 for Δ and a mean intensity error due to noise of 0.6×10^{-26}.

The errors in the phase of the visibility function were treated in the same way as the errors in amplitude. For all but the very weakest sources, these errors were dominated by the uncertainty in the calibration of the instrumental phase shift, as was noted on page 41. Explicit errors were calculated for all phase observations and are included in table 5.

The principal weakness of these observations was the amount of subjectivity involved in the gain and phase-shift calibrations. Uncertainties in these calibrations were the most serious sources of error. After these observations were taken, the receiver was redesigned to reduce the instabilities responsible for these errors. Stabilization of the receiver is made difficult by the large daily range of temperature in the Owens Valley, which may be as great as 40°C.

Errors due to confusion set a lower intensity limit on any investigation of discrete sources. As we shall see, the effects of confusion on the present work were small, but they would become quite important in a study of fainter

sources than those included in the present program.

We may estimate the effect of confusion by calculating the flux level at which we might expect to find one source per primary beam area, in this case per 0.5 square degree. A recent Cambridge survey at 1.7 m (52) has found a density of one source per 30 square degrees having a flux of $7.5 \times 10^{-26} wm^{-2}(c/s)^{-1}$ or more. This intensity would correspond to about 2.2×10^{-26} at 31.3 cm, assuming a spectral index* of -0.7. The density of sources for other flux limits will vary approximately as the inverse square of the flux, so we may say that at 31.3 cm there is about one source per 0.5 square degree with a flux of 0.3×10^{-26} or greater. The faintest source in the present program had a flux of 1.2×10^{-26}, but there were only nine sources with fluxes of less than 3×10^{-26}. Thus for only the nine faintest sources should the error due to confusion be much greater than 0.10 in the visibility amplitude or 0.10 radian, about 6^{o}, in the phase. The amplitude error due to confusion is about equal to that due to receiver noise. The nine sources which may have been seriously affected by confusion are the following: 3C 28, 3C 46, 3C 135, 3C 191, 3C 243, MSH 19-16, 3C 413, and 3C 469.

---

*The wavelength dependence of the flux from a source can usually be approximated by a power law, $S \propto \lambda^{-x} \propto \nu^{x}$. The exponent x is called the spectral index and for most sources is approximately -0.7, as was demonstrated in CTA.

Two other possible sources of error should be mentioned. If the antennas were not pointed at the source, the apparent intensity would, of course, be reduced. Provided the same erroneous position were used for all observations of a source, and provided the real position of the source were still within the primary antenna beam, the relative visibility amplitudes observed would still be nearly correct, but the flux obtained from them would be too low. Every effort was made to point the antennas at the best available position for each source. These positions were supplied by Matthews (46) and were precessed to the date of observation. In the few cases in which a better position has become available since the observations were made (usually the result of adding a lobe shift to a 3C right ascension), the source intensity has been corrected for this effect. It is believed that there were few pointing errors in individual observations. The only very likely ways to mis-set an antenna position all result in the absence of any interference pattern. About two questionable records have been discarded (out of a total of over 1600); in these there was some evidence for such a gross pointing error.

Finally, we note that there was a very large amount of bookkeeping involved in taking and analyzing the observations. Every reasonable precaution has been taken to prevent or detect clerical errors, but a few may remain.

CHAPTER IV

Visibility Functions

Data are presented in this chapter on the visibility functions of the 127 sources observed. All the data are given in tables 4-9, while the visibility amplitudes for 51 sources are plotted in figures 5-17. These latter sources have been chosen because their visibility functions are reasonably complete and show interesting features. Generally this means that these sources have major structural details with characteristic sizes between 1'.5 and 15'.

Table 4 includes all the sources, and in it are given the visibility amplitudes, as observed at the four transit spacings, and the source intensities. For sources included in the CTA or CTB lists, a visibility amplitude at "zero spacing" is also given. This zero spacing amplitude is equal to the CTA or CTB flux divided by the flux of table 4. In most cases this ratio is unity, within the error of measurement, but there are some exceptions. In a case where this ratio is larger than unity, the source may possibly have a broad emission feature which was completely resolved by the interferometer at the smallest spacing available.

The fluxes have been determined by comparison of the east-west interferometer data, the CTA and CTB data, and

the north-south interferometer data obtained by Maltby. The comparison was made by Maltby and the writer, and the results are believed to be the best available estimates of the fluxes from these sources at 31.3 cm. All fluxes are based on an assumed value for the total flux from M 87, at 31.3 cm, of $300 \times 10^{-26} w\, m^{-2} (c/s)^{-1}$, which is the same value assumed in preparing the CTA and CTB lists. A recent re-evaluation by Wilson (53) of the published data on absolute flux measurements suggests that this assumed value is 3% ± 1.5% high. In the few cases where this change would be significant, the fluxes in table 4 may be scaled accordingly. Since the correction is small and still somewhat uncertain, it was not thought worthwhile to revise table 4.

The fluxes have been corrected for atmospheric extinction and are the values which would be observed if no atmosphere were present.* A value of 0.00763 was assumed for the 31.3 cm sea-level extinction at the zenith.

For a source with a large diameter, the apparent intensities observed with the interferometer cannot be extrapolated back to zero spacing to give the total flux. For such sources, the CTA or CTB flux, corrected for extinction, has been adopted, and these are indicated by a flux value enclosed in parentheses. Wilson has provided improved estimates of the fluxes for several of the CTB

---

*For a discussion of extinction corrections, see Broten and Medd (54).

sources (53). Some sources were large enough to be partially resolved by the primary antenna beam. For these sources the peak apparent intensity from CTA or CTB is tabulated, and these fluxes are marked with a dagger. Three sources for which fluxes are given in table 4, 3C 17, 3C 28, and 3C 41, were observed only off transit. All fluxes are given in units of $10^{-26} wm^{-2}(c/s)^{-1}$.

A source marked with an asterisk is one for which the visibility amplitude is plotted in figures 5-17. A visibility amplitude based on only one observation is marked with a colon. The sources are identified either with familiar names of long standing*, or by their numbers in the 3C, CTA, or CTB surveys or in the first survey of Mills, Slee, and Hill (44). "Coma A" is the source so designated in the Jodrell Bank survey of the region containing the Coma cluster of galaxies (56).

Table 5 gives the visibility phases for the transit observations. Unless otherwise noted, they are normalized to Matthews' 195λ positions in the way indicated by equation 32. As was stated in Chapter III, about half the sources observed were virtually unresolved at the longest available spacing. These sources would be expected to have no appreciable phase shift, and the method of calibration assumed that this was so. In table 5 are listed only those sources for which the phase was measured and found to

---

*See, for example, the IAU list (55).

be significantly different from zero at one or more spacings. Phases were measured for all source-spacing combinations for which an amplitude (not an upper limit) is entered in table 4, except for the following: 3C 40, 3C 58, and 3C 66 at 389λ; CTA 26 at 1557λ; 3C 280 at 779λ; 3C 298 at 1557λ; 3C 380 at 779λ; and MSH 19-16, CTB 87, CTA 97, and 3C 469 at all spacings.

The convention as to the sign of the phase is given by the definitions in Chapter II. A positive phase shift corresponds to an apparent displacement of the source toward the west. This is consistent with the definition of Jennison and Latham (35), but contrary to that adopted by Twiss, Carter, and Little (36). Again in table 5, a colon denotes a value based on a single observation.

In tables 6-9 are listed the visibility amplitudes measured in the off-transit observations. In these tables the absolute value of the rotation angle ρ is given for each source. The direction of resolution, i.e. the direction of the baseline when projected against the sky, is given by the following position angles:

$$(40)\qquad \begin{aligned} &90^\circ + |\rho| \quad \text{for} \quad \delta>0,\ h<0 \quad \text{or for} \quad \delta<0,\ h>0 \\ &90^\circ - |\rho| \quad \text{for} \quad \delta<0,\ h<0 \quad \text{or for} \quad \delta>0,\ h>0 \quad . \end{aligned}$$

For some sources near the equator, for which ρ was very small, the observations taken east and west of the meridian at a given effective spacing have been averaged. Such averages are indicated by an A . Except for these averages

and except for many of the observations made with the 1168λ effective spacing, most of the entries in tables 6-9 are the result of single observations.

In figures 5-17 the visibility amplitudes for 51 sources are plotted. In the graphs, the filled circles refer to transit observations, while the open circles refer to off-transit observations. Unless otherwise noted, all curves are of one-dimensional visibility amplitudes with resolution in PA 90°. Open circles appearing on PA 90° curves represent measurements for which the effect of a non-zero rotation ρ was judged to be negligible. Some off-transit points, generally those for which the effects of fringe rotation are not particularly clear, have been omitted from the graphs. A dashed line indicates that the behavior of the visibility function in that region is not well determined by the available data.

Table 4

Fluxes and Visibility Amplitudes for

Transit Observations

Source	Flux	Spacing 0	195λ	389λ	779λ	1557λ
3C 2	5.1±0.4	---	.87±.17:	---	---	1.00±.10
SN 1572*	(57±3)	1.00±.05	.69±.07	---	.17±.02:	.08±.01:
3C 15	5.5±0.4	.93±.21	1.07±.15:	---	---	---
3C 17	7.8±0.5	1.30±.30	---	---	---	---
3C 20	14.7±1.8	.93±.11	.92±.15:	---	.90±.08:	.80±.08:
3C 26	3.2±0.6	---	.92±.15	---	.97±.15	1.06±.20:
3C 28	2.7±0.3	.89±.33	---	---	---	---
3C 33*	18.6±0.9	.97±.03	.86±.10:	.84±.07:	.64±.06:	.35±.05:
3C 38	7.0±0.7	1.19±.22	.64±.11	---	---	.65±.10:
3C 40*	8.0±1.2	1.0±.22	.81±.12	.29±.05:	.49±.07:	.11±.05:
3C 41	(6.9±0.9)	1.00±.13	---	---	---	---
3C 46	2.2±0.5	---	1.11±.15:	.75±.14:	.42±.22:	---
3C 48	21.5±1.1	.98±.08	---	---	---	1.00±.07
3C 58*	35.0±2.4	.95±.05	.63±.06:	.36±.03:	.08±.01:	.06±.01
3C 63	5.3±0.8	1.15±.19	.91±.16	---	---	---
3C 66*	(12.9±0.9)	1.00±.08	.46±.10:	.46±.06:	.20±.04:	.20±.02
MSH02-110	6.4±0.4	---	1.04±.16	---	---	---
3C 71	6.9±0.3	---	.82±.14:	---	.95±.11:	.91±.06
3C 75*	8.1±0.4	.92±.07	.81±.13:	.72±.12:	.11±.06:	.31±.07
3C 78	9.1±1.4	---	.88±.13:	---	.76±.10:	---
3C 79	7.0±0.5	.97±.08	---	.90±.18:	.88±.12:	.36±.04
CTA 21	9.3±0.7	.97±.11	.89±.10	---	---	---
NGC 1275*	20.4±2.0	1.05±.11	.90±.09	.88±.05:	.77±.05:	.71±.04
Fornax A	(125±6)†	1.00±.04	.05±.01:	.03±.01:	.01±.00:	---
3C 89*	(6.3±0.9)	1.00±.16	.59±.09	.70±.09:	.63±.08:	.47±.08:
CTA 26	2.8±0.4	1.25±.41	.77±.22:	---	.79±.17:	.69±.21
3C 98*	(14.1±1.2)	1.00±.08	.92±.04	.88±.10	.55±.05:	.33±.03
3C 103	7.2±0.5	.92±.08	.97±.05:	---	.99±.12:	.99±.11:
3C 109	5.9±0.6	.86±.16	.92±.05	.96±.09:	.97±.09:	---
3C 111*	20.4±2.0	1.00±.08	.89±.04:	.69±.04:	.07±.03:	.33±.05
3C 123	64.3±1.9	1.050±.03		standard source		
3C 129*	10.6±1.1	.89±.11	.46±.02	.48±.03	.23±.03	.31±.03
3C 134*	15.1±0.8	1.00±.08	.99±.04:	1.01±.04	.90±.06:	.81±.03
3C 135	2.9±0.9	---	.83±.15:	.57±.11:	---	.66±.17:
Pictor A*	(86.8±2.6)	1.01±.07	.54±.03:	.06±.01:	.17±.01:	.09±.01:

Table 4 (continued)

Source	Flux	Spacing 0	195λ	389λ	779λ	1557λ
Crab Neb*	(1030±45)	1.00±.04	.92±.06	.64±.02	.28±.01:	.04±.00:
Orion N.*	(361±9)	1.00±.03	.64±.03	.31±.02:	.11±.01:	.02±.00:
3C 147	29.2±0.9	.99±.03		standard source		
3C 154	7.2±0.5	.95±.08	.99±.05	.97±.06	.87±.09	.80±.08:
3C 161	25.6±1.3	.93±.06	1.00±.05	.97±.05	1.00±.06	.97±.05:
3C 171	5.7±0.4	1.05±.16	.95±.05	.97±.08	1.00±.10	.92±.19:
3C 175	4.1±0.4	---	.94±.09	.98±.05	.96±.05	.69±.13:
3C 180	4.3±0.6	---	.94±.11	1.00±.09	.98±.07	.75±.14:
3C 191	2.9±0.4	---	1.01±.11	.98±.15	.97±.15	1.19±.33:
3C 196	20.4±0.8	1.03±0.8		standard source		
3C 198*	3.4±0.3	---	.92±.07	.73±.10:	.27±.14:	.30±.13:
Puppis A	(105±6)†	1.00±.06	.13±.02:	.02±.01:	.01±.00:	---
3C 208*	4.9±1.2	---	.83±.06	.57±.08	1.03±.11:	.99±.10
CTB 31*	(212±21)†	1.00±.10	.48±.04:	.40±.02:	.20±.01:	.04±.00:
CTB 32*	(34.3±5)†	1.00±.15	.74±.08:	.52±.02:	.23±.02:	---
3C 216	6.0±0.4	---	.95±.05	1.03±.05	1.01±.11:	.96±.11:
Hydra A*	(67.5±1.8)	1.00±.03	.97±.04	.95±.04	.83±.03	.71±.02
3C 219*	12.3±0.9	---	.95±.05	.91±.04	.67±.06:	<.10:
3C 227*	11.2±1.1	.91±.09	.83±.05	.69±.05	.22±.02	.11±.03
3C 230	5.9±0.4	---	.85±.07:	.77±.10	.70±.13:	.84±.11:
3C 234*	8.3±0.8	.88±.12	1.00±.04	.65±.04	.62±.05	.43±.08
3C 237	9.6±0.7	.57±.10	1.01±.08:	1.00±.04	.86±.10:	.99±.11
3C 243	2.1±0.5	---	---	.67±.11	.61±.15	.56±.22
3C 254	5.1±0.4	---	.99±.06	1.02±.05	.95±.08	.99±.06
3C 264*	(10.5±3.0)	1.00±.29	.72±.06	.59±.05	.47±.06	.31±.05
3C 265	4.8±0.5	---	.95±.08	.86±.09	.72±.10:	.37±.10:
3C 270*	(28.5±1.5)	1.00±.05	.56±.03	.07±.01	.23±.02	.08±.02
3C 273	45.4±1.4	1.11±.05	1.00±.04	1.00±.03	.97±.05	.94±.04:
M 87*	300 ---	1.00±.05	.84±.03	.59±.02	.50±.02:	.38±.01
Coma A	4.0±0.6	---	---	.89±.13:	1.12±.15:	.98±.24
3C 278*	10.6±1.1	.91±.15	.94±.13:	.74±.06:	.42±.05:	<.15:
3C 279	9.8±0.7	.70±.12	1.01±.08	.99±.08:	.82±.10:	.92±.10:
3C 280	7.2±0.7	.95±.16	.96±.06:	1.02±.08:	.93±.12:	.90±.09:
3C 283	8.6±0.9	1.18±.18	.98±.04	1.01±.09	.97±.06	.83±.08
NGC 5128*	(442±35)†	1.00±.07	.53±.02:	.15±.01	.33±.01	.08±.01
3C 286	19.8±1.4	.99±.08	.99±.05:	1.03±.05:	1.00±.05:	1.02±.06:
3C 287	9.6±0.9	.88±.13	.85±.05	1.09±.08:	.95±.10:	.91±.09:
3C 295	32.0±1.0	.95±.07		standard source		
3C 298	9.7±0.5	1.15±.16	.97±.05	1.07±.06:	1.05±.09:	.94±.05
MSH14+010	3.4±0.7	---	.85±.12:	.64±.11	.81±.16	.70±.19

Table 4 (continued)

Source	Flux	Spacing 0	195λ	389λ	779λ	1557λ
3C 310*	12.7±0.9	.85±.14	.98±.07:	.89±.06	.60±.06	.17±.04
3C 313*	6.0±0.9	.91±.16	.85±.15:	.85±.09:	.43±.06:	.62±.17
3C 315	6.1±0.6	1.00±.16	.97±.05:	.94±.09:	.87±.06	.52±.06
3C 317	10.0±0.7	1.00±.10	1.00±.10:	.97±.07:	.96±.06:	.93±.06
3C 318	4.1±0.6	.72±.24	.97±.20:	.94±.07	1.03±.06:	1.04±.18:
3C 324	4.2±0.6	1.50±.37	.88±.08	.93±.06	.91±.07	.98±.16
3C 327*	12.3±1.2	.95±.17	.91±.04	.63±.09	.58±.06	.28±.04
MSH16+02	6.5±1.0	---	.94±.14	---	.97±.10:	.68±.26
3C 330	10.6±0.7	.83±.15	.99±.06	.93±.08	.82±.05	.35±.04
3C 338*	6.7±0.5	1.08±.17	.97±.06	.93±.05	.78±.04	.38±.05
3C 343*	(10.5±0.9)	1.00±.09	.32±.02	.98±.06:	.17±.02:	.85±.07:
3C 345	8.4±0.8	1.00±.14	.95±.08:	.98±.07	.96±.09:	.82±.07:
3C 347*	2.5±0.6	---	.96±.12:	.54±.20:	.59±.11:	.88±.20:
Herc A*	73.5±3.7	1.00±.08	.93±.03:	.76±.03:	.27±.01	.61±.02
CTB 38	(38±13)†	1.00±.30	.56±.06:	.59±.03:	.18±.03	.08±.02:
3C 353*	81.5±1.8	1.04±.02	.88±.03	.61±.02	.27±.01	.25±.01
SN 1604*	21.3±2.1	.95±.10	.97±.08	.84±.07	.41±.02	.19±.02
Sgtr A*	(700±140)†	1.00±.20	.30±.06:	---	.07±.00	.02±.00
3C 365	3.5±0.5	---	1.03±.12:	---	.78±.12	.98±.07
Omega N.*	(502±75)†	1.00±.15	.55±.04:	.26±.01	.05±.00	.02±.00
3C 380	19.8±1.0	.93±.03	.98±.12:	1.00±.05:	1.00±.05:	1.02±.04
CTA 80*	7.8±0.8	.88±.07	1.00±.12:	.75±.07:	.52±.07	.38±.06:
3C 386*	10.2±0.5	.94±.06	---	.87±.07:	.64±.04	.17±.05:
3C 388	(9.9±1.2)	1.00±.12	.86±.10:	.81±.05	.90±.07	.69±.08
3C 397*	(25±13)†	1.00±.50	.53±.07:	.36±.02	.13±.03	.10±.06
3C 398*	(92±14)†	1.00±.15	.45±.07	.19±.01:	.08±.01	.06±.01
MSH19-16	1.2±0.4	---	.95±.35:	---	.82±.22	1.12±.60
3C 401	7.2±0.5	1.09±.14	---	1.00±.07:	.99±.08	1.01±.09:
3C 402*	4.9±1.0	.92±.24	.90±.15	---	.43±.05:	.35±.07:
3C 403*	(9.6±0.6)	1.00±.06	.71±.13:	---	.47±.05:	.25±.04
Cygnus A	(2160±120)	1.00±.06	---	---	.49±.03	.41±.02
3C 409	21.0±1.5	1.05±.06	---	---	.98±.05	1.00±.10
CTB 87	(10.0±4.0)†	1.00±.40	.81±.12:	---	.11±.03:	.27±.08:
3C 410	12.7±0.9	1.02±.08	---	---	.98±.05	.93±.06
3C 413*	1.5±0.4	---	.95±.20:	---	.41±.11	.62±.37:
3C 424	3.9±0.4	1.60±.25	.98±.09	---	.94±.08	1.09±.16
3C 430	11.2±1.1	1.00±.14	1.00±.10:	---	---	.75±.10:
3C 433	17.4±0.9	.89±.09	---	---	.93±.04	.93±.04
3C 436	(6.3±0.6)	1.00±.10	.81±.13:	---	.76±.07	.77±.09
CTA 97	(4.5±0.6)	1.00±.13	.29±.07:	---	---	---

Table 4 (continued)

Source	Flux	Spacing 0	195λ	389λ	779λ	1557λ
3C 438	10.6±0.5	1.00±.06	1.08±.15:	---	.97±.05	1.06±.09
3C 444	13.6±0.7	1.00±.04	---	---	.92±.05	.79±.09
3C 445*	(8.2±1.2)	1.00±.14	.95±.11	---	.59±.07:	.16±.05:
3C 446*	(7.8±0.9)	1.00±.12	.96±.12	---	.74±.10:	1.01±.09
CTA 102	7.8±0.5	.93±.08	---	---	1.00±.12:	.99±.15
3C 452*	15.3±1.5	.91±.06	.86±.08	---	.09±.02:	.10±.01
3C 456*	3.4±0.9	---	1.05±.15:	---	.73±.10:	1.00±.16
3C 459	(7.2±0.6)	1.00±.08	---	---	.94±.11:	.82±.10
Cass A	(3120±150)	1.00±.05	---	---	.08±.01:	.06±.00
MSH23-112	3.2±0.5	---	1.00±.18:	---	.97±.16:	.86±.08
3C 465*	(11.7±0.9)	1.00±.08	.78±.10	---	.26±.05:	.37±.07
3C 469	2.3±0.6	---	.60±.25	---	---	.62±.10

Notes--

All fluxes given in units of 10^{-26} w m^{-2} $(c/s)^{-1}$

* Amplitudes for these sources are plotted in figures 5-17

( ) CTA or CTB flux

† Peak apparent flux from CTA or CTB

: Based on single observation

Table 5

Visibility Phases for Transit Observations

(Only those sources are listed which have phases differing significantly from zero.)

Source	Spacing 389λ	779λ	1557λ
SN 1572	----	-170° ± 30:	-70° ± 50:
3C 33	----	00 ± 30:	+120 ± 50:
3C 40	----	-130 ± 30:	-180 ± 60:
3C 58	----	+70 ± 50:	+75 ± 50:
3C 66	----	+120 ± 30:	+230 ± 50:
3C 75	00° ± 20:	+70 ± 30:	+155 ± 40:
Fornax A (1)	-110 ± 20:	+60 ± 40:	----
3C 89	-20 ± 20:	-25 ± 40:	-85 ± 70:
3C 98	00 ± 15	-25 ± 20:	-210 ± 40:
3C 111	00 ± 15:	+50 ± 40:	+170 ± 40:
3C 129	-45 ± 20	-90 ± 30	-250 ± 80
3C 135	-30 ± 20:	----	-235 ± 80
Pictor A	+120 ± 20:	+40 ± 20:	----
Crab Neb.	00 ± 10	00 ± 10:	-90 ± 30:
Orion Neb.	00 ± 10:	+20 ± 10:	+140 ± 30:
Puppis A	-115 ± 10:	00 ± 40:	----
3C 208	+40 ± 20	+90 ± 30:	+120 ± 30
CTB 31 (2)	+20 ± 20:	-15 ± 30:	-70 ± 40:
CTB 32 (2)	+50 ± 20:	+90 ± 30:	----
Hydra A	-10 ± 10	-40 ± 15	-90 ± 40
3C 227	-10 ± 20	-110 ± 30	-230 ± 70
3C 270	+95 ± 10	+125 ± 30	+270 ± 40
M 87	-10 ± 10	-25 ± 30:	-80 ± 40
3C 278	-25 ± 20:	-50 ± 20:	----
NGC 5128	-145 ± 20	-185 ± 15	-550 ± 40
3C 287	-45 ± 20:	-90 ± 30:	-170 ± 40:
3C 313	00 ± 15:	00 ± 30:	+115 ± 50
3C 327	-30 ± 20	-155 ± 15	-280 ± 40
3C 343	+90 ± 20:	+50 ± 30:	+30 ± 40
3C 347	-120 ± 20:	-180 ± 40:	-510 ± 60:
Herc A	-10 ± 10:	-50 ± 15	-190 ± 30
CTB 38 (2)	+15 ± 20:	+140 ± 30	+290 ± 50:
3C 353	-10 ± 10	-130 ± 15	-230 ± 30
SN 1604	00 ± 10	-50 ± 20	+70 ± 30
Sgtr A (2)	----	+10 ± 20	+200 ± 30

Table 5 Continued

Source	Spacing 389λ	779λ	1557λ
Omega Neb. (2)	-55° ± 10°	-90° ± 20°	-190° ± 30°
CTA 80	-40 ± 10:	-10 ± 20	-160 ± 60:
3C 397	+70 ± 20:	-140 ± 20	+140 ± 40
3C 398	+135 ± 20:	+170 ± 20	+300 ± 60
3C 402	----	-65 ± 40:	-190 ± 80:
3C 403	----	-60 ± 30:	-290 ± 50
Cyg A	00 ± 10:	-10 ± 10	-150 ± 30
3C 413	----	+50 ± 40	+280 ± 60:
3C 452	----	-140 ± 50:	-30 ± 40
Cass A	----	+65 ± 20:	-90 ± 30
3C 465	----	-115 ± 40:	-230 ± 50

Notes: (1) Based on CTA position
(2) Based on CTB position
: Based on single observation

Table 6

Visibility Amplitudes for Observations

with $\cos\theta_o = 5/8$

Source	Effective Spacing 126λ E	126λ W	487λ E	487λ W	973λ E	973λ W	$\lvert\rho\rvert$
3C 2	--	--	.94	--	.95	--	00
3C 15	--	--	--	--	.70	--	02
3C 26	--	.86	--	--	--	--	03
3C 33	--	--	.87	--	.87	--	16
3C 38	--	--	--	--	.78	--	19
3C 40	--	.95	.44	--	<.15	--	02
3C 63	--	.96	--	--	.96	--	03
3C 75	--	.93	--	--	.15	--	07
3C 79	--	--	--	--	.53	--	05
CTA 21	--	.89	--	--	.95	--	21
3C 89	--	--	--	--	.40	--	02
CTA 26	--	--	--	--	.88	--	03
3C 98	--	.93	--	.65	--	--	12
3C 109	--	.94	--	1.06	--	--	13
3C 135	--	.98	--	.62	--	--	02
Crab Neb.	--	.93	--	.65	--	.14	28
Orion Neb.	--	--	--	.21	--	.05	07
3C 154	--	1.00	--	--	--	--	35
3C 175	.84	.95	--	.96	--	.85	14
3C 180	1.02	--	--	--	--	--	03
3C 191	1.11	.99	--	--	--	--	12
3C 198	.99	.81	--	.56	--	--	07
3C 208	.75	1.19	--	.57	--	.93	16
Hydra A	1.00	1.02	--	--	--	.74	14
3C 227	--	.98	--	--	--	.24	09
3C 230	.80	--	--	--	--	.55	00
3C 237	--	.99	.99	--	--	.83	09
3C 243	--	--	.67	--	--	--	08
3C 264	.73	.80	.62	--	--	.29	25
3C 270	--	.78	.23	.28	.04A		07
M 87	1.02	--	.55	.49	.49	.53	03
3C 278	--	.98	.70	.71	.28	.27	15
3C 279	--	--	.86	--	.94	1.14	07
3C 283	1.00	--	1.00	--	--	.99	28
3C 298	--	1.01	--	--	.99A		08

Table 6 (continued)

Source	Effective Spacing 126λ E	126λ W	487λ E	487λ W	973λ E	973λ W	|ρ|
MSH 14+010	--	--	.91A		.60A		04
3C 313	--	--	--	.69	.36	.18	10
3C 317	--	--	--	.98	.94A		09
3C 318	--	--	--	1.02	.92	.92	26
3C 324	.81	--	--	--	.89	--	28
3C 327	1.02	--	--	.50	.56A		03
MSH 16+02	--	--	--	.98	.89A		02
3C 347	--	--	--	--	.86	--	16
Herc A	.98	--	--	--	.21	.17	06
3C 353	.94	--	.42A		.34A		01
SN 1604	--	--	.69	.67	.19	.18	27
3C 365	--	--	.96	--	1.00	.46	16
Omega Neb.	.77	--	.16	.07	.09	.02	20
3C 386	1.00	--	.79	.78	.44	.31	22
3C 397	.66	--	--	.38	--	.05	08
3C 398	.19	--	.31	.21	.11	.12	10
MSH 19-16	--	--	.53	--	--	--	17
3C 403	--	--	.68	--	.25A		03
3C 413	--	--	.77	--	--	--	09
3C 424	.94	--	1.14	.77	--	--	08
3C 433	--	--	--	--	.96	--	33
3C 444	--	--	.93	--	.88	--	21
3C 445	--	--	.73	--	.51	--	03
3C 446	--	--	--	--	.90	--	06
3C 456	--	--	.75	--	.75	--	11
3C 459	--	--	.94	--	.87	--	05

Note-- For the observations at effective spacings of 126λ, the value of $\cos\theta_o$ was 0.646.

Table 7

Visibility Amplitudes for Observations

with $\cos\theta_o = 3/4$

Source	Effective Spacing 292λ E	292λ W	584λ E	584λ W	1168λ E	1168λ W	$\lvert\rho\rvert$
3C 2	--	--	--	--	.96± .08	----	00°
3C 17	--	--	1.05	--	----	----	02
3C 26	--	--	.99	--	1.13± .19	----	03
3C 28	--	--	1.14	--	.79± .07	----	25
3C 33	--	.79	.89	--	.81± .05	----	11
3C 38	--	--	.89	--	.72± .04	----	14
3C 40	--	.71	.47	--	.20± .08	----	01
3C 41	--	.77	--	--	.68± .04	----	35
3C 46	--	--	--	--	.67± .22	----	43
3C 48	--	--	--	--	1.00± .05	----	35
3C 63	--	.84	--	--	.93± .10	----	02
MSH 02-110	--	.88	--	--	.84± .12	----	18
3C 71	--	.97	--	--	.91± .20	----	00
3C 75	--	.71	--	--	.24± .07	----	05
3C 78	--	.88	--	--	.67± .10	----	03
3C 79	--	.97	--	--	.50± .10	----	15
CTA 21	--	.93	--	--	.92± .12	----	15
CTA 26	--	.91	--	--	----	----	02
3C 98	--	.89	--	--	----	----	09
3C 109	--	.96	--	--	----	----	10
3C 111	--	.81	--	.32	.20± .04	.32± .02	44
3C 123		standard		source			30
3C 134	--	.97	--	.81	----	.21± .03	44
3C 135	--	.39	--	--	----	----	01
Crab Neb.	--	.82	--	.46	----	.03± .00	21
Orion Neb.	--	.46	--	.17	----	.03± .00	04
3C 154	--	.92	--	.83	----	.85± .07	24
3C 161	--	1.00	--	.99	----	.98± .05	05
3C 175	--	.89	--	.88	----	.76± .12	10
3C 180	--	.93	--	.81	----	.84± .13	02
3C 191	--	.89	--	.92	----	1.18± .26	09
3C 198	--	.71	--	.33	----	.27± .13	05
3C 208	--	1.06	--	.75	----	.74± .06	12
Hydra A	--	1.00	.86	.93	----	.82± .05	10
3C 227	--	.74	.37	.29	----	.21± .04	06

Table 7 (continued)

Source	Effective Spacing 292λ E	292λ W	584λ E	584λ W	1168λ E	1168λ W	|ρ|
3C 230	--	1.07	--	1.01	----	1.04± .12	00°
3C 234	--	.86	.86	.83	----	.37± .06	29
3C 237	--	1.01	1.00	.92	----	.99± .10	06
3C 243	--	.78	.67A		----	.67± .21	05
3C 264	.61	.65	.52	.52	.30± .10	.30± .03	18
3C 265	.87	1.07	.76	--	----	.68± .10	33
3C 270	.27A		.33A		.04± .01A		05
3C 273	1.00A		.99A		.97± .04A		02
M 87	.72	.67	.53	.49	.47± .02	.49± .02	11
Coma A	.88	1.06	--	.97	----	1.04± .16	27
3C 278	.79	.85	.59	.58	.18± .06	.09± .03	11
3C 279	.94A		.97A		1.00± .05		05
3C 283	1.01	1.01	--	--	----	----	21
3C 286	--	--	--	--	----	----	31
3C 287	.96	.92	.95	.95	.86± .08	.83± .06	25
3C 298	1.05A		.97A		.98± .07A		05
MSH 14+010	.91A		--	--	----	.54± .19	03
3C 310	.84	.96	.72	--	.16± .01	.27± .04	26
3C 313	.87A		.67	--	.26± .10	.43± .06	07
3C 315	.97	1.08	.88	.86	.60± .09	.67± .08	26
3C 317	.99A		.98A		.93± .03A		06
3C 318	.95	1.01	--	.95	1.02± .14	.91± .14	19
3C 324	.93	.99	.79	--	.85± .17	----	20
3C 327	.77A		--	.49	.43± .03A		02
MSH 16+02	.98	--	.93	--	.93± .05A		01
3C 338	.87	--	--	--	.63± .09	.65± .14	47
3C 345	1.02	--	--	--	.92± .08	.59± .14	48
3C 347	.62		.71	.44	.71± .05	1.07± .21	11
Herc A	.87	--	.53A		.39± .03A		04
3C 353	--	--	.31A		.39± .04A		01
SN 1604	.93	--	.60	.58	<.06	.08± .02	20
Sgtr A	--	--	.11	.13	.00	.05± .00	29
3C 365	.98	--	--	.66	----	.71± .15	12
Omega Neb.	.42	--	.15	.03	.05± .00	.01± .00	14
CTA 80	.94	--	.88	--	.72± .07	.27± .05	34

Table 7 (continued)

Source	Effective Spacing 292λ E	292λ W	584λ E	584λ W	1168λ E	1168λ W	$\lvert\rho\rvert$
3C 386	.95	--	.72	.65	.35± .05	.27± .05	15
3C 397	.39	--	.31A		.14± .02A		06
3C 398	.63	--	.26A		.12± .01A		08
MSH 19-16	--	--	--	--	.4± .26	----	13
3C 403	.76	--	.60	--	.14± .05A		02
3C 409	--	--	--	--	1.02± .05A		22
CTB 87	.66	--	.27	--	.21± .06	.12± .04	42
3C 410	.99	--	--	--	.92± .09	----	30
3C 413	.77	--	.59	--	<.67	----	06
3C 424	.92	--	.90	--	1.01± .17	1.12± .14	05
3C 433	.95	--	--	--	.91± .09	----	24
3C 436	.71	--	--	--	.68± .04	----	28
3C 438	.95	--	--	--	.86± .07	----	44
3C 444	.97	--	.94	--	.90± .05	----	15
3C 445	.89	--	.82	--	.35± .06	----	02
3C 446	.99	--	.90	--	.78± .09	----	04
CTA 102	.94	--	--	--	----	----	10
3C 452	.52	--	.67	--	.11± .05	----	47
3C 456	--	--	--	--	.72± .14	----	08
3C 459	--	--	--	--	.96± .09	----	03
MSH 23-112	--	--	--	--	1.14± .18	----	11
3C 465	--	--	.28	--	.23± .04	----	26

Table 8

Visibility Amplitudes for Observations

with $\cos\theta_0 = 7/8$

Source	Effective Spacing 169λ E	169λ W	681λ E	681λ W	1363λ E	1363λ W	$\lvert\rho\rvert$
3C 2	--	--	.93	--	1.09	--	00
3C 20	--	.94	.87	--	.83	--	47
3C 26	--	--	--	--	1.08	--	02
3C 28	--	--	--	--	.86	--	17
3C 33	--	--	--	--	.57	--	07
3C 38	--	--	--	--	.76	--	10
3C 46	--	.89	--	--	--	--	26
3C 66	--	.82	--	--	.08	--	32
3C 75	--	.88	--	--	--	--	03
NGC 1275	--	.93	--	--	.66	.66	30
Fornax A	--	.13	--	--	--	--	26
3C 109	--	--	--	--	--	.77	06
3C 111	--	.91	--	--	--	.33	26
3C 129	--	.47	--	--	--	--	35
3C 134	--	.94	--	--	--	--	27
3C 135	--	--	--	.47	--	--	00
Crab Neb.	--	--	--	.31	--	.00	13
Orion Neb.	--	--	--	.13	--	.02	03
3C 161	--	--	--	.01	--	--	03
3C 171	--	.98	--	.92	--	.79	53
3C 175	--	--	--	--	--	.58	06
3C 180	--	--	--	.77	--	.68	01
3C 198	--	--	--	.34	--	.16	03
3C 208	--	--	--	.62	--	.62	08
3C 216	--	.98	--	--	--	--	35
Hydra A	--	--	--	.88	--	.81	06
3C 219	--	.92	--	.36	--	.38	37
3C 227	--	--	.31	.19	--	.20	04
3C 230	--	--	.88	--	--	.95	00
3C 237	--	--	1.01	1.02	--	1.06	04
3C 254	.98	--	1.16	--	--	--	30
3C 264	--	--	.52	.49	.39	.22	12
3C 265	.96	1.01	.90	.84	--	.43	21
3C 270	--	--	.32A		.05A		03
3C 273	--	--	--	.99	--	.97	01

Table 8 (continued)

Source	Effective Spacing 169λ E	169λ W	681λ E	681λ W	1363λ E	1363λ W	|ρ|
M 87	--	.89	.53	.46	.41	.43	07
Coma A	1.05	--	--	--	--	.97	18
3C 278	--	--	.56	.48	.17	--	07
3C 279	--	--	--	--	.89	--	03
3C 280	--	--	1.03A		1.01A		39
3C 283	--	--	--	.96	--	--	13
3C 287	--	--	1.03	.93	1.01	.75	16
3C 298	1.06	--	--	--	1.01A		03
MSH 14+010	--	--	.97A		.62A		01
3C 310	.95	.98	.60	.73	.11	.27	17
3C 313	--	--	.56	.58	.30	.39	04
3C 315	--	--	.84	.69	.54	.59	17
3C 317	1.03	--	1.06	--	.95	--	03
3C 324	--	--	.95	.85	.89	--	13
3C 327	--	--	.61	--	.31	--	01
MSH 16+02	--	--	.86	--	--	.90	00
3C 338	1.02	--	--	.85	.52	.45	28
3C 345	1.05	--	--	.88	1.10	.89	29
3C 347	--	--	.84	.69	.68	.49	07
Herc A	--	--	.40A		.56A		02
3C 353	--	--	.25	--	--	--	00
SN 1604	--	--	--	.50	.10	.10	13
Sgtr A	--	--	--	.11	.03	.02	18
Omega Neb.	--	--	--	.03	--	.02	09
CTA 80	1.02	--	.77	.35	.39	.21	22
3C 386	1.02	--	.66	.64	--	.22	10
3C 388	.85	--	.78	.64	.80	.65	36
3C 397	--	--	.21A		--	--	03
3C 398	--	--	.04A		.10A		05
MSH 19-16	--	--	<.6	--	--	--	08
3C 402	--	--	.41	--	.21	--	44
Cygnus A	--	--	--	--	.31	.24	29
CTB 87	.80	--	.42	--	.16	--	25
3C 410	--	--	1.01	--	.95	--	19
3C 413	--	--	.61	--	--	--	04
3C 424	--	--	.95	--	.88	--	03
3C 433	--	--	--	--	1.00	--	16
3C 436	--	--	.75	--	.62	.68	18
3C 438	--	--	.94	--	1.00	--	26
3C 445	--	--	.56	--	--	.08	01

Table 8 (continued)

Source	Effective Spacing 169λ E	169λ W	681λ E	681λ W	1363λ E	1363λ W	|ρ|
3C 446	--	--	.76	--	--	--	02
3C 452	--	--	.30	--	.26	--	28
3C 465	--	--	.28	--	.11	--	17

Note-- For the observations at effective spacings of 169λ, the value of $\cos\theta_o$ was 0.867.

Table 9

Visibility Amplitudes for Observations

with $\cos\theta_o = 0.788$

Source	Effective Spacing 1226λ E	1226λ W	|ρ|
3C 66	.36	.27	46°
3C 75	.24	--	04
NGC 1275	.63	.70	42
3C 98	--	.34	08
3C 111	.19	.36	36
3C 134	<.16	.50	36

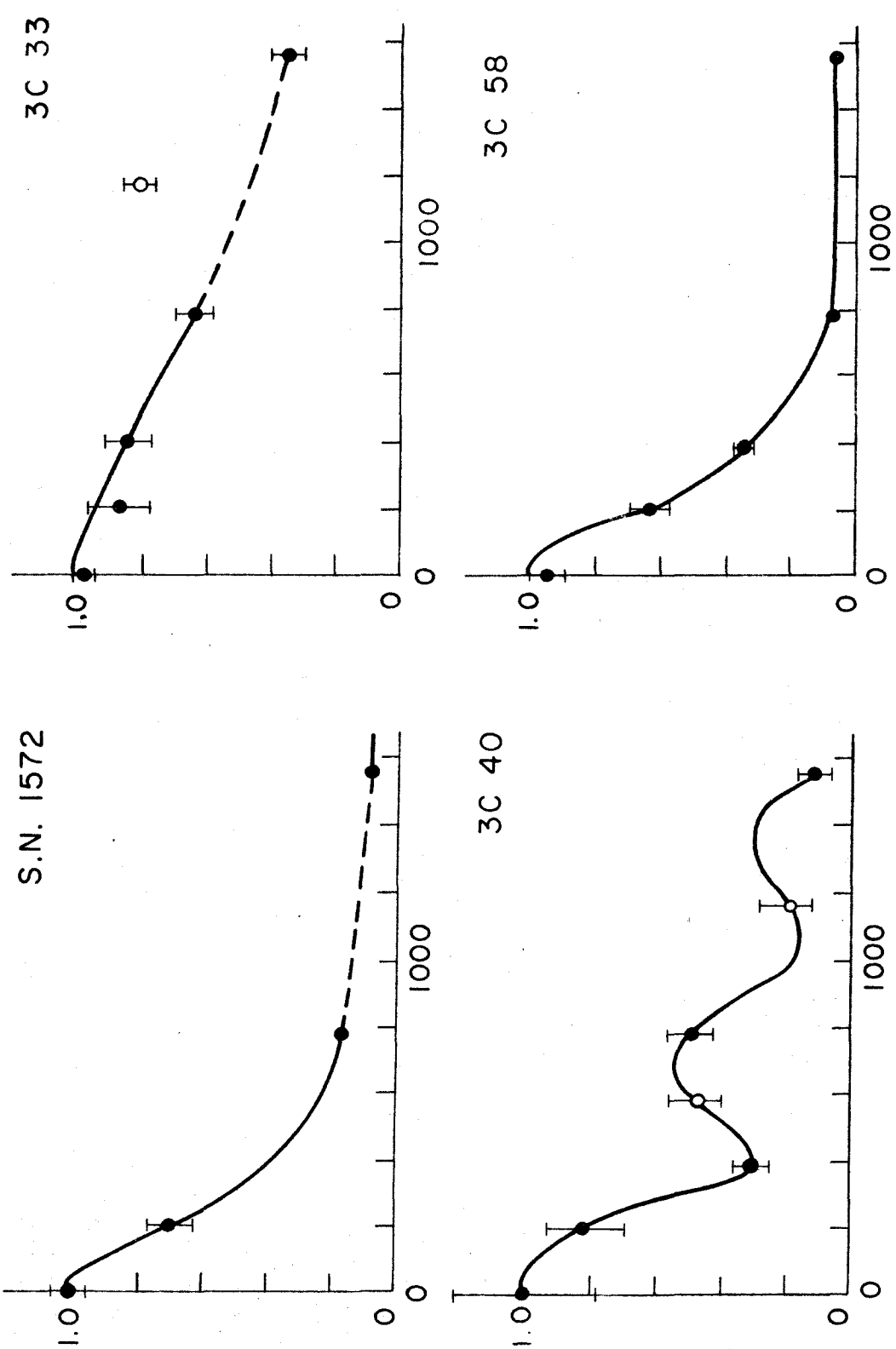

Figure 5. Visibility amplitudes for SN 1572, 3C 33, 3C 40, and 3C 58. Abscissae are effective antenna spacings, in wavelengths.

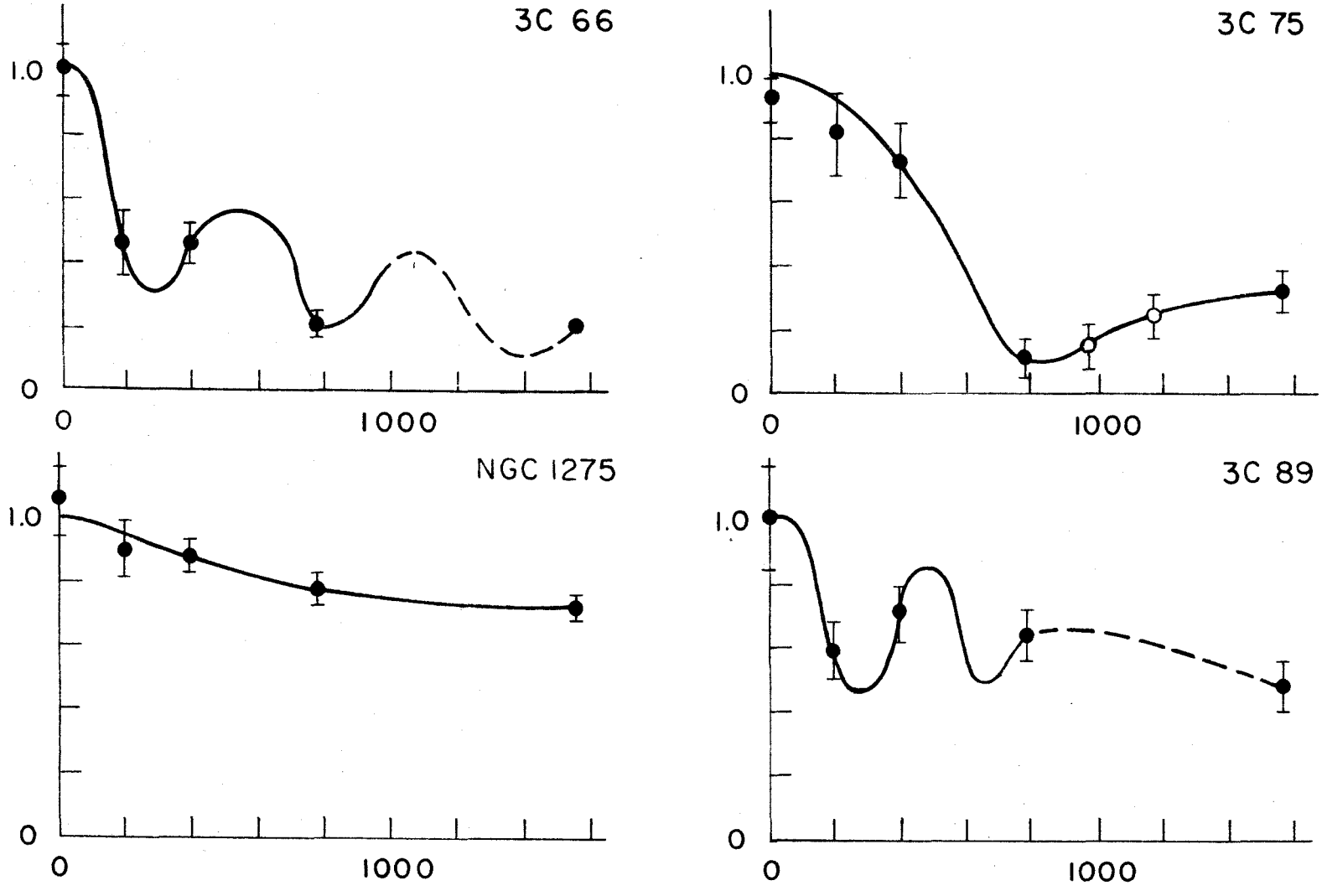

Figure 6. Visibility amplitudes for 3C 66, 3C 75, NGC 1275, and 3C 89. Abscissae are effective antenna spacings, in wavelengths.

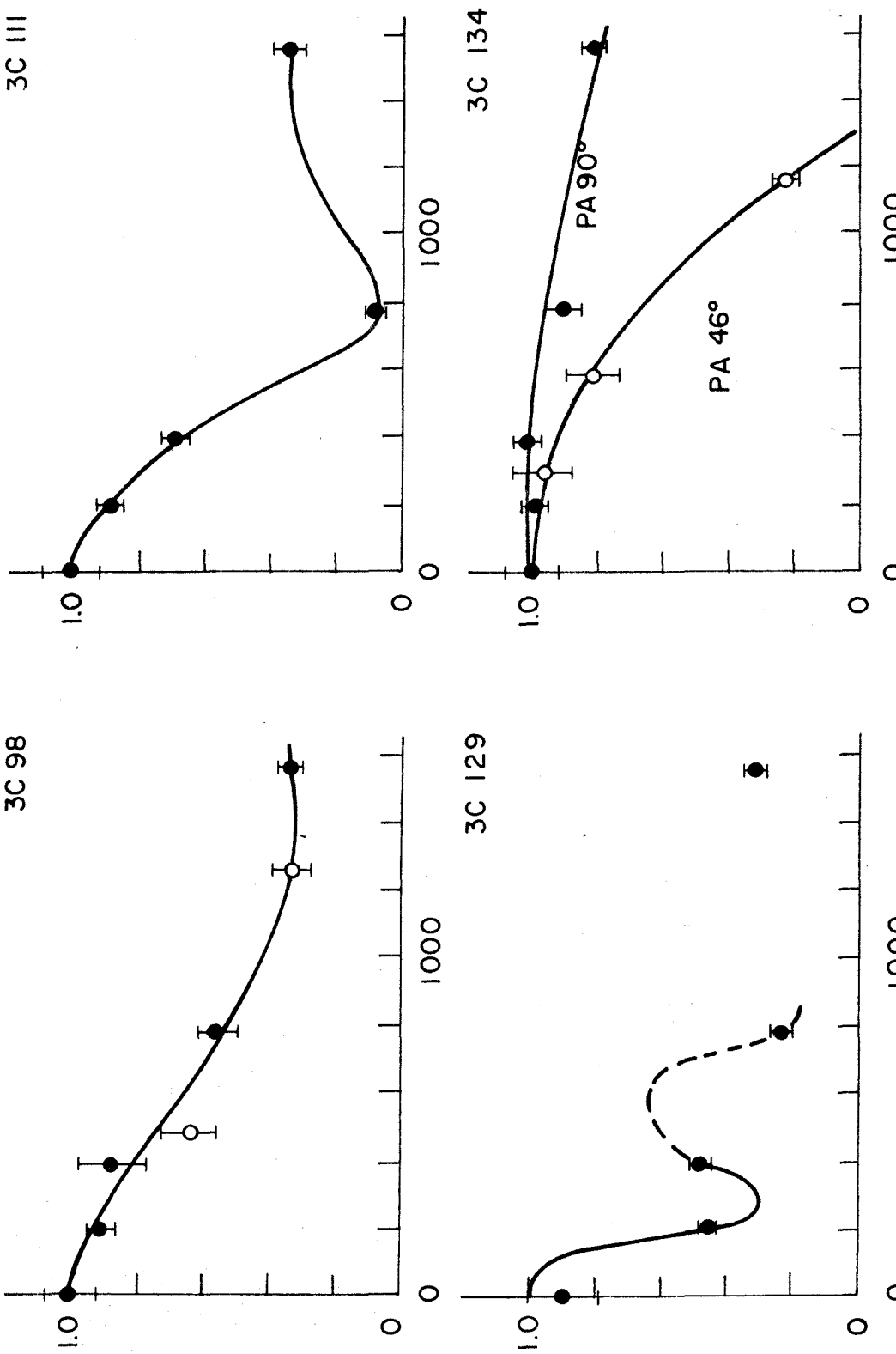

Figure 7. Visibility amplitudes for 3C 98, 3C 111, 3C 129, and 3C 134. Abscissae are effective antenna spacings, in wavelengths.

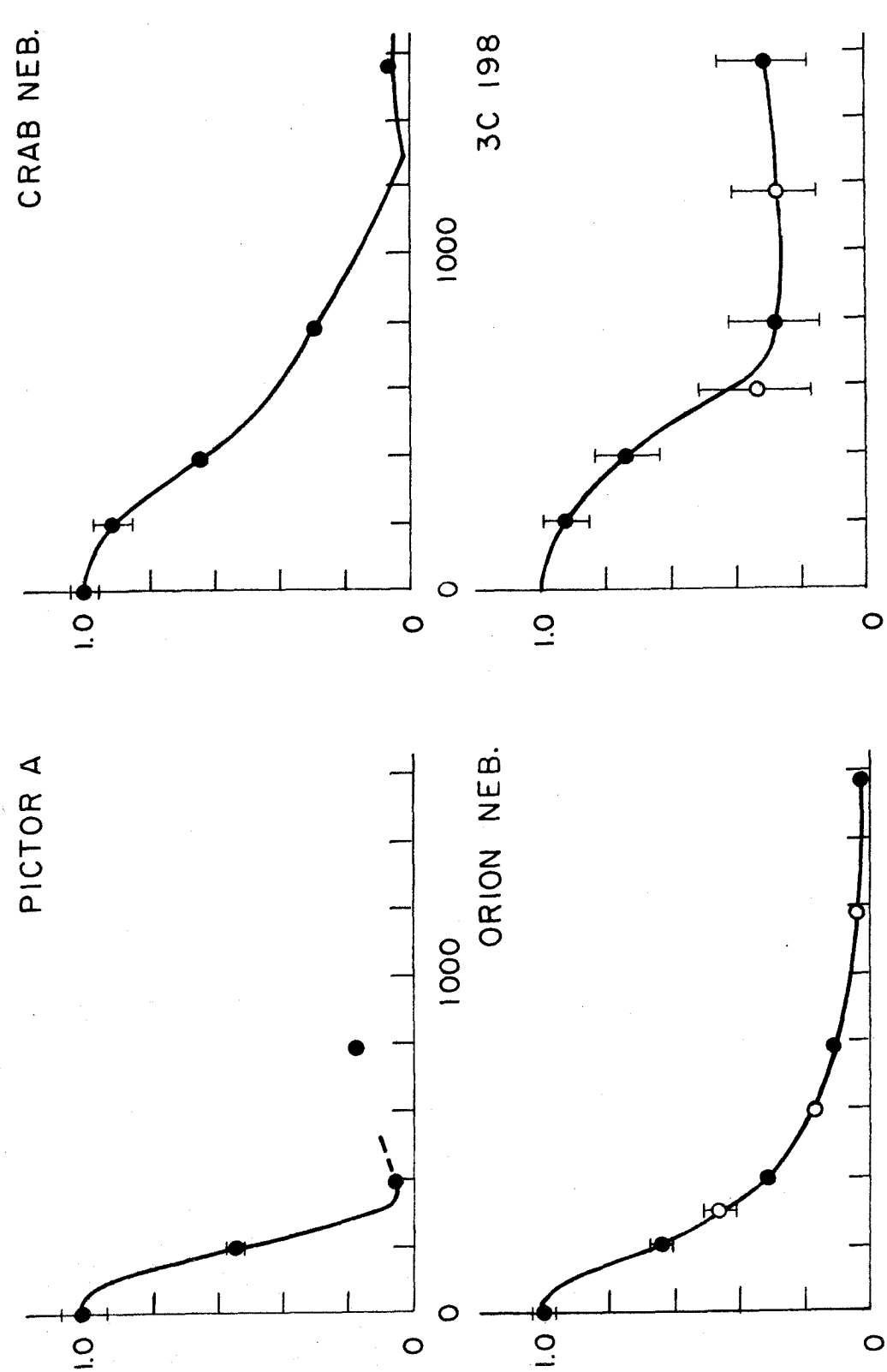

Figure 8. Visibility amplitudes for Pictor A, the Crab Nebula, the Orion Nebula, and 3C 198. Abscissae are effective antenna spacings, in wavelengths.

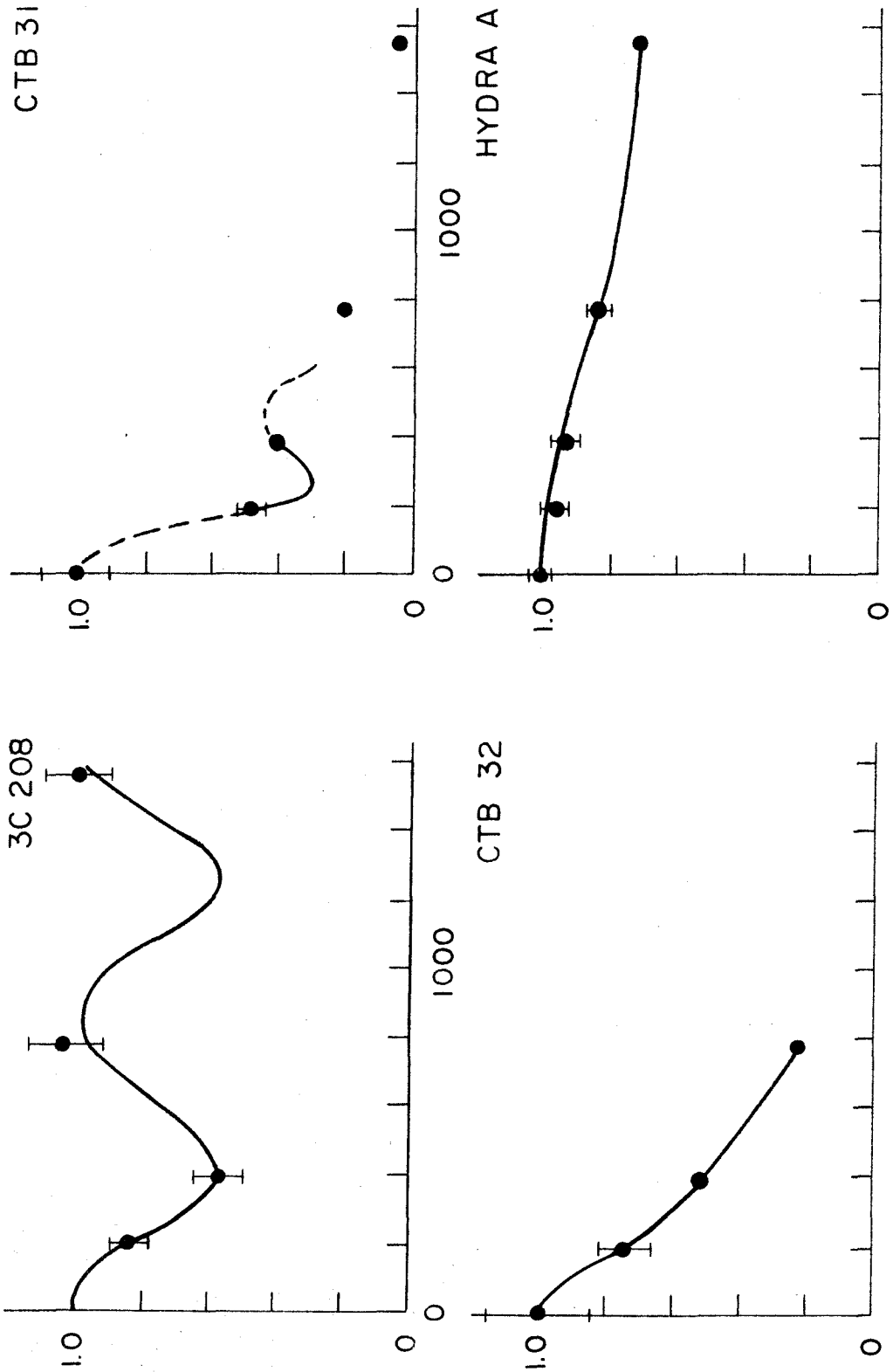

Figure 9. Visibility amplitudes for 3C 208, CTB 31, CTB 32, and Hydra A. Abscissae are effective antenna spacings, in wavelengths.

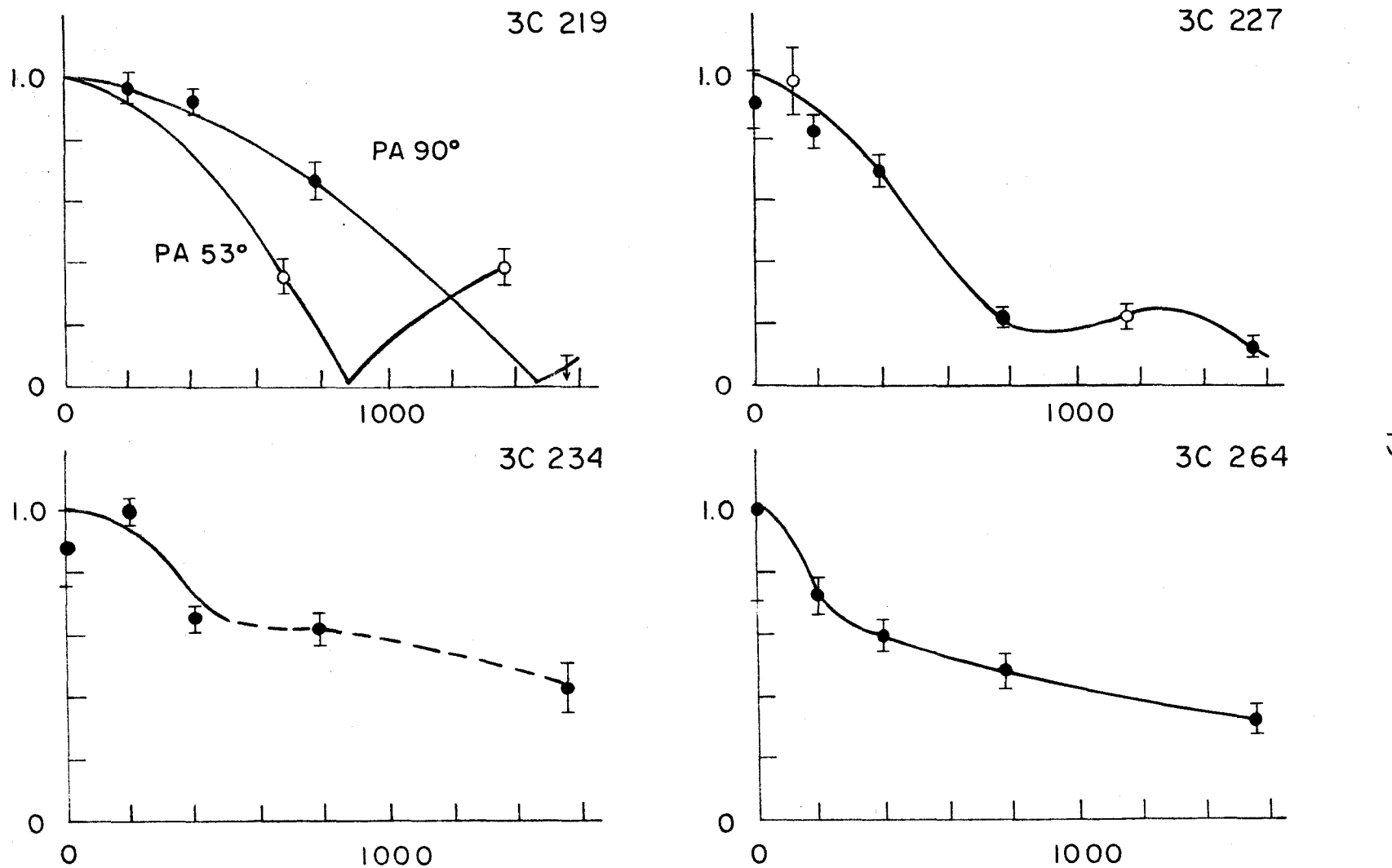

Figure 10. Visibility amplitudes for 3C 219, 3C 227, 3C 234, and 3C 264. Abscissae are effective antenna spacings, in wavelengths.

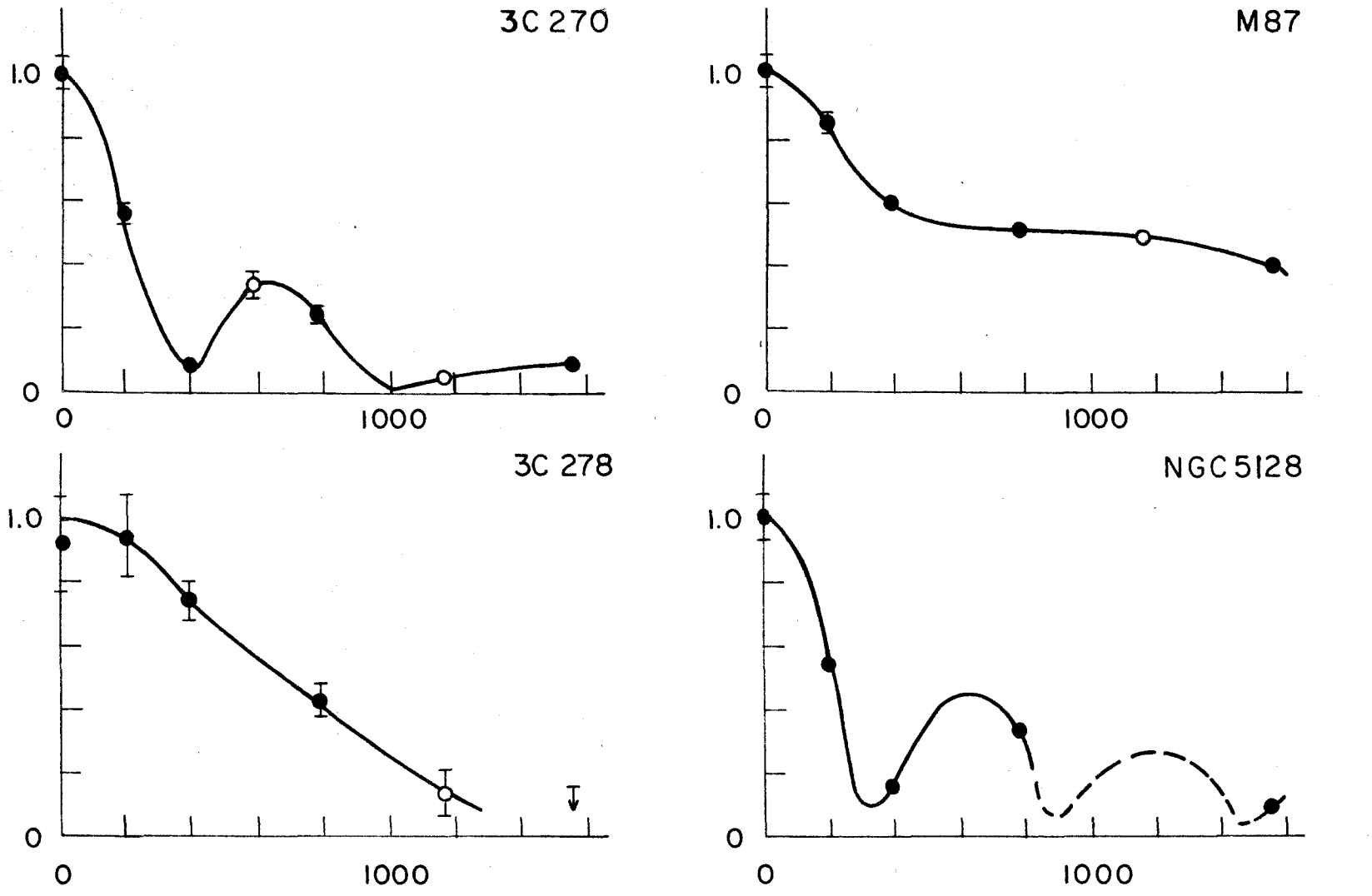

Figure 11. Visibility amplitudes for 3C 270, M 87, 3C 278, and NGC 5128. Abscissae are effective antenna spacings, in wavelengths.

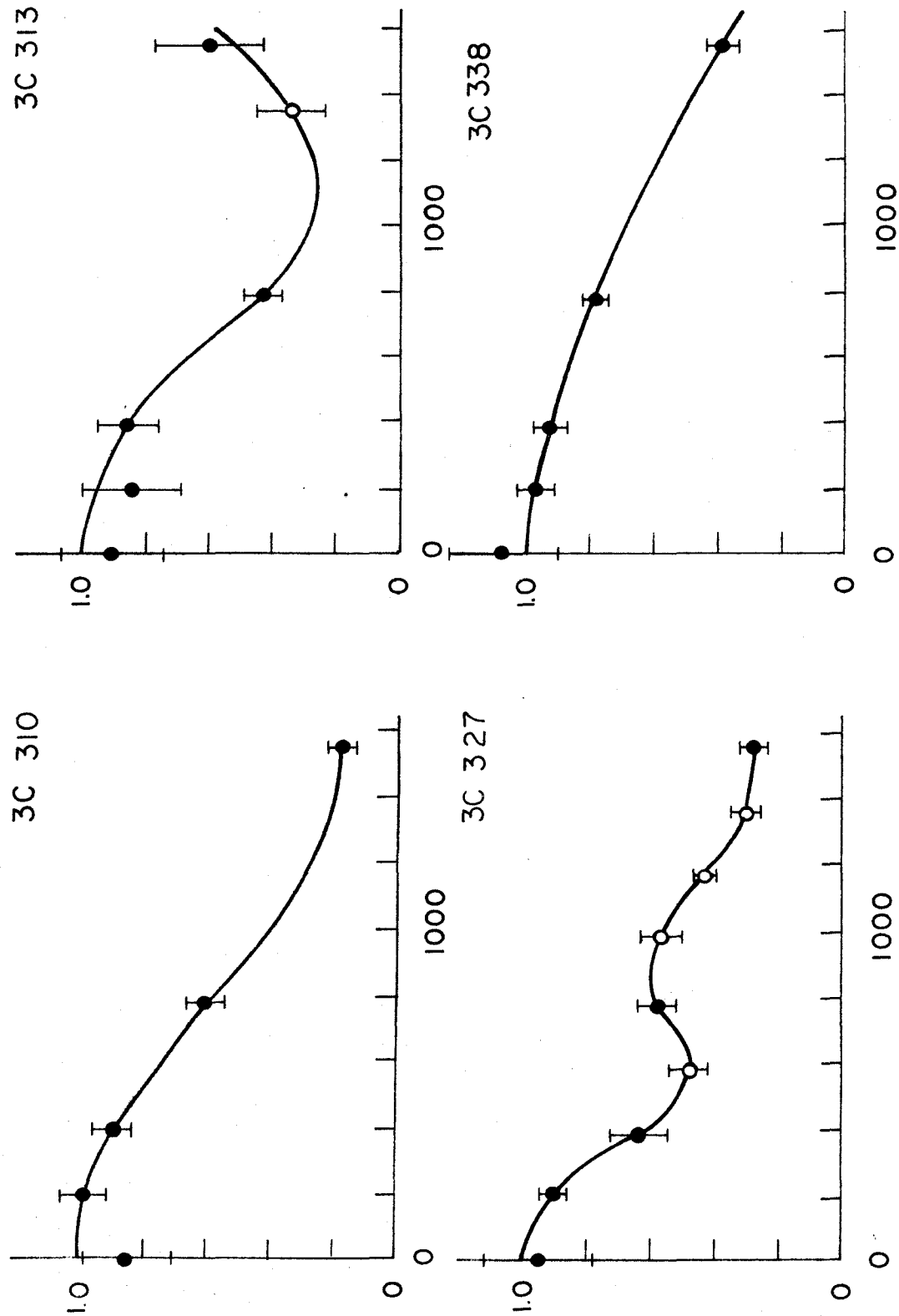

Figure 12. Visibility amplitudes for 3C 310, 3C 313, 3C 327, and 3C 338. Abscissae are effective antenna spacings, in wavelengths.

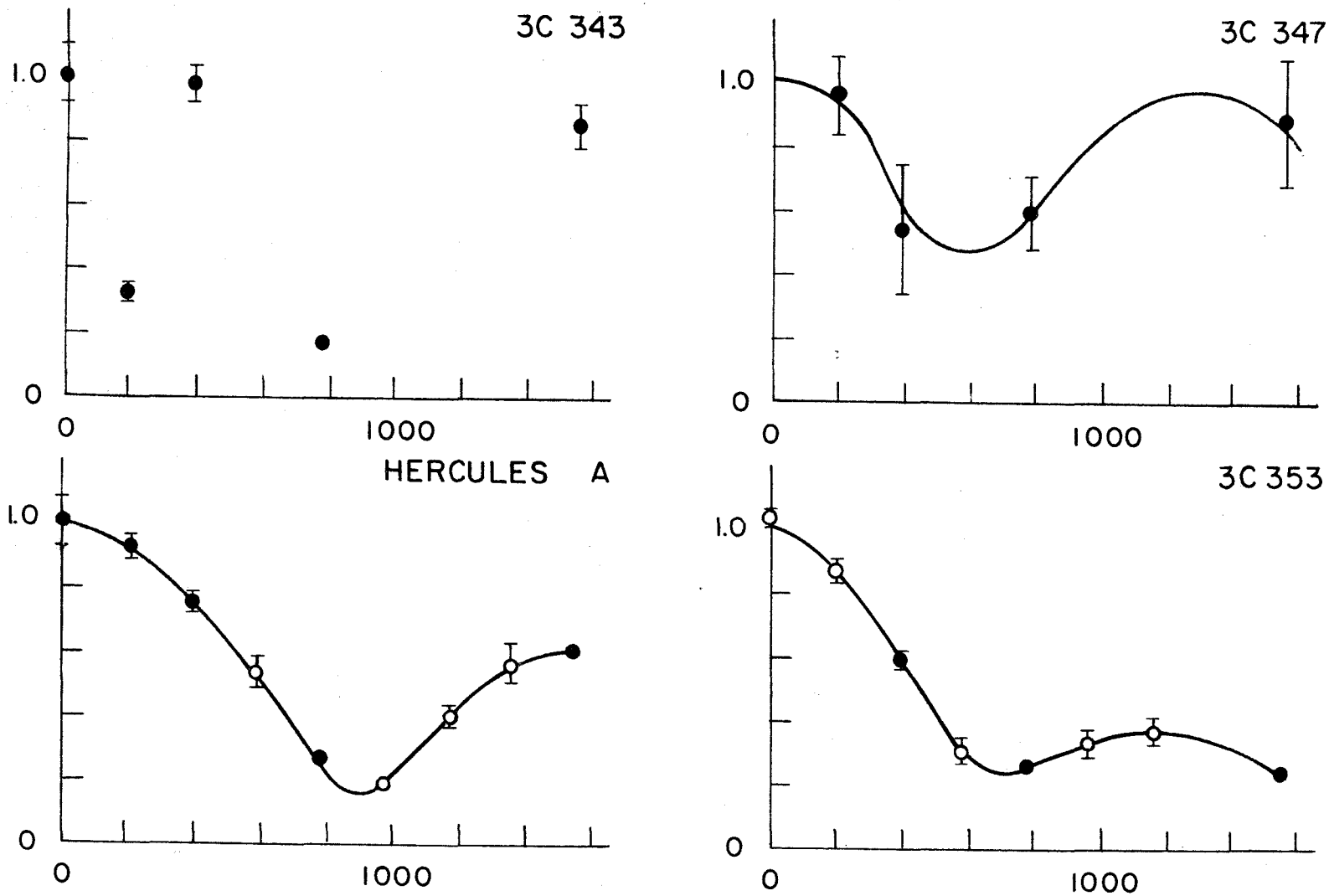

Figure 13. Visibility amplitudes for 3C 343, 3C 347, Hercules A, and 3C 353. Abscissae are effective antenna spacings, in wavelengths.

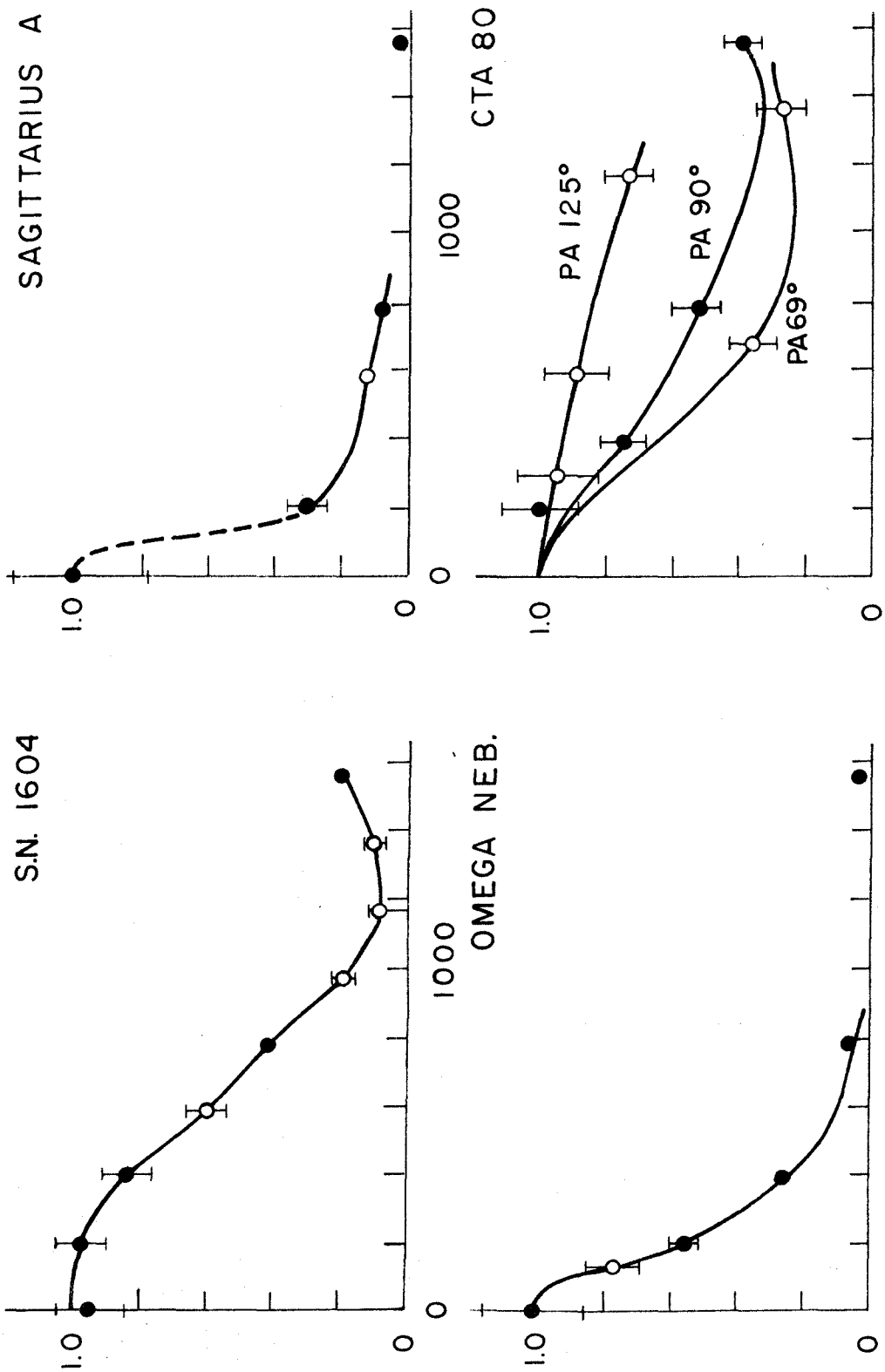

Figure 14. Visibility amplitudes for SN 1604, Sagittarius A, the Omega Nebula, and CTA 80. Abscissae are effective antenna spacings, in wavelengths.

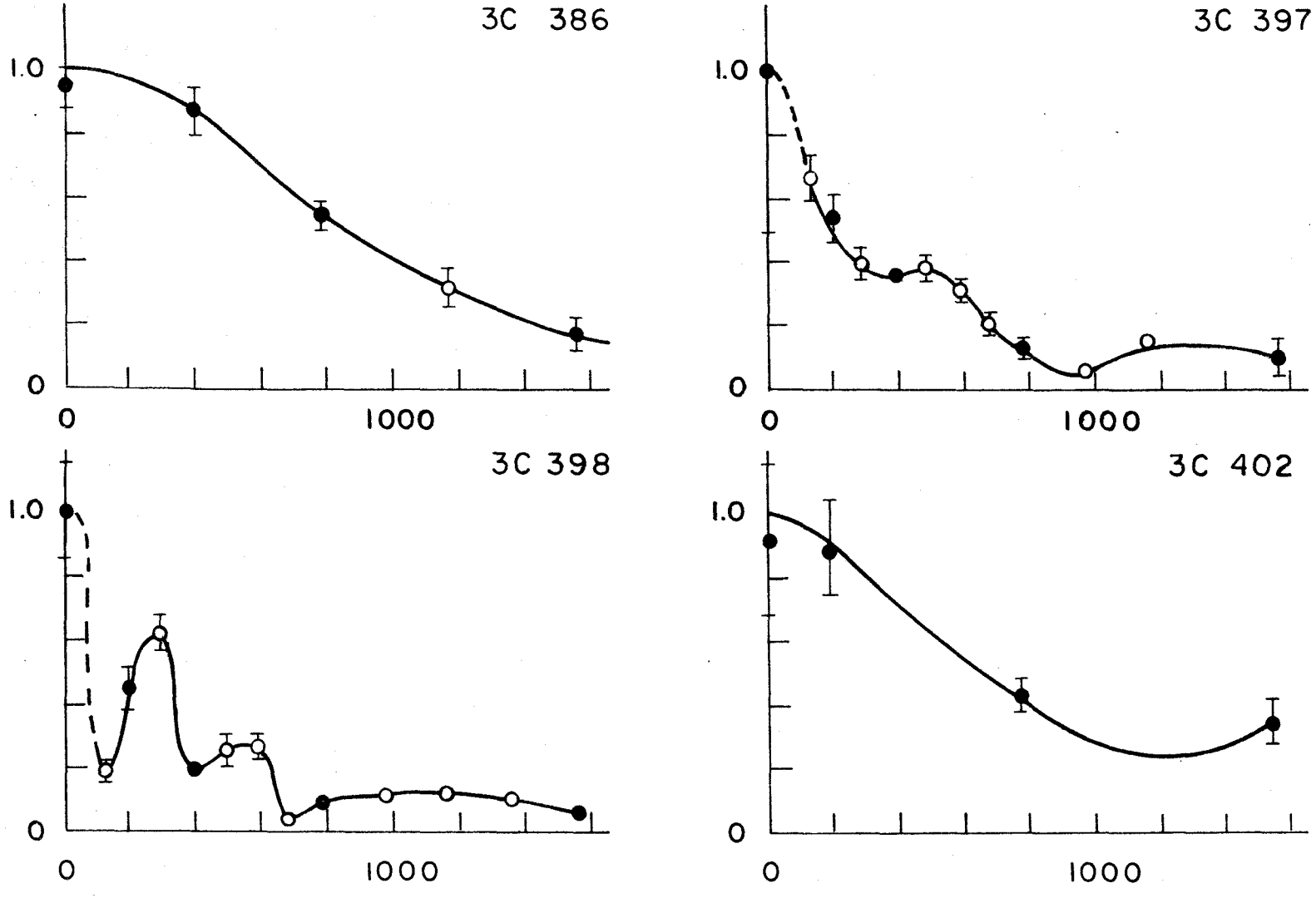

Figure 15. Visibility amplitudes for 3C 386, 3C 397, 3C 398, and 3C 402. Abscissae are effective antenna spacings, in wavelengths.

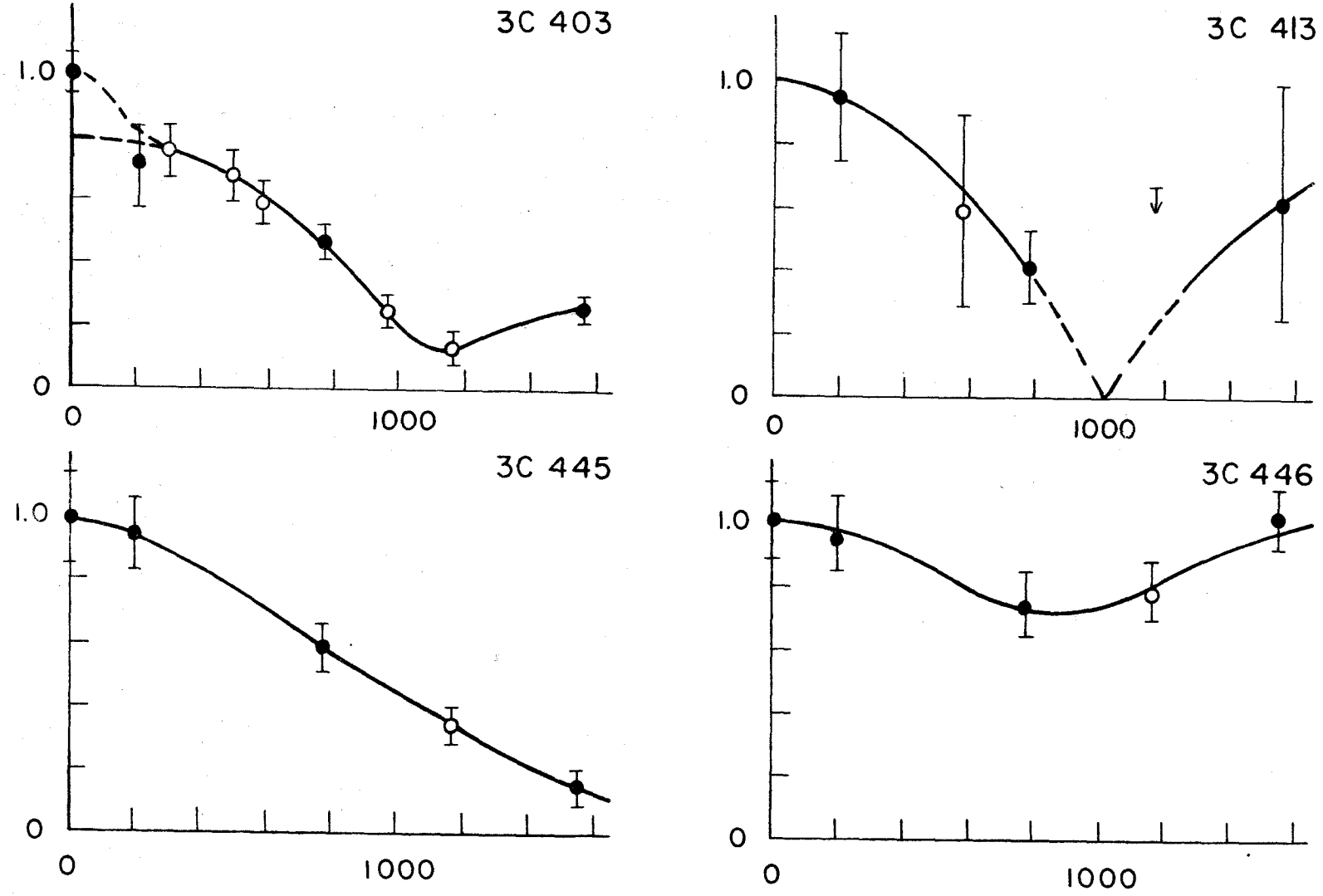

Figure 16. Visibility amplitudes for 3C 403, 3C 413, 3C 445, and 3C 446. Abscissae are effective antenna spacings, in wavelengths.

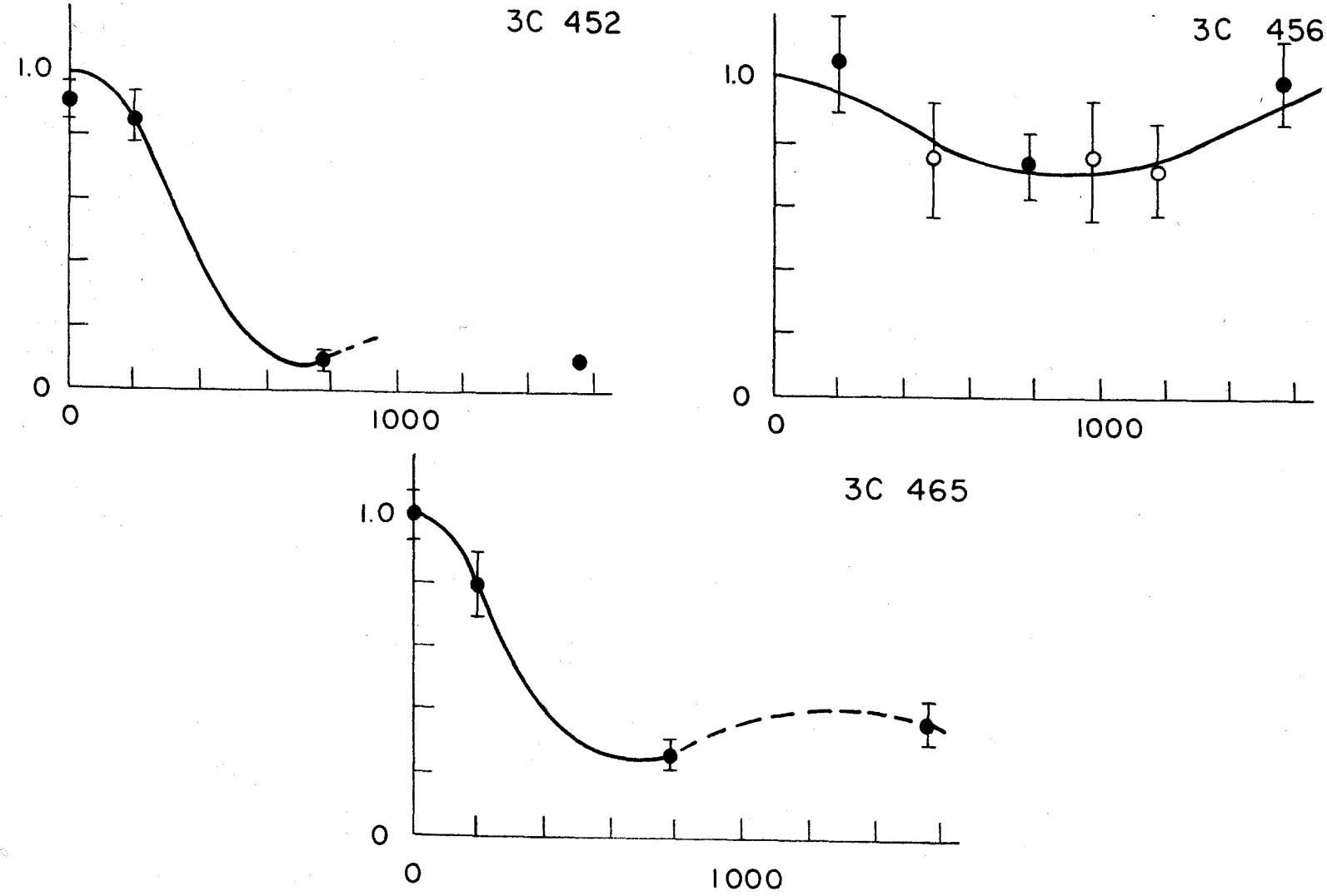

Figure 17. Visibility amplitudes for 3C 452, 3C 456, and 3C 465. Abscissae are effective antenna spacings, in wavelengths.

CHAPTER V

Interpretation

The observed data on the visibility functions have been presented in the previous chapter. We now consider the interpretation of these data in terms of the source brightness distributions. The method used has been that of model fitting, as described in Chapter II; the models which were employed are worked out in the Appendix. Although a few of the sources are not well suited to this method of analysis, it has been decided to postpone any efforts at numerical integration of the visibility functions until the results from the east-west baseline reported here can be combined with Maltby's results from the north-south baseline.

The reason for this decision is that in many cases the two visibility functions complement each other, and a much more satisfactory interpretation can be made if both are considered together. Because of improvements which have been made in receiver performance, the errors in the north-south measurements are generally smaller than in those reported here. Thus the north-south data can often be helpful in pointing out features of the east-west visibility functions which were partially masked by the uncertainty in the observed points. The east-west measurements, however, were made at a greater number of effective spacings than could be used north-south. These

extra points on the visibility curve are often very helpful in determining the structure of a moderately complicated source, and once the general type of structure is known, the interpretation of the north-south data is made easier. Inasmuch as both sets of data now exist, exhaustive analysis of either set by itself would be pointless.

The sources were analyzed in the following manner: For each source the visibility amplitudes were plotted on a sheet of graph paper as a function of effective antenna spacing. A smooth curve was steered as nearly as possible through the transit points and any of the off-transit points for which the rotation of the fringes could be neglected. If there were one or more groups of observations having a common, non-negligible value of the rotation angle ρ, a separate curve was drawn for each group. The curves representing the calculated models were then compared with the observed visibility curves, and a tentative model assignment was made. Since the phase information was not available for all effective spacings, and since the errors in the phases were rather large, this information was used primarily to confirm the tentative model assignment or to decide between possible models. Parameters in the model were adjusted to give the best fit to the observed data. Because of the uncertainty in the observed values of the visibility function, an adequate fit could be obtained for a range of values of the model parameters, and this range was noted.

In figures 18 and 19 are shown examples of the fits for two sources. The observed data on the visibility function for NGC 5128 are shown in figure 18. The curves are those for a model consisting of two circular Gaussians of equal intensity, spaced 5.'6 apart. The components have individual diameters of 2.'0. The fit of the phase at 1557λ is fortuitous, since the source is very heavily resolved at that spacing, and relatively insignificant structural details (contributing perhaps 5% of the total flux) could combine to give almost any phase. The departure, at the observed point near the first minimum, of both the amplitude and phase from the calculated curves indicates some difference between the source and the model. The region of a minimum is very sensitive to any such differences, since the major components of the source have there largely canceled each other out. Because the observed points are so widely spaced, the visibility function is not completely determined, and the uncertainties in the final description of the source are correspondingly increased.

The observed amplitudes and phases for 3C 353 are shown in figure 19. This source is within one degree of the equator; therefore, the observations at any effective baseline can be combined directly with the transit observations, since the fringe rotation will be negligible. The curves are those for a model consisting of two circular

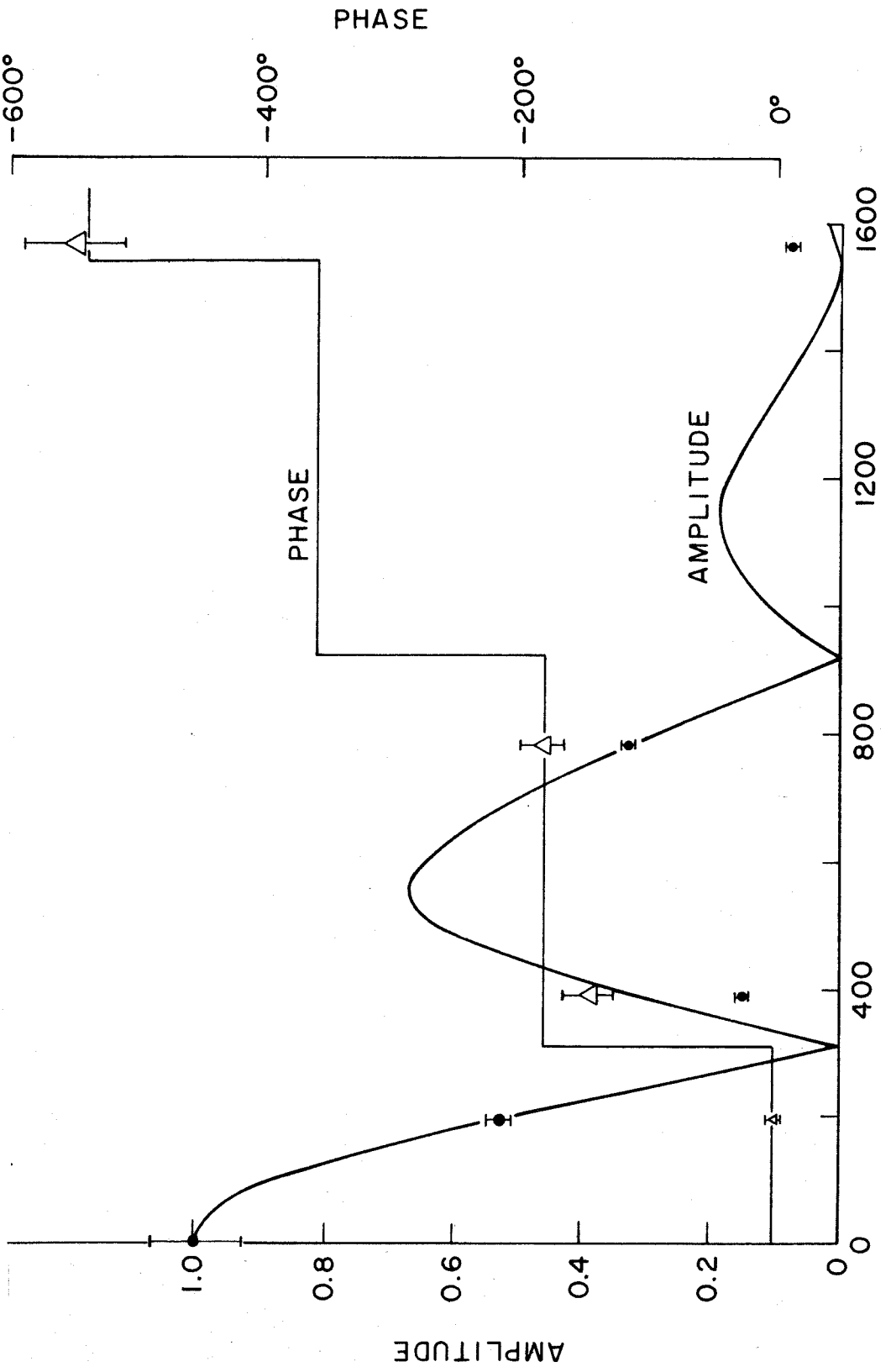

Figure 18. Illustration of the model fit for NGC 5128. See text for details.

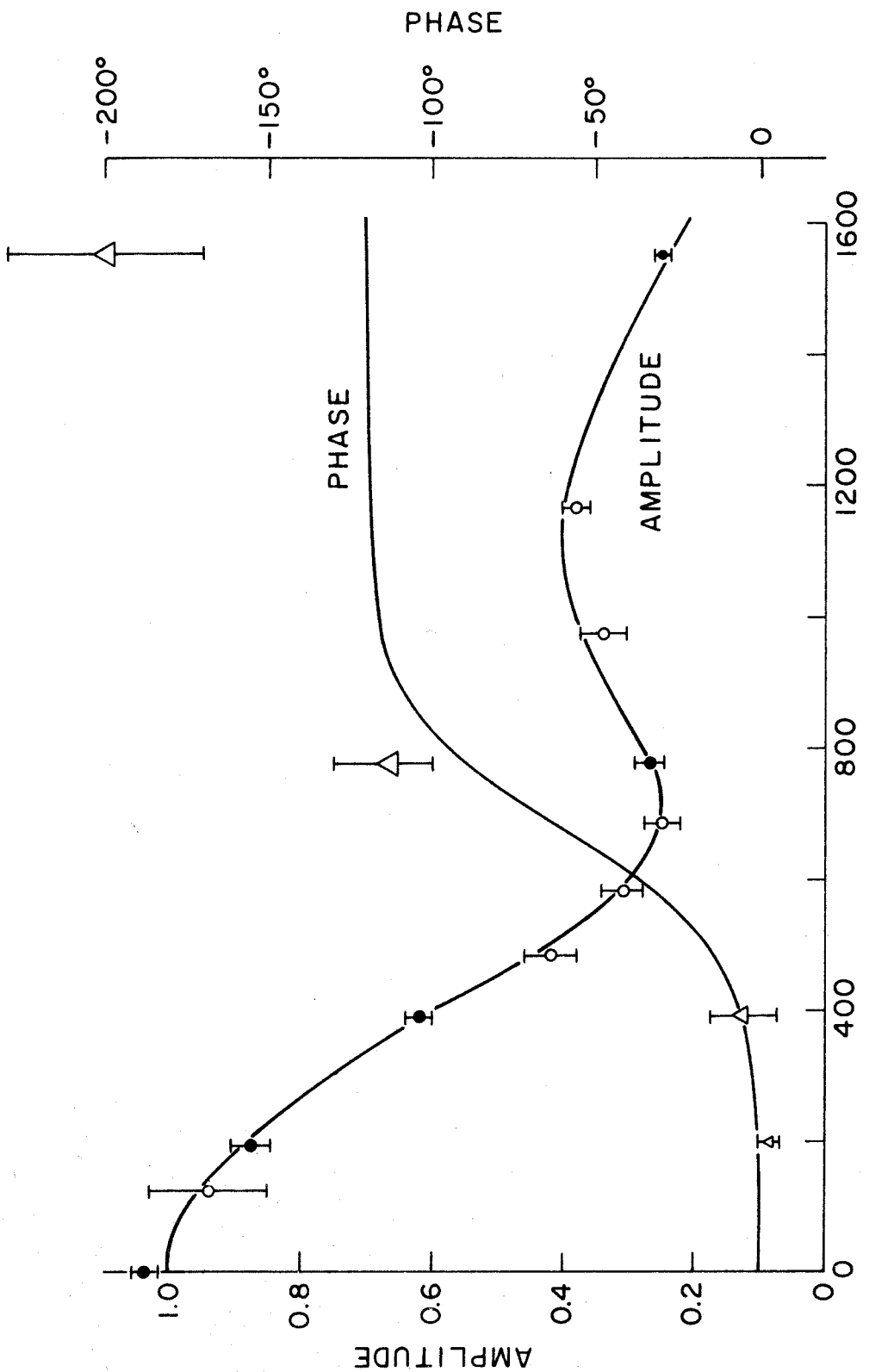

Figure 19. Illustration of the model fit for 3C 353. See text for details.

Gaussians with individual diameters of 1'.4. The ratio of their intensities is 2.0 to 1, with the stronger source 3'.0 east of the weaker one. The phase values have been adjusted for best fit by assuming that the centroid of the source lies 0^{s}.6 east of Matthews' 195λ position, which is just beyond the limit of his quoted mean error. Thus the phases plotted differ from those given for 3C 353 in table 5 by a linear function of antenna spacing. The departure of the 1557λ point from the calculated phase curve is not considered too serious, since the source is fairly well resolved at this point. A more exact knowledge of the phase variations between spacings of 779λ and 1557λ would clearly be desirable.

Description of the Sources.

When models had been fitted to all the sources, it was evident that they could be divided into several categories. Many sources were unresolved or barely resolved, having diameters of less than 1'.5. Their visibility amplitudes remained close to unity at the largest spacing. For these sources a diameter, or an upper limit on a diameter, was assigned on the basis of a circular Gaussian model. The resultant diameter value is that of the half-brightness contour in the Gaussian which has the same second moment as does the source along its east-west axis (see equation 31). A few sources showed a smooth decline of the visibility amplitude to low values with no very large phase shift.

These were fitted by Gaussian models having diameters between 1'.5 and 2'.5. An example of such a source is 3C 445, the visibility amplitude for which is given in figure 16.

A majority of the well-resolved sources showed more complicated structure. Some were fitted by models with two equal components, while others were fitted by asymmetrical models with two unequal components. In some of the double sources, the position angle of the major axis could be determined from the off-transit measurements, since the apparent separation of the components was a function of the rotation angle ρ. A few sources were fitted by models having a sharp, small-diameter core superimposed on a broad halo. No source was found for which the data were sufficiently complex and yet were known with sufficient precision to make a three-component model useful. In every case the source components were adequately represented by circular Gaussians. Examples of the symmetrical and asymmetrical double sources are NGC 5128 and 3C 353, which have been discussed previously. The core-and-halo is typified by M 87, for which the visibility amplitude is given in figure 11.

A final category, labeled merely "complex", contained sources which obviously had complicated structure, but for which the observations were not sufficient to determine the structure in detail. Some of these were faint sources for which the errors were large. Others were sources for

which observations had not been taken at enough spacings, either because the available spacings were too widely separated or because observations were lacking at some of the spacings. An example of a "complex" source is 3C 129.

The sources were also divided rather arbitrarily into two groups, those of extragalactic, and those of galactic origin. Small-diameter ($< 3'$) objects with normal non-thermal spectra were included in the extragalactic group, even when found at low galactic latitudes, while large-diameter objects occurring near the galactic plane, and generally also having abnormally flat spectra, were considered to be of galactic origin. The source 3C 48 was included in the galactic group on the basis of its identification with a peculiar star (46).

The distribution of the 110 presumably extragalactic sources among the structural categories described above is given in table 10.

The 17 galactic sources have been classified somewhat differently, as is shown in table 11. The sources in the last two categories of table 11 are all H_{II} regions, as far as is known, except for one large supernova remnant, Puppis A. Each of the four small supernova remnants consists of a single main center of emission, but each displays some indication of smaller-scale structure as well. The H_{II} regions are generally rather complex. Accurate measurements of amplitude and phase at frequent intervals in the range of spacings from 0 to 800λ will be necessary for an

adequate description of most of these objects. Some of them have been observed by Wilson with the north-south interferometer and will be discussed in his thesis (57).

Table 10

Classification of the 110 Extragalactic Sources

Category	Number
Diameter $< 1'.5$	63
Simple: diameter between $1'.5$ and $2'.5$	4
Core and halo	5
Symmetrical double: intensity ratio < 1.3 to 1	11
Asymmetrical or unequal double: intensity ratio ≤ 1.3 to 1	15
Complex	12

Table 11

Classification of the 17 Galactic Sources

Category	Number
Peculiar star	1
Small supernova remnant	4
Others: diameter $< 10'$	5
Others: diameter $\geq 10'$	7

The interpretations of the individual sources are given in tables 12 and 13. All values tabulated in the

diameters column refer to a circular Gaussian model, as has been explained above. Other structural details, where known, are given in the comments column. Most of the dimensions quoted are accompanied by limits. These are based on the range of the model parameters over which the model will give a satisfactory fit to the observed visibility function. The probability that the dimensions of the major features of a source lie within the quoted range is estimated as 80%. Additional comments are needed for a few sources, and these are given in the next section of this chapter.

The information in tables 12 and 13 should not be used without some regard for the way in which it was derived. In each case it describes a model which has a visibility function which fits that of the source within the range of the observations and within the observational uncertainty. Interpretation of the source by this method will ignore any structural details which would cause only slight changes in the observed part of the visibility function. For example, if the uncertainty in the visibility amplitude were ± 0.10 at all the measured points, it would be possible to have about 10% of the emission from the source distributed almost arbitrarily within a box centered on the main part of the source and up to 10' wide in the east-west direction by as much as 40' north-south. This type of uncertainty is common to all the sources, and some may very possibly have faint features which were over-

Table 12

Diameters and Comments on Structure for the

Extragalactic Sources Observed

Source	Diameter	Comments
3C 2	< 0!5	
3C 15	1!2± 0!5	
3C 17	< 1!5	poor data
3C 20	< 0!7	
3C 26	< 0!7	
3C 28	< 0!7	
3C 33		Has components <1!2, indication of larger-scale structure.
3C 38	0!7± 0!2	
3C 40		2 sources, relative intensities 3±1 and 1, stronger source to east, separation 4!4± 0!6.
3C 41		Components < 1!2, data insufficient to exclude larger-scale structure.
3C 46	2!0± 1!0	possibly 2 sources
3C 63	< 0!8	
3C 66		2 sources, relative intensities 3±1 and 1, stronger source to east, separation 6'±1'.
MSH 02-110	< 1!0	
3C 71	< 0!5	
3C 75		2 sources, equal intensities ±25%, equal diameters 1!2± 0!2, separation 2!0± 0!2.
3C 78	1!0± 0!5	
3C 79	1!2± 0!2	
CTA 21	< 0!8	
NGC 1275		4!5 halo with 15% of flux, core diameter < 0!5.
Fornax A	> 15'	
3C 89		Probably 2 sources ≈6' apart, relative intensities about 3 and 1, diameter of stronger source <1!0.
CTA 26	< 1!2	
3C 98		Possibly 2 sources of unequal intensities, separation 2!5, diameter of stronger ≈1!2.
3C 103	< 0!5	
3C 109	< 1!0	
3C 111		2 sources, equal intensities ±15%, equal diameters 1!2± 0!3, separation 2!5 along major axis in PA 60°± 7°.
3C 123	< 0!4	standard source
3C 129		Complex source, ≥6' overall, fine structure <1'.
3C 134		2 sources, equal intensities ±15%, separation 2!0± 0!2 along major axis in PA 175°± 5°. EW diameter 0!6± 0!2.
3C 135		Complex source, overall diameter ≥ 4', fine structure < 1'.

Table 12 Continued

Source	Diameter	Comments
Pictor A	7!5± 1!0	some smaller scale structure
3C 147	< 0!4	standard source
3C 154	0!6± 0!3	
3C 161	< 0!4	
3C 171	< 0!7	
3C 175	0!7± 0!3	
3C 180	< 1!0	
3C 191	< 0!7	
3C 196	< 0!4	standard source
3C 198	3!5± 1!0	some smaller scale structure, possibly a 20-35% core with diameter < 1!0
3C 208		2 sources, relative intensities 4 and 1, separation 4!1± 0!5, faint component following. Both have diameters < 1!0.
3C 216	< 0!6	
Hydra A	< 0!7	possibly a 4' halo with 10% of flux
3C 219		2 sources, equal intensities ±20%, both diameters <1!2, separation 2!0± 0!1 in PA 35°± 3°.
3C 227	2!8± 0!5	highly asymmetric with peak on the east side
3C 230		Complex structure with components < 1'.
3C 234		Complex structure, overall diameter ≈3', components < 1!2.
3C 237	< 0!6	
3C 243	< 3'	
3C 254	< 0!5	
3C 264	2!0± 0!5	strong central concentration
3C 265	1!2± 0!3	
3C 270		2 sources, equal intensities ±15%, equal diameters 2!9± 0!5, separation 4!7± 0!3.
3C 273	< 0!4	
M 87		6!5± 0!5 halo with 48%± 5% of flux, core diameter 0!6± 0!2 .
Coma A	< 0!8	
3C 278	2!5± 0!5	slight central concentration
3C 279	< 0!6	
3C 280	< 0!6	
3C 283	< 0!7	
NGC 5128		2 sources, equal intensities ±30%, both diameters 2!0± 0!7, separation 5!6± 0!7.
3C 286	< 0!4	
3C 287	< 0!8	possibly a faint second source ≈9' west
3C 295	< 0!4	standard source
3C 298	< 0!5	
MSH 14+010	< 1!2	some larger-scale structure possible
3C 310	1!8± 0!2	
3C 313		2 sources, relative intensities 1.6± 0.4 and 1.0, both diameters < 1!0, separation 1!6± 0!2, stronger component to west.

Table 12 Continued

Source	Diameter	Comments
3C 315	1!0± 0!2	
3C 317	< 0!5	
3C 318	< 0!6	
3C 324	< 0!7	
3C 327		2 sources, either unequal intensities or diameters, separation 3!5± 0!5.
MSH 16+02	< 0!7	
3C 330	1!2± 0!2	
3C 338	1!2± 0!2	very nearly circular, since diameters in PA's 43° and 137° are both 1!1± 0!3
3C 343		2 sources, equal intensities ±30%, both diameters <0!7. Separation certainly ≥ 6', possible separation 11'.
3C 345	< 0!7	
3C 347		Possibly 2 sources, relative intensities 3±1 and 1, both diameters <1!0, separation 2!9± 0!6.
Herc A		2 sources, relative intensities 1.25± 0.15 and 1, equal diameters 0!7± 0!2, separation 1!92± 0!10.
3C 353		2 sources, relative intensities 2.0± 0.2 and 1, equal diameters 1!4± 0!2, separation 2!5± 0!1 with stronger component towards east.
3C 365	≤ 2!0	possibly complex structure with components <0!7
3C 380	< 0!4	
CTA 80	2!0± 0!5	highly elongated, possibly 2 sources of unequal intensity, separation 1!7± 0!4 in PA 55°± 15°
3C 386	1!9± 0!2	slight central concentration
3C 388	< 0!8	possibly a faint (≈10%) companion 3!5 away
MSH 19-16	< 1!5	
3C 401	< 0!5	
3C 402	2!0± 0!5	possibly double, with components <1' in diameter, separation 1!5± 0!3
3C 403		2 sources, relative intensities 1.2± 0.2 and 1, diameters 1!2± 0!3, separation 1!56± 0!10.
Cygnus A		2 sources, relative intensities 1.2± 0.2 and 1, both diameters 0!7± 0!2, separation 1!58± 0!10 along major axis in PA 106°± 5°. E-W separation 1!52± 0!14.
3C 409	< 0!5	
3C 410	< 0!5	
3C 413		Probably double, equal intensities ±60%, separation 1!7± 0!3.
3C 424	< 0!6	
3C 430	0!6± 0!3	
3C 433	< 0!5	

Table 12 Continued

Source	Diameter	Comments
3C 436	< 0!6	possible larger-scale structure, overall extent ≤4'
3C 438	< 0!5	
3C 444	0!6± 0!3	
3C 445	1!6± 0!3	
3C 446		Probably 2 sources, relative intensities 6± 3 and 1, both diameters <0!6, separation 1!8± 0!2.
CTA 102	< 0!6	
3C 452	4!0± 2!0	complex
3C 456		Probably 2 sources, relative intensities 6± 3 and 1, diameters <0!8, separation 1!9± 0!3.
3C 459	< 0!7	
MSH 23-112	< 0!8	
3C 465	5!0± 1!0	with fine structure
3C 469	< 1!2	

Table 13

Diameters and Comments on Structure for the

Galactic Sources Observed

Source	Diameter	Comments
SN 1572	6'± 2'	some central concentration or fine structure
3C 48	< 0!4	
3C 58	6'± 1'	some fine structure
Crab Neb.	3!3± 0!4	some central concentration
Orion Neb.	7'± 1'	strong central concentration
Puppis A	> 15'	
CTB 31	≈10'	about 35% of flux in 2' core
CTB 32	≈6'	strong central concentration
CTB 38		Complex structure, overall size >8', components <3'.
SN 1604	2!2± 0!5	considerable evidence of structure
Sgtr A	> 15'	25%± 5% of flux in 3!0± 0!5 core
Omega Neb.	6!5± 1!0	
3C 397	≥ 10'	complex, with components <2'
3C 398	> 10'	complex, 2 principal components have relative intensities 1.6±0.3 and 1, diameters 4'± 1', separation 13'± 2'
CTB 87	4!5± 1!0	complex, with some components <1!0
CTA 97	10'± 3'	
Cass A	> 3!5	

looked in this way. The possibility of confusion, as discussed on pages 48 and 49, should also be borne in mind.

As another example, a source with a quoted diameter of 1!2 might have 20% of its flux coming from a core of very small diameter or might consist of two small-diameter sources spaced 1!0 apart. The distinction between these possibilities can be made only with larger antenna spacings since the visibility functions of all three are virtually identical for spacings up to 1600λ.

Many of the double sources are described as having components with unequal intensities and equal diameters. In each of these cases it would be possible to have unequal component diameters and a slightly different ratio of intensities. Very much better and more complete phase information would be required to decide between these possibilities. In general, however, the component diameters should lie somewhere within the range quoted in table 12 or 13.

Remarks on Individual Sources

Several sources require more extensive comments than could be placed in the tables, and these are given here. In general these comments involve comparison of the present results either with information about an associated optical object or with radio information obtained at other wavelengths.

Extragalactic Sources

3C 40.-- This source has been identified by Minkowski (58) with a double elliptical galaxy, NGC 545-47. The radio object is also double, with the centroid falling between NGC 545-47 and another galaxy 4!5 to the southwest. The radio separation is somewhat greater than the optical separation, but all three galaxies may be involved in the source.

3C 66.-- Minkowski (quoted in CTA) has identified this source with an elliptical galaxy having a jet similar to the well-known one in M 87. As in 3C 40, the radio object is double, with one component probably associated with Minkowski's peculiar galaxy. It is a rich field, and there are several other galaxies in the vicinity, but none seems to be in the position of the second component (46).

Fornax A.-- Known to be associated with NGC 1316, this source has been investigated by Wade, using an 18' pencil beam at 10 cm (59). Wade finds that it is an unequal double, with components separated by about 13'. It is too large for study with the antenna spacings used in the present work, but the very low visibility amplitudes which were observed suggest that the two components have smooth brightness distributions and do not contain small, bright cores.

Pictor A.-- This source might be a symmetrical double with a separation of 4!6 ± 0!5 and component diameters >2', but the phase observed at the 779 spacing does not agree

with this interpretation. Maltby finds a north-south diameter of <2', which suggests a very elongated source, if not a double one.

3C 219.-- This source definitely has two components, but the observations reported here do not exclude the possibility of a 5' separation in PA 166°. Maltby's north-south observations confirm the alternative orientation of PA 35°, which is given in table 12.

M 87.-- Comparison of the 3 m observations of Mills (22) and the 21 cm observations of the Nancay group (31) with the present results shows that the core becomes less prominent with increasing wavelength. Over this range of wavelengths, the core has a spectral index of about -0.3, while the halo has a steeper spectrum with an index of about -1.0. The core is presumably to be identified with the jet, which optically has a length of 20" and projects in PA 290° from the center of the galaxy (60). The halo is somewhat larger in diameter at 21 cm than at 31 cm or 3 m -- 10' at 21 cm, versus 6'.5 at the two longer wavelengths.

NGC 5128.-- This source has two major parts, a compact core and a very extended halo, the latter being more than 4° across. The brightness distribution within the halo has been measured at various wavelengths with pencil-beam antennas, and is found to consist of two diffuse centers of emission (61,62). The flux listed in table 4 is that which Bolton and Clark find for the core at 31 cm (62).

The central source has been shown in the Sydney observations at 21 cm (36) to also consist of two, roughly equal components with an east-west separation of about 5'. This structure is confirmed by the present measurements at 31 cm, which place the separation at $5'.6 \pm 0'.7$. Observations at 10 cm by Little, with a $2'.3$ fan beam (63), also show the twin-peaked structure but with a separation at that wavelength of $4'.6$. The intensity ratio of the two components of the central source is 1.5 to 1 at 10 cm, while at 31 cm it is no more than 1.3 to 1. It would seem that both the spacing and the relative intensities of the two components change with the wavelength of observation. The early study of this source by Mills at 3 m (22) was seriously disturbed by the presence of the extended halo in the primary antenna beam, but it did suggest that the central source is elongated in PA 130°.

3C 343.-- There is a possibility that this is a chance association of two small-diameter sources. The north-south separation is not known and might be quite large.

Cygnus A.-- This is the most completely investigated of all the extragalactic radio sources. In 1953, Jennison and Das Gupta (64) discovered that at a wavelength of 2.4 m it appears to consist of two, roughly equal components. In 1959, Rowson (29) showed that it has a similar structure at 10 cm. The identification with a distant pair

of galaxies was made by Baade and Minkowski in 1954 (65). In the present study, it happened that observations were made only in the range of spacings near the first minimum in the visibility function. Given a two component model, they were sufficient to determine the separation of the components and the position angle of the major axis. A summary of these and similar measurements at other wavelengths is given in table 14.

Table 14

Features of Cygnus A Observed at Different Wavelengths

Wavelength	Observing Group	Reference	E-W Separation	PA of Major Axis
2.63 m	Jodrell Bank	(35)	1'.34	97°
31.3 cm	Caltech	--	1'.52 ± 0'.14	106° ± 5°
21.1 cm	Nancay	(31)	1'.52	--
21.0 cm	Sydney	(36)	1'.47	--
10.7 cm	Jodrell Bank	(29)	1'.59 (derived from 1'.69 in PA 109°)	109° ± 2°

The results contained in table 14 indicate that as the wavelength of observation increases, the two components appear to draw together and to rotate toward an east-west orientation.

Jennison and Latham (35) found that the two components of the source differed in intensity by 20%, with the

stronger component toward the west. This result was based on the phase measurements at antenna spacings of 1540λ and 2160λ east-west. In the present work, the phase measured at the 1557λ spacing indicates a ratio of component intensities of 1.3 ± 0.3 to 1 but with the inequality in the opposite sense, i.e. with the stronger component toward the east. Although no analysis of the source is given in the preliminary Sydney paper (36), the 21 cm phase measurements reported there agree with the 31 cm result. Thus a third change in the structure of the source as a function of wavelength would seem to be indicated. It is worth noting that the different sets of phase measurements agree on other sources, at least within their errors.

Galactic Sources

Crab Nebula.-- Both the amplitude and phase are in agreement with the Sydney results, provided the Sydney phases are renormalized to zero at a spacing of 195λ to correspond with the normalization used in the present measurements.

Orion Nebula.-- The remarks for the Crab Nebula also apply here. The diameter quoted in table 13 is that of the Gaussian with the same second moment as that of the source. Since a Gaussian was such an obviously bad fit to the visibility curve, an approximate numerical inversion was done by hand. The result is a distribution with broad

wings which blend into a relatively sharp central concentration. The diameter at half-intensity is 3'.5.

Sagittarius A.-- The results are in agreement with those of the Nancay group (31), though the Nancay results are more meaningful for such a large source because they are based on observations taken with smaller antenna spacings.

CTA 97.-- A possible identification with an H_{II} region, IC 5146, is suggested in CTA. The radio diameter, which agrees with the optical diameter of IC 5146, confirms the identification.

Cassiopeia A.-- The data obtained was fragmentary, but the phases at 779λ and 1557λ agree very well with those measured by Jennison and Latham (35) at 2.4 m, suggesting little change in structure with wavelength.

The Complex Nature of the Sources

The work reported here has yielded a ten-fold increase in the number of extragalactic radio sources for which brightness distributions are known in some detail. Excluding normal galaxies such as the Clouds of Magellan or M 31, detailed brightness distributions have previously been available only for Cygnus A, M 87, NGC 5128, and Fornax A. Forty-seven of the objects included in the present study were well enough resolved to give a fair idea of their structure, at least along an east-west axis.

A most important characteristic of these 47 sources

is apparent on consideration of their distribution among the last four categories of table 10. Only four sources display a simple, smooth brightness distribution*. The remaining sources all have complex structure of one sort or another. Although the sample is small, and may not be fully representative**, this result certainly suggests that the majority of the extragalactic sources cannot be represented by simple symmetrical brightness distributions. Detailed observations with longer baselines will be required to fully test this suggestion on the many sources which were not resolved in the present study. However, it receives strong support from observations at Jodrell Bank (47) of the 64 sources in the list of Elsmore, Ryle and Leslie (39). At Jodrell Bank, the visibility amplitudes for these sources were observed at about 2 m wavelength, using east-west antenna spacings of 310λ, 2200λ, and 9700λ. Of the 59 extragalactic sources in the list, 27 were among those which were observed but not resolved in the present study at 31 cm. Of these, 8 were not well resolved at even the 9700λ spacing. For 14 of the remaining 19 sources, it

---

*Furthermore, Maltby has observed three of these, and found two to be complex along a north-south axis! The only source for which he confirms a simple structure is 3C 278.

**One may argue that the sources observed were not a representative sample since they were mainly selected from a catalog (3C) which excludes sources of large angular diameter. The seriousness of this effect is now being argued (66), but it seems unlikely that more than 20% of the sources in the regions covered by 3C, and above the 3C intensity limit, could have been excluded.

was necessary to assume at least two components in order to explain the observed visibility amplitudes. Since the observations were not made at a sufficient number of spacings to give a detailed indication of the structure of the sources, it is probable that some sources with complex structure were overlooked. Thus it would seem that the tendency toward complex structure is not a characteristic peculiar to the 47 relatively large-diameter sources which were resolved in the present study.

About thirty of the extragalactic sources described in table 12 have been identified with optical objects (41,46, 58,65,67,68,69). A comparison of the radio and optical structures of these objects was made in the hope that some reason for the high incidence of radio complexity might be apparent. The results were inconclusive. It appears that a complex radio source can be associated with either a single or a multiple galaxy, while the one source known to have a reasonably simple radio structure, 3C 278, is associated with a double system, NGC 4782-83. In some cases, notably 3C 40 and 3C 66 (which were discussed above), the components of a multiple radio source may be associated with separate members of a cluster of galaxies. However, 3C 270 is a complex source which is associated with a single member of the Virgo cluster, NGC 4261. The number of identified sources is still too small for valid statistical conclusions to be drawn about the frequency of the

various combinations of radio and optical structure.

It is interesting to consider this result, namely, that most of the extragalactic radio sources are complex, in terms of the available theoretical explanations of such objects. These theories can be grouped into two general schools, the "colliding galaxies" school and the "internal sources" school. The first of these was founded by Baade and Minkowski when they identified Cygnus A with a pair of very distant galaxies (65). The optical spectrum of this object displayed very powerful emission lines, and Baade and Minkowski concluded that the source of excitation was a collision between the two galaxies. Minkowski has also cited NGC 1275 as an example of a galactic collision which is associated with a radio source (70). A quantitative analysis of this process in Cygnus A was given by Shklovsky in his text (71). He concluded that the radio source was generated by a collision of the gaseous coronas of two spiral galaxies and that the two centers of radio emission were the recoiling, highly excited coronas.

Since this theory provides an easy explanation for the many radio sources in which there are two well-separated centers of emission, it is quite satisfactory in the light of the present observational result. Asymmetrical double sources would presumably arise from collisions of different-sized galaxies. However, this theory has severe difficulty in providing sufficient energy to account for the observed radio emission in sources such as Cygnus A. Burbidge (72)

has shown that the total energy of magnetic fields and high energy particles in Cygnus A must be $\sim 10^{60}$ ergs. The total kinetic energy of the collision can be at most $\sim 10^{61}$ ergs, provided a collision is taking place. There seems to be no known mechanism for the conversion of even a few percent of the collision energy into fields and particles in the radio corona. Another difficulty is that there are radio sources which are identified with single galaxies, for example M 87 and NGC 1316. The collision theory has never provided an explanation for these objects.

The other school, which relies on internal energy sources, is now headed by Shklovsky, who has abandoned his previous explanation of Cygnus A. Even in his text, Shklovsky gave an explanation for the optical jet and the radio emission from M 87 in terms of an internal process. At that time he suggested that collisions of individual stars in the nucleus of this galaxy were capable of supplying the necessary energy (73). In a more recent article (74), Shklovsky proposes an explanation for all radio galaxies in terms of a different energy source. He argues that many radio sources are associated with galaxies of greater than average luminosity, a fact which has also been noted by Bolton (69). During the early life of a giant system it is possible that the number of supernova explosions is very great, and much greater than in a less massive galaxy. In Shklovsky's view, a sufficient number

of supernova explosions could occur to provide the energy necessary to account for the emission in the strongest radio sources. Shklovsky's explanation for the extended regions of radio emission in Cygnus A and NGC 5128 is that clouds of relativistic electrons and hot gas leak out along the lines of the galactic magnetic field and expand rapidly away from the main galactic mass. In the jet of M 87 we presumably see such a breakout of highly excited material.

An attractive feature of this theory is that successive escapes of material could presumably lead to a variety of shapes for radio sources. For instance, the halos in NGC 5128 and in M 87 might be due to previous emissions and the central sources in both these galaxies to current activity within the nucleus.

It would seem that the observed complexity of the radio sources can be satisfactorily explained by either type of theory. In fact, both theories are at present couched in such general terms that they can explain almost any type of radio structure. More detailed theories will presumably result when distances, physical dimensions and surface brightnesses as a function of wavelength are known for a greater number of radio sources. Any future theory should provide some explanation for the predominance of radio sources having two major components.

Concluding Remarks

Because so many sources are highly elongated double

objects, it is clear that measurements of source structure made with only a single baseline orientation are incomplete. A preliminary comparison of the data in table 12 with those resulting from Maltby's north-south observations shows that a large number of the sources have very different diameters in the two directions. For this reason, further study of the implications of the brightness distributions will be made only after the results of the two investigations have been combined to yield a maximum of information about each source.

It is expected that the Caltech interferometer will be used for further measurements of brightness distributions. Additional observing stations have been constructed which will permit measurement of the visibility function, at transit, at additional antenna spacings. The stability and sensitivity of the receiving equipment will be improved, as will the techniques of data handling. Measurements will almost certainly be made at a shorter wavelength, thus reducing the size of the primary beam pattern and lowering the confusion limit.

An important suggestion for possible further investigations comes from the three extragalactic sources for which there were studies comparable to the present measurements, but at other wavelengths. In each case significant changes in structure with wavelength were noted. It will be recalled that in M 87, and possibly also in Cygnus A

and in NGC 5128, the principal components were found to have different spectral characteristics. In the latter two sources, the relative positions of the two components were also found to change. This strongly suggests that all those sources studied here should be studied in detail at other wavelengths as well. Detailed knowledge of the radio spectra of the various features of the sources will afford us a much better knowledge than we now have of the physical processes and conditions involved in these objects. The present work is a first step toward that goal.

APPENDIX

Model Sources

As was indicated in Chapter II, model fitting is a valuable method for the interpretation of measured visibility functions. Presented here are the visibility functions calculated for certain simple models. We have assumed models which are either circularly symmetric or which have circularly symmetric components. In these cases the orientation of the baseline enters in an obvious way, and the one-dimensional analysis is essentially general.

The visibility function for a source distribution $T(x,y)$ is given by equation 19. We may re-write this equation, replacing the exponential within the integral by its equivalent trigonometrical form.

$$(41)\quad V(s_x,s_y)e^{i\Phi(s_x,s_y)} = \frac{\int T'(x,y)\begin{bmatrix}\cos 2\pi(s_x x+s_y y)\\ +i\ \sin 2\pi(s_x x+s_y y)\end{bmatrix} dx\ dy}{\int T'(x,y)\ dx\ dy}$$

We will evaluate this for the chosen models, using the one-dimensional modification of equations 26-28, i.e. we assume $s_y = 0$.

Circular Gaussian

We consider the visibility function for a circular Gaussian "mound". Let us define

$$T(x,y) = T\, e^{-\left(\frac{x^2+y^2}{\sigma^2}\right)}$$

$$A(x,y) = A\, e^{-\left(\frac{x^2+y^2}{a^2}\right)} \qquad (42)$$

$$T'(x,y) = A(x,y)T(x,y) \quad .$$

Here σ is the dispersion of the Gaussian source, equal to 0.610 times the half-brightness diameter d. Also, a is the dispersion of a Gaussian representing the primary power response pattern of the antenna. Then $T'(x,y)$ is given by

$$T'(x,y) = T\, A\, e^{-(x^2+y^2)\left(\frac{1}{\sigma^2}+\frac{1}{a^2}\right)} \quad . \qquad (43)$$

Since the source is symmetric about the origin, the sine transform term in equation 41 vanishes, and since we assume $s_y = 0$, the y dependence factors out. We are left with a one-dimensional visibility function of the form of equation 28:

$$V(s_x)\, e^{i\Phi(s_x)} = \frac{\int e^{-x^2\left(\frac{\sigma^2+a^2}{\sigma^2 a^2}\right)} \cos 2\pi s_x x \, dx}{\int e^{-x^2\left(\frac{\sigma^2+a^2}{\sigma^2 a^2}\right)} dx} \quad , \qquad (44)$$

or

$$V(s_x) = e^{-(\pi s_x \sigma)^2\left(1+\frac{\sigma^2}{a^2}\right)^{-1}} \quad , \quad \Phi(s_x) = 0 \quad . \qquad (45)$$

As is well known, the Fourier transform of a Gaussian is itself a Gaussian. For the Caltech 90 ft antennas operating at 31.3 cm, the primary beamwidth to half power is 48', corresponding to $a = 28.8$ or 0.0084 radians. The visibility

amplitude from equation 45 has been plotted in figure 20 for source diameters between 0'.3 and 30'. The correction for the primary beamwidth is significant only for sources 10' in diameter or greater. Since it is difficult to include this correction in the calculation of other types of models, we will neglect it and consider only models with diameters of 10' or less.

Uniformly Bright Disk

The visibility functions for this model and for various limb-darkened disk models have been calculated by Michelson and Pease (75). Here we include only the uniform disk. Let r be the radius of the disk, and let T(x,y) be defined by

$$T(x,y) = \begin{cases} T & \text{for } (x^2 + y^2) \leq r^2 \\ 0 & \text{for } (x^2 + y^2) > r^2 \end{cases} \tag{46}$$

Again, because of symmetry the sine transform vanishes, and the phase Φ must be either 0 or π. We can dispense with Φ if we allow negative values of V. We have

$$V(s_x) = \frac{\int_{-r}^{r} \int_{-\sqrt{r^2 - x^2}}^{\sqrt{r^2 - x^2}} T \cos 2\pi s_x x \, dy \, dx}{\int_{-r}^{r} \int_{-\sqrt{r^2 - x^2}}^{\sqrt{r^2 - x^2}} T \, dy \, dx} \tag{47}$$

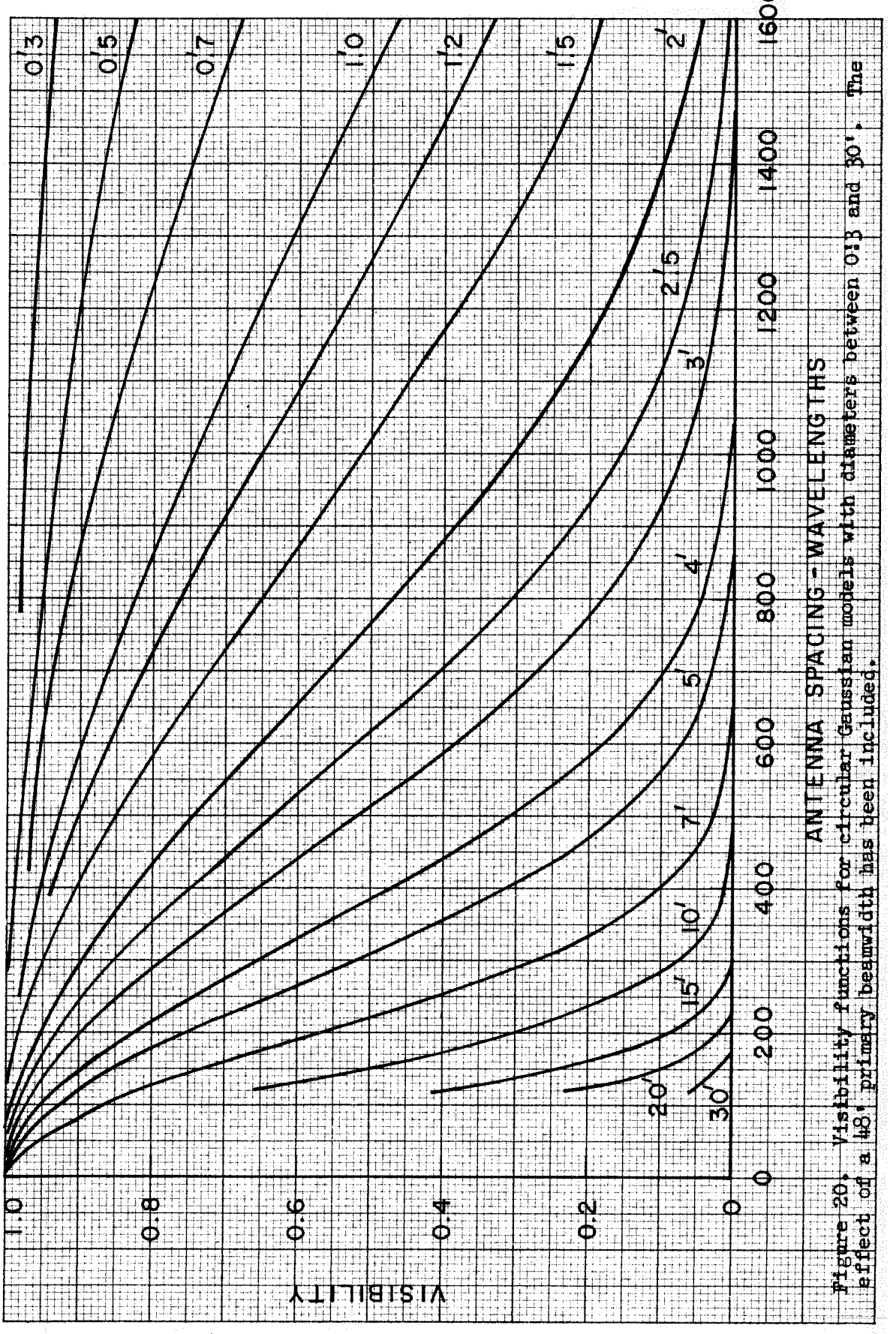

Figure 20. Visibility functions for circular Gaussian models with diameters between 0'3 and 30'. The effect of a 40' primary beamwidth has been included.

or

$$(48) \qquad V(s_x) = \frac{4T \int_0^r \sqrt{r^2 - x^2} \cos 2\pi s_x x \, dx}{4T \int_0^r \sqrt{r^2 - x^2} \, dx}$$

The integral in the numerator of equation 48 is given by Oberhettinger (76). Making use of his result, we obtain

$$(49) \qquad V(s_x) = \frac{\frac{r}{s_x} J_1(2\pi s_x r)}{\pi r^2} = \frac{J_1(2\pi s_x r)}{\pi s_x r} \quad .$$

This function has been plotted in figure 21 for values of $D = 2r$ from 1'.0 to 10'.

Two-Gaussian Models

Consider the one-dimensional visibility function for the sum of two source distributions, $T_1(x-x_1)$ with its centroid at $x = x_1$, and $T_2(x-x_2)$ with its centroid at $x = x_2$. We have

$$(50) \qquad V(s_x)e^{i\Phi(s_x)} = \frac{\int \left[T_1(x-x_1) + T_2(x-x_2)\right] e^{i2\pi s_x x} \, dx}{\int \left[T_1(x-x_1) + T_2(x-x_2)\right] dx} \quad .$$

or

$$(51) \qquad V(s_x)e^{i\Phi(s_x)} = \frac{\int T_1(x-x_1)e^{i2\pi s_x x} \, dx + \int T_2(x-x_2)e^{i2\pi s_x x} \, dx}{\int T_1(x-x_1) \, dx + \int T_2(x-x_2) \, dx}$$

Let S_1 and S_2 be the fluxes from the two components, S be their sum, and ν_1 and ν_2 be the visibility functions

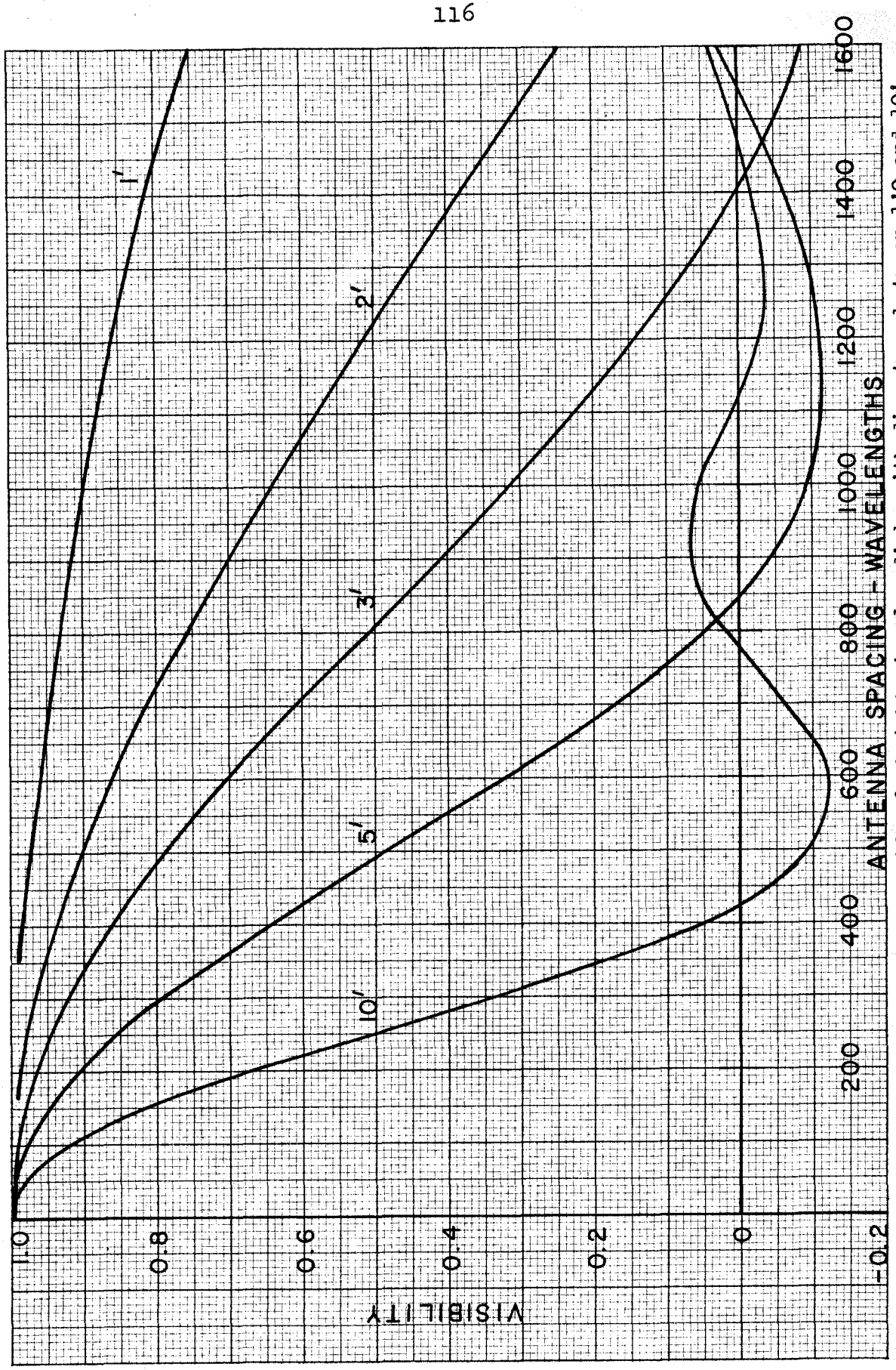

Figure 21. Visibility functions for uniformly bright circular disks with diameters between 1.0 and 10'.

of the two components. Recalling the definition of the flux from equation 15, we can re-write equation 51 as

$$(52)\quad V(s_x)e^{i\Phi(s_x)} = \frac{S_1}{S}\nu_1(s_x)e^{i2\pi s_x x_1} + \frac{S_2}{S}\nu_2(s_x)e^{i2\pi s_x x_2} \quad .$$

Let us choose x_1 and x_2 such that the centroid of the total source distribution is at $x = 0$. We can do this without changing the value of $x_1 - x_2$, the distance between the centroids of the two components, which we will call X. The required condition is that

$$(53)\qquad \frac{x_1}{X} = \frac{S_2}{S} \quad , \quad \frac{-x_2}{X} = \frac{S_1}{S} \quad .$$

We can then write equation 52 as

$$(54)\quad V(s_x)e^{i\Phi(s_x)} = \frac{S_1}{S}\nu_1(s_x)e^{+i2\pi s_x\frac{S_2 X}{S}} + \frac{S_2}{S}\nu_2(s_x)e^{-i2\pi s_x\frac{S_1 X}{S}} \quad .$$

This is a general expression, valid for the superposition of any two source distributions.

Equal Diameters.-- We now consider the special case of a source with two Gaussian components having equal diameters. Let $V_d(s_x)$ be the Gaussian visibility function of equation 45, evaluated for a source with diameter d. Substituting in equation 54, we may factor out the common diameter dependence, $V_d(s_x)$. We obtain

$$(55)\quad V(s_x)e^{i\Phi(s_x)} = V_d(s_x)\left[\frac{S_1}{S}\, e^{+i2\pi s_x\frac{S_2 X}{S}} + \frac{S_2}{S}\, e^{-i2\pi s_x\frac{S_1 X}{S}}\right] \quad .$$

If the component intensities as well as the diameters are equal, we have $S_1 = S_2 = \frac{1}{2}S$, and equation 55 becomes simply

$$(56) \qquad V(s_x) = V_d(s_x) \cos \pi s_x X \quad , \quad \Phi(s_x) = 0 \quad .$$

This expression for $V(s_x)$ is plotted in figure 22 for $X = 5'$, and $d = 1'$, $3'$, and $5'$.

We notice in equation 55 that the expression in brackets is dependent only on the component separation X and the ratio of the component intensities S_2/S_1. (We can write S_1/S as $(1 + S_1/S_2)^{-1}$, etc.) By representing the two terms in the brackets as two vectors rotating in the complex plane, we may derive the following expressions for the amplitude and phase of the visibility function:

$$(57) \quad V(s_x) = V_d(s_x)\left[\left(\frac{S_1}{S}\right)^2 + \left(\frac{S_2}{S}\right)^2 + \frac{S_1 S_2}{S^2} \cos 2\pi s_x X\right]^{\frac{1}{2}} \quad ,$$

$$(58) \quad \Phi(s_x) = \tan^{-1}\left[\frac{S_1 - S_2}{S} \tan \pi s_x X\right] - \frac{S_1 - S_2}{S} \pi s_x X \quad .$$

The amplitude, given in equation 57, is seen to equal the visibility amplitude of one component multiplied by an interference term. This interference term is plotted in figure 23 as a function of the component separation (in units of the fringe period) for several values of the intensity ratio S_2/S_1. The fringe period is equal to $1/s_x$, and it is convenient to remember that a spacing of 343.8λ produces a fringe period of $10'$. The phase, given in

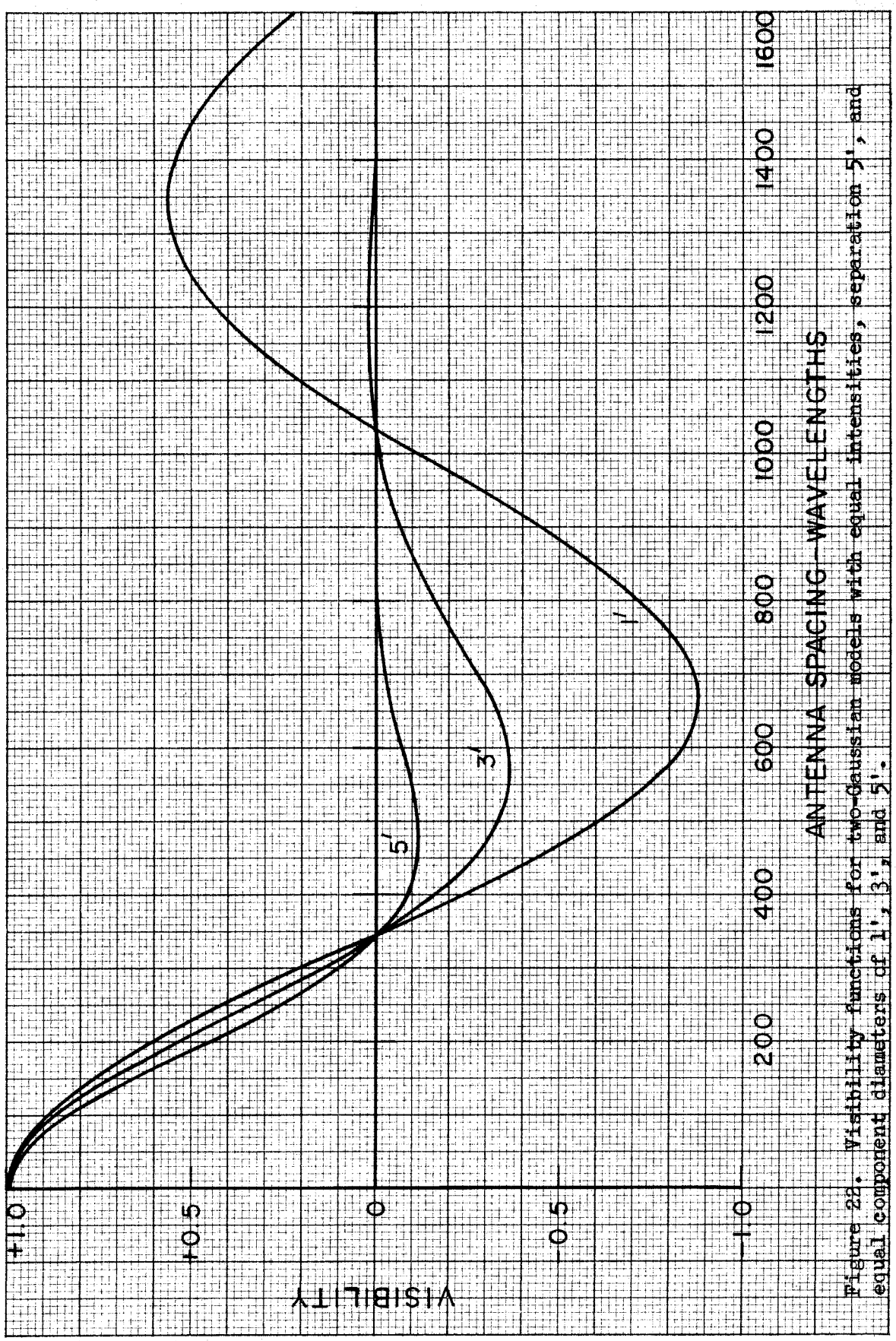

Figure 22. Visibility functions for two-Gaussian models with equal intensities, separation 5', and equal component diameters of 1', 3', and 5'.

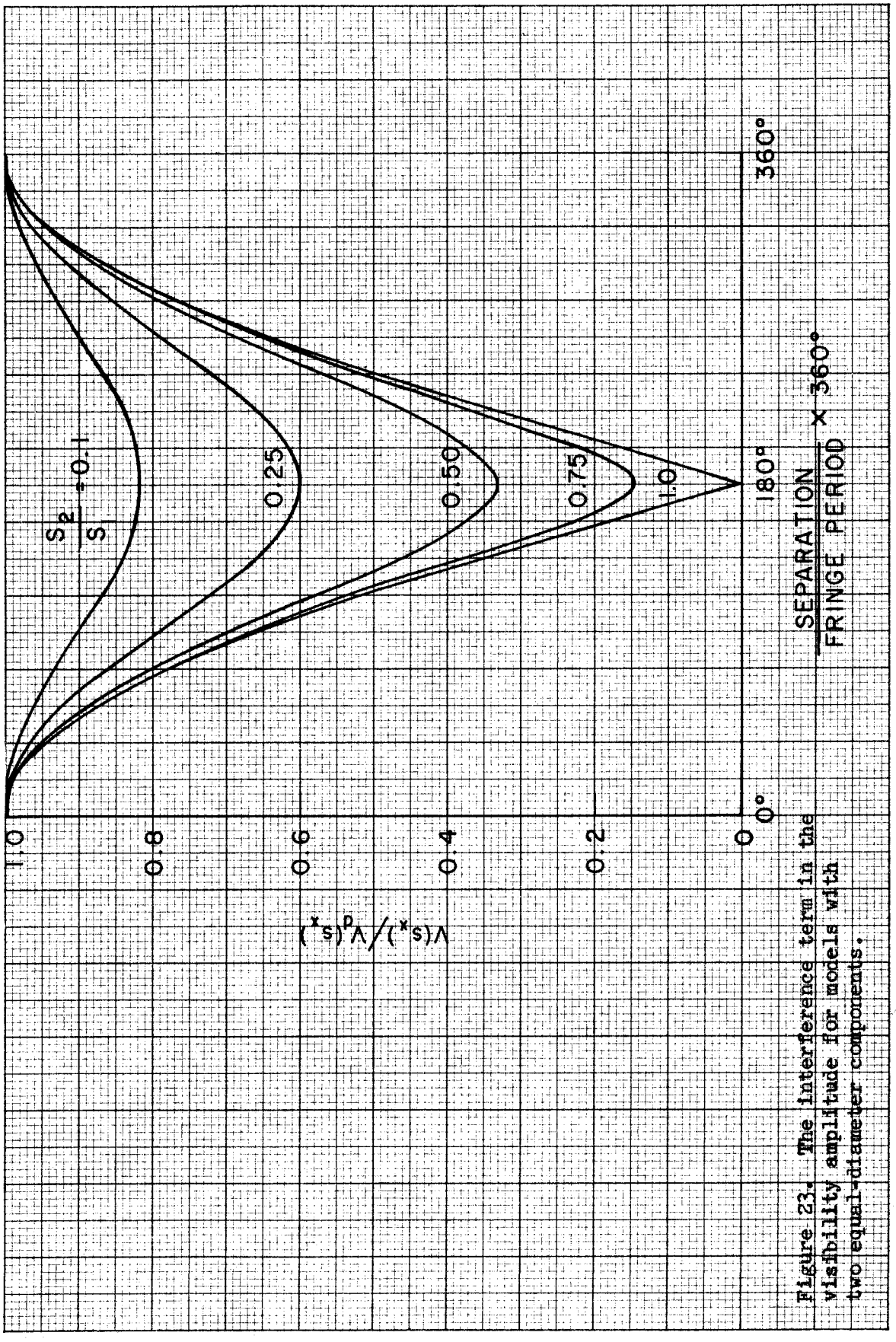

Figure 23. The interference term in the visibility amplitude for models with two equal-diameter components.

equation 58, is plotted in figure 24, using the same independent variable as in the preceding figure. We note that for sources with equal-diameter components, the phase contains no explicit diameter dependence. For antenna spacings which produce fringe periods smaller than the component separation, the amplitude function of figure 23 merely repeats itself, while the phase function of figure 24 continues to increase in stair-step fashion (see figure 18).

In order to obtain the visibility amplitude for a double source with equal-diameter components, we must scale the abscissa in figure 23 according to the separation of the components and multiply by the visibility of the components V_d, which is obtained from figure 20. An example, given in figure 25, is the visibility amplitude for a source with components having intensities of 2 and 1, a separation of 5', and individual diameters of 3'. The source distribution is shown in the inset. The phase for this source is obtained by suitably scaling the abscissa in figure 24.

Unequal Diameters.-- Finally we consider models consisting of two Gaussian components with unequal diameters. The visibility function for these models is given by equation 54, but a common diameter dependence can no longer be factored out as was done in deriving equation 55. Instead, let $V_{d_1}(s_x)$ be the visibility function for component 1, which is a Gaussian having intensity S_1 and diameter d_1, and make similar definitions for component 2. The total intensity is

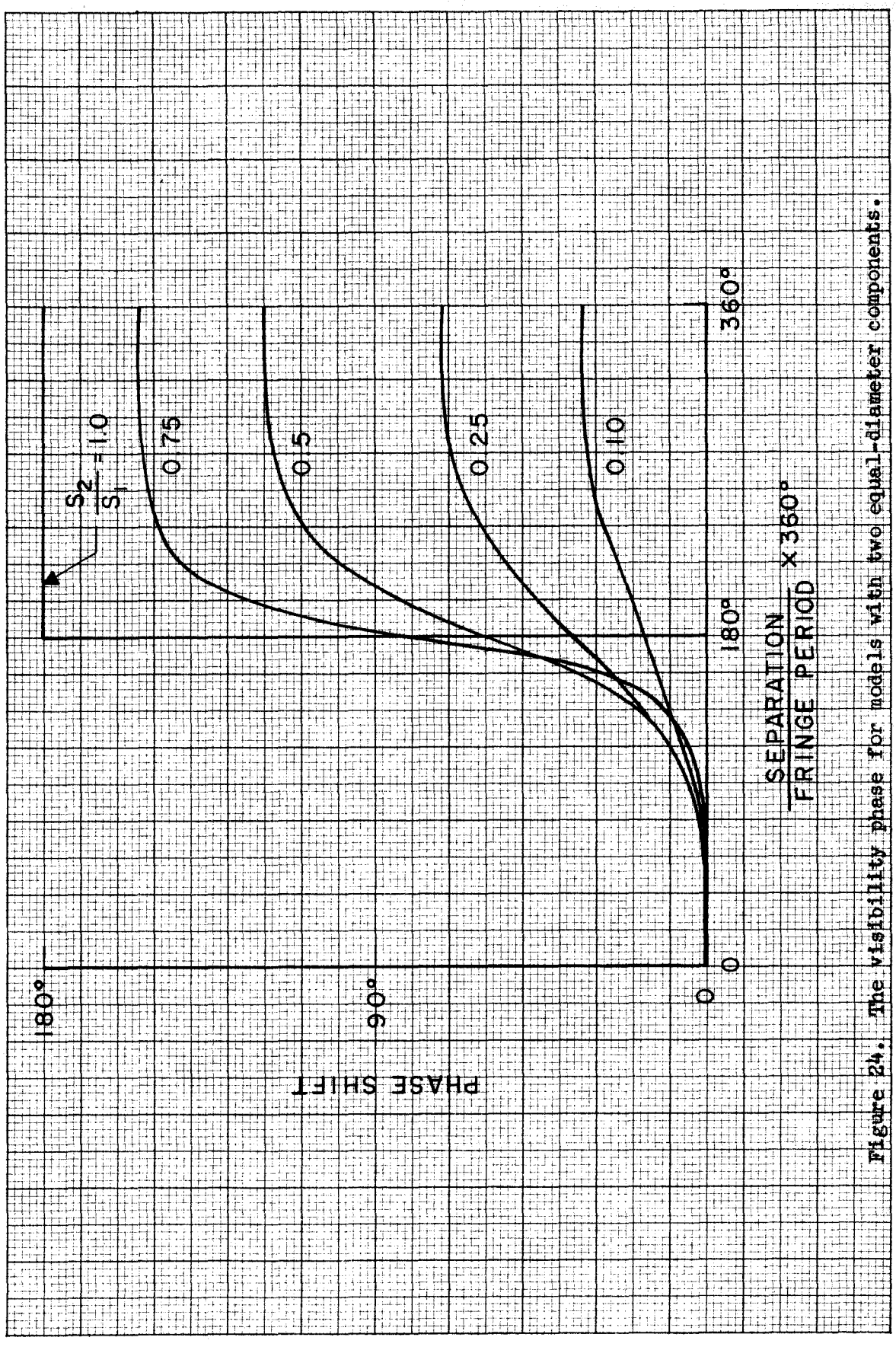

Figure 24. The visibility phase for models with two equal-diameter components.

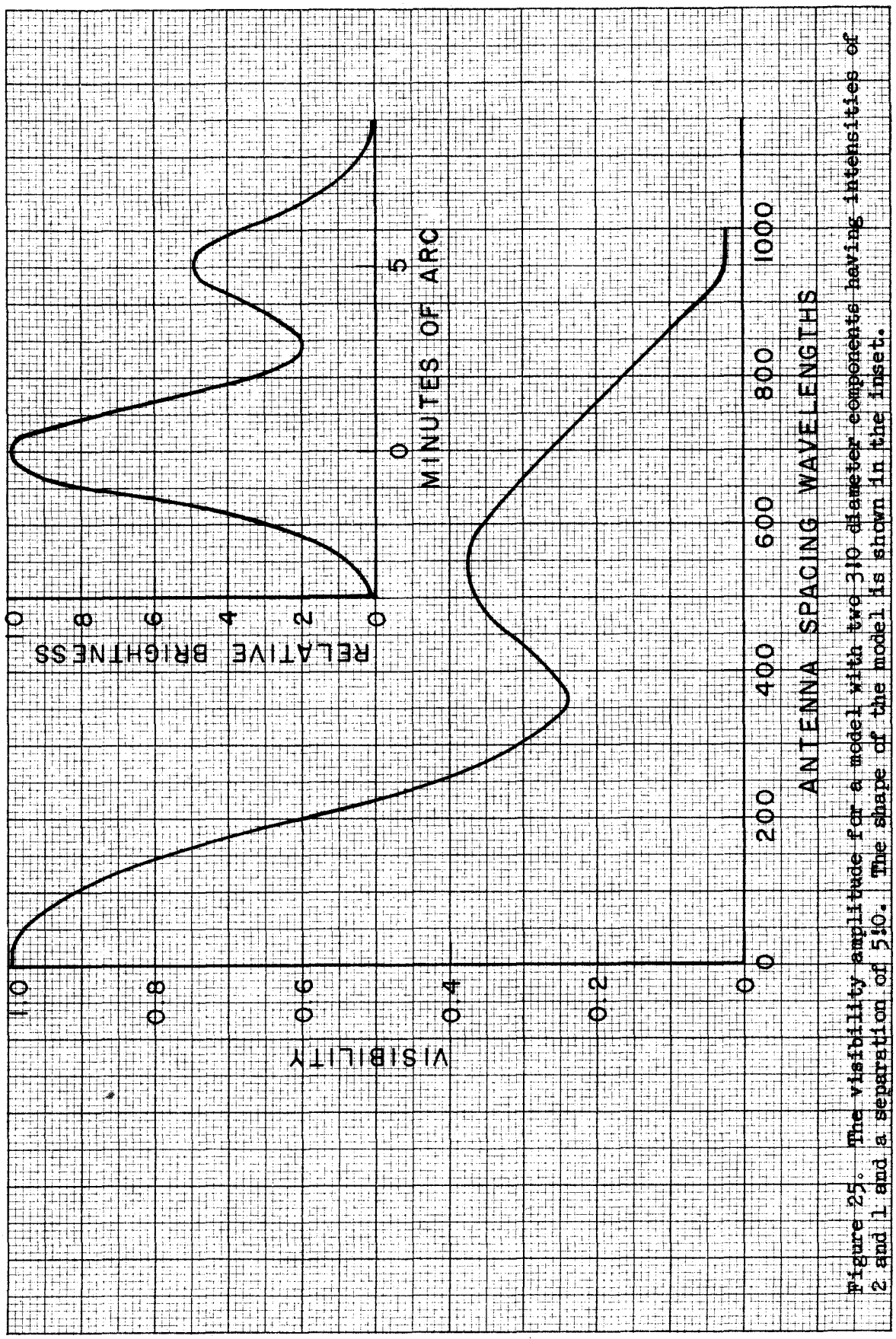

Figure 25. The visibility amplitude for a model with two 3.0 diameter components having intensities of 2 and 1 and a separation of 5.0. The shape of the model is shown in the inset.

still $S = S_1 + S_2$. Let us also define the apparent intensities and their sum as

$$S_1' = S_1 V_{d_1}(s_x)$$

$$S_2' = S_2 V_{d_2}(s_x) \tag{59}$$

$$S' = S_1' + S_2' \quad .$$

Then we can write equation 54 as

$$V(s_x)e^{i\Phi(s_x)} = \frac{S_1'}{S} e^{-i2\pi s_x \frac{S_2 X}{S}} + \frac{S_2'}{S} e^{+i2\pi s_x \frac{S_1 X}{S}} \quad . \tag{60}$$

Again by representing this expression as the sum of two vectors in the complex plane, we may derive relations for the amplitude and phase of the visibility function:

$$V(s_x) = \left[\left(\frac{S_1'}{S}\right)^2 + \left(\frac{S_2'}{S}\right)^2 + 2\frac{S_1' S_2'}{S^2} \cos 2\pi s_x X \right]^{\frac{1}{2}} \tag{61}$$

$$\Phi(s_x) = \tan^{-1}\left[\frac{S_1' - S_2'}{S'} \tan \pi s_x X \right] - \frac{S_1 - S_2}{S} \pi s_x X \quad . \tag{62}$$

Because of their complicated dependence on the two diameters, these relations cannot be plotted as could the analogous results for the equal-diameter model. The only general feature we can note is that the upper and lower envelopes of the amplitude are given by the sum and difference of the weighted amplitudes of the two components.

As an example of this type of model, in figure 26 are

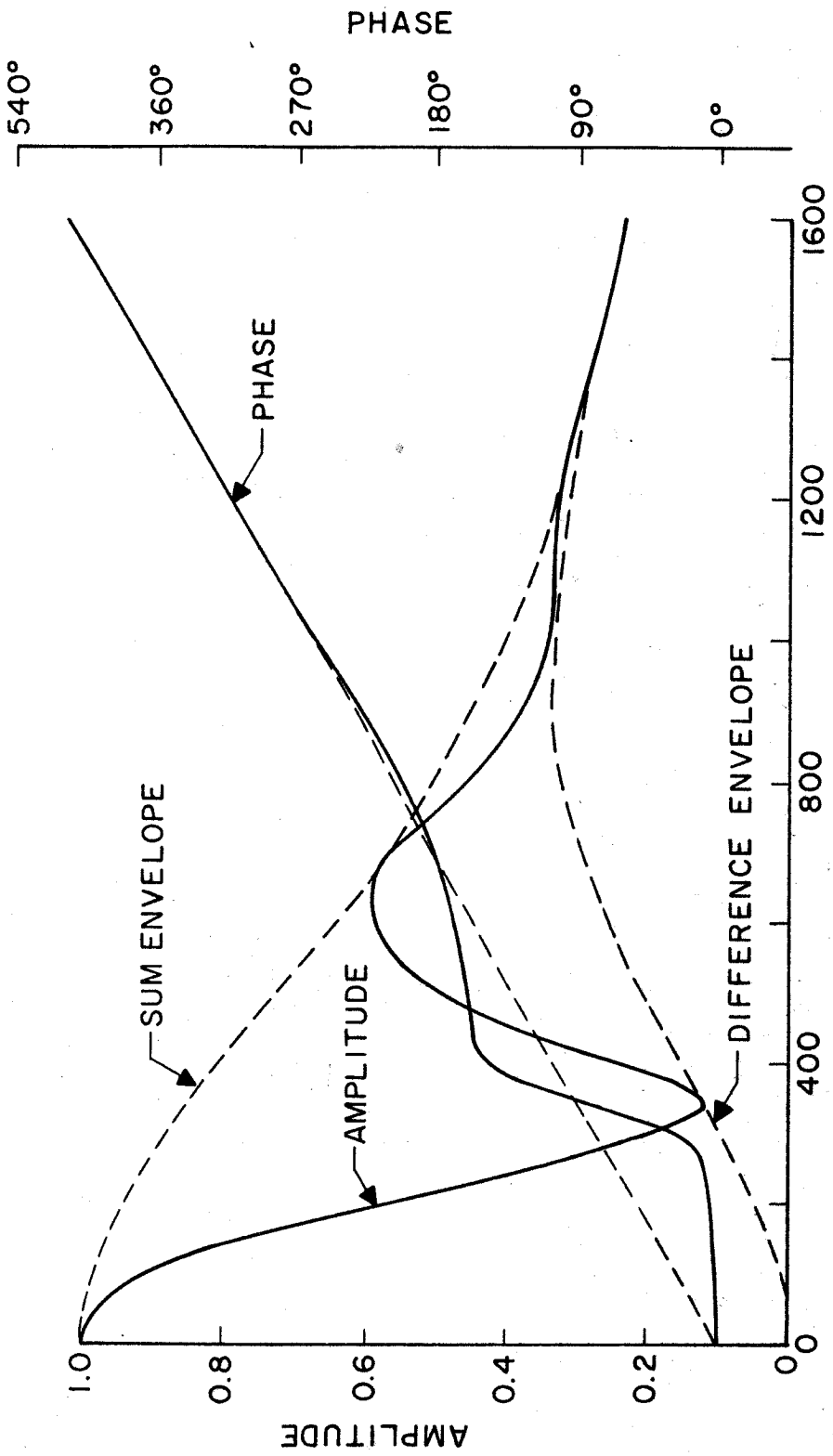

Figure 26. Amplitude and phase for a model with two components of equal intensity, diameters of 1:0 and 3:0, and a separation of 5:0.

plotted the amplitude and phase for a source with two Gaussian components of equal intensity, separated by 5', and with diameters of 1' and 3'. After the large component has become heavily resolved, the smaller one dominates the visibility function. The linear phase shift at large spacings indicates the displacement of the apparent position to that of the center of the smaller component.

REFERENCES

1. J. S. Hey, S. J. Parsons, and J. W. Phillips, Nature 158, 234 (1946).

2. J. G. Bolton and G. J. Stanley, Australian J. Sci. Research A1, 58 (1948).

3. A. A. Michelson, Phil. Mag. 30, 1 (1890).

4. A. A. Michelson, Phil. Mag. 31, 256 (1891).

5. M. Ryle and D. D. Vonberg, Nature 158, 339 (1946).

6. L. L. McReady, J. L. Pawsey, and R. Payne-Scott, Proc. Roy. Soc. (London) A187, 357 (1947).

7. R. N. Bracewell, Proc. Inst. Radio Engrs. 46, 97 (1958).

8. R. N. Bracewell, Trans. Inst. Radio Engrs. AP-9, 59 (1961).

9. R. B. Read, Trans. Inst. Radio Engrs. AP-9, 31 (1961).

10. J. Lequeux, E. Le Roux, and M. Vinokur, Compt. rend. 249, 634 (1959).

11. J. S. Hey, Quarterly Jour. Roy. Astron. Soc. 1, 103 (1960).

12. M. Ryle, Proc. Roy. Soc. (London) A211, 351 (1952).

13. I. N. Sneddon, Fourier Transforms (McGraw-Hill Book Company, Inc., New York, 1951), p. 24.

14. R. N. Bracewell and J. A. Roberts, Australian J. Phys. 7, 615 (1954).

15. J. Waser and V. Schomaker, Revs. Modern Phys. 25, 671 (1953).

16. A. E. Covington and G. A. Harvey, Can. J. Phys. 37, 1216 (1959).

17. M. Ryle and A. Hewish, Monthly Notices Roy. Astron. Soc. 120, 220 (1960).

18. I. S. Shklovsky, Cosmic Radio Waves (Harvard University Press, Cambridge, Mass., 1960), pp. 97-117.

19. R. H. Brown, R. C. Jennison, and M. K. Das Gupta, Nature 170, 1061 (1952).

20. B. Y. Mills, Nature 170, 1063 (1952).

21. F. G. Smith, Nature 170, 1065 (1952).

22. B. Y. Mills, Australian J. Phys. 6, 452 (1953).

23. R. C. Jennison and M. K. Das Gupta, Phil. Mag. 1, 65 (1956).

24. J. E. Baldwin, Nature 174, 320 (1954).

25. J. E. Baldwin and F. G. Smith, Observatory 76, 141 (1956).

26. J. E. Baldwin and D. W. Dewhirst, Nature 173, 164 (1954).

27. R. H. Brown, H. P. Palmer, and A. R. Thompson, Nature 173, 945 (1954).

28. R. G. Conway, Observatory 76, 235 (1956).

29. B. Rowson, Monthly Notices Roy. Astron. Soc. 119, 26 (1959).

30. B. Rowson, Proc. Phys. Soc. (London) B70, 328 (1957).

31. F. Biraud, J. Lequeux, and E. Le Roux, Observatory 80, 116 (1960).

32. D. Morris, H. P. Palmer, and A. R. Thompson, Observatory 77, 103 (1957).

33. L. R. Allen, H. P. Palmer, and B. Rowson, Nature 188, 731 (1960).

34. R. C. Jennison, Monthly Notices Roy. Astron. Soc. 118, 276 (1958).

35. R. C. Jennison and V. Latham, Monthly Notices Roy. Astron. Soc. 119, 174 (1959).

36. R. Q. Twiss, A. W. L. Carter, and A. G. Little, Observatory 80, 153 (1960).

37. J. R. Shakeshaft, M. Ryle, J. E. Baldwin, B. Elsmore, and J. H. Thompson, Memoirs Roy. Astron. Soc. 67, 106 (1955).

38. D. O. Edge, J. R. Shakeshaft, W. B. McAdam, J. E. Baldwin, and S. Archer, Memoirs Roy. Astron. Soc. 68, 37 (1959).

39. B. Elsmore, M. Ryle, and P. R. R. Leslie, Memoirs Roy. Astron. Soc. 68, 61 (1959).

40. B. Y. Mills, O. B. Slee, and E. R. Hill, Australian J. Phys. 13, 676 (1960).

41. B. Y. Mills, Australian J. Phys. 13, 550 (1960).

42. D. E. Harris and J. A. Roberts, Publs. Astron. Soc. Pacific 72, 237 (1960).

43. R. W. Wilson and J. G. Bolton, Publs. Astron. Soc. Pacific 72, 331 (1960).

44. B. Y. Mills, O. B. Slee, and E. R. Hill, Australian J. Phys. 11, 360 (1958).

45. R. B. Read (Ph.D. thesis, California Institute of Technology, in preparation).

46. T. A. Matthews, private communication (1961).

47. H. P. Palmer, private communication via R. H. Brown (1960).

48. J. A. Högbom and J. R. Shakeshaft, Nature 189, 561 (1961).

49. O. B. Slee, Australian J. Phys. 8, 498 (1955).

50. A. W. L. Carter, Australian J. Phys. 8, 564 (1955).

51. P. Maltby, private communication (1961).

52. P. R. R. Leslie, Monthly Notices Roy. Astron. Soc. 122, 51 (1961).

53. R. W. Wilson, private communication (1961).

54. N. W. Broten and W. J. Medd, Astrophys. J. 132, 279 (1960).

55. J. L. Pawsey, Astrophys. J. 121, 1 (1955).

56. M. I. Large, D. S. Matthewson, and C. G. T. Haslam, Nature 183, 1663 (1959).

57. R. W. Wilson (Ph.D thesis, California Institute of Technology, in preparation).

58. R. Minkowski, Publs. Astron. Soc. Pacific 70, 143 (1958).

59. C. M. Wade, private communication (1961).

60. W. Baade, Astrophys. J. 123, 550 (1956).

61. C. M. Wade, Australian J. Phys. 12, 472 (1959).

62. J. G. Bolton and B. G. Clark, Publs. Astron. Soc. Pacific 72, 29 (1960).

63. A. G. Little, private communication (1961).

64. R. C. Jennison and M. K. Das Gupta, Nature 172, 996 (1953).

65. W. Baade and R. Minkowski, Astrophys. J. 119, 206 (1954).

66. F. G. Smith, Monthly Notices Roy. Astron. Soc. 122, 71 (1961).

67. D. W. Dewhirst, in Paris Symposium on Radio Astronomy, R. N. Bracewell, ed. (Stanford Univ. Press, Stanford, Calif., 1959), p. 507.

68. R. Minkowski, Proc. Natl. Acad. Sci. U. S. 46, 13 (1960).

69. J. G. Bolton, introductory talk at session on discrete sources at U.R.S.I. General Assembly, London, 1960 --also Obs. Calif. Inst. of Technology Radio Observatory, 5 (1960).

70. R. Minkowski, in Radio Astronomy, I.A.U. Symposium No. 4, H. C. van de Hulst, ed. (Cambridge Univ. Press, Cambridge, England, 1957), p. 107.

71. I. S. Shklovsky, opus cit., p. 357.

72. G. R. Burbidge, in Paris Symposium on Radio Astronomy, R. N. Bracewell, ed. (Stanford Univ. Press, Stanford, Calif. 1959), p. 541.

73. I. S. Shklovsky, opus cit., p. 370.

74. I. S. Shklovsky, Astron. J. U.S.S.R. 37, 945 (1960).

75. A. A. Michelson and F. G. Pease, Astrophys. J. 53, 249 (1921).

76. F. Oberhettinger, Tabellen zur Fourier Transformation (Springer Verlag, Berlin, 1957), p. 6.